



PB95266607



**Method for Developing Motion Damage
Relationships for Reinforced Concrete Frames**

by

A. Singhal¹ and A.S. Kiremidjian²

May 11, 1995

Technical Report NCEER-95-0008

NCEER Task Number 93-4101

NSF Master Contract Number BCS 90-25010

and

NYSSTF Grant Number NEC-91029

- 1 Doctoral Candidate, The John A. Blume Earthquake Engineering Center, Department of Civil Engineering, Stanford University
- 2 Professor and Co-Director, The John A. Blume Earthquake Engineering Center, Department of Civil Engineering, Stanford University

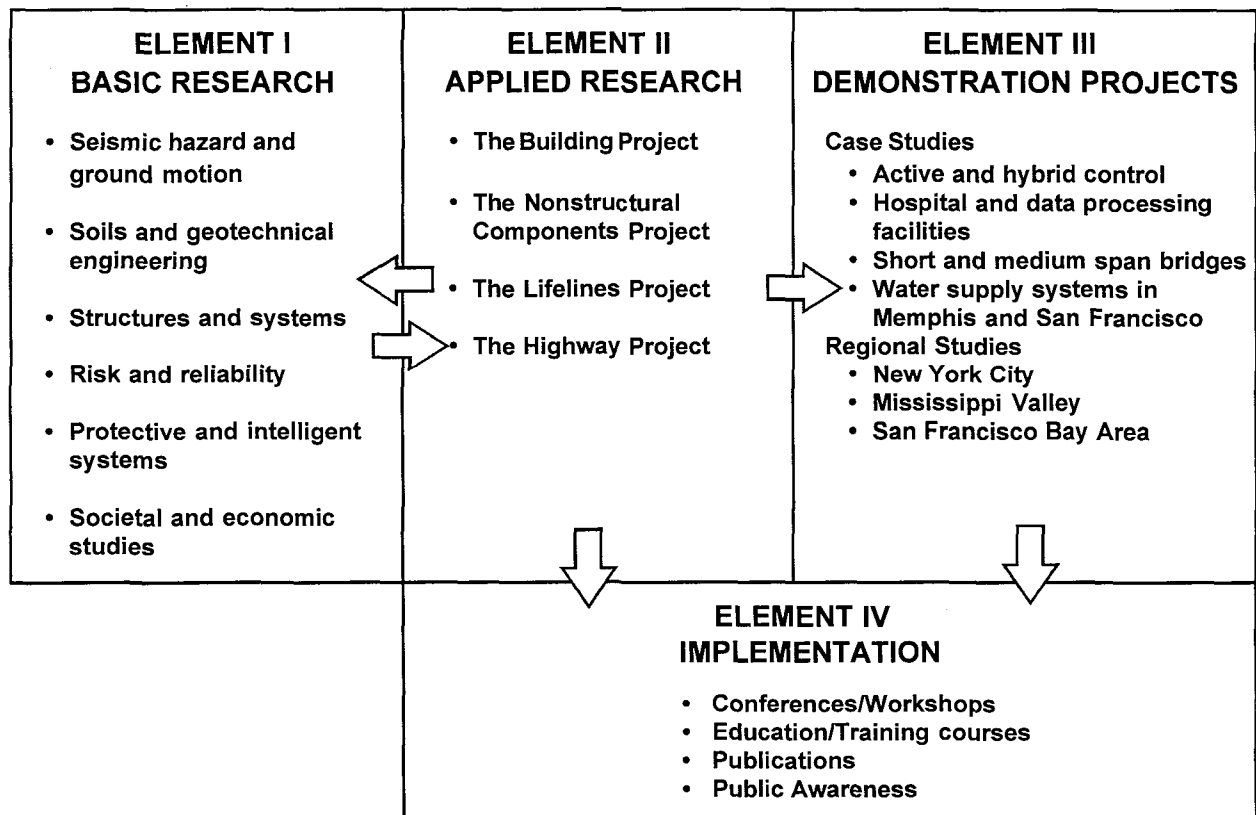
NATIONAL CENTER FOR EARTHQUAKE ENGINEERING RESEARCH
State University of New York at Buffalo
Red Jacket Quadrangle, Buffalo, NY 14261



PREFACE

The National Center for Earthquake Engineering Research (NCEER) was established to expand and disseminate knowledge about earthquakes, improve earthquake-resistant design, and implement seismic hazard mitigation procedures to minimize loss of lives and property. The emphasis is on structures in the eastern and central United States and lifelines throughout the country that are found in zones of low, moderate, and high seismicity.

NCEER's research and implementation plan in years six through ten (1991-1996) comprises four interlocked elements, as shown in the figure below. Element I, Basic Research, is carried out to support projects in the Applied Research area. Element II, Applied Research, is the major focus of work for years six through ten. Element III, Demonstration Projects, have been planned to support Applied Research projects, and will be either case studies or regional studies. Element IV, Implementation, will result from activity in the four Applied Research projects, and from Demonstration Projects.



Research in the **Building Project** focuses on the evaluation and retrofit of buildings in regions of moderate seismicity. Emphasis is on lightly reinforced concrete buildings, steel semi-rigid frames, and masonry walls or infills. The research involves small- and medium-scale shake table tests and full-scale component tests at several institutions. In a parallel effort, analytical models and computer programs are being developed to aid in the prediction of the response of these buildings to various types of ground motion.

Two of the short-term products of the **Building Project** will be a monograph on the evaluation of lightly reinforced concrete buildings and a state-of-the-art report on unreinforced masonry.

The **risk and reliability program** constitutes one of the important areas of research in the **Building Project**. The program is concerned with reducing the uncertainty in current models which characterize and predict seismically induced ground motion, and resulting structural damage and system unavailability. The goal of the program is to provide analytical and empirical procedures to bridge the gap between traditional earthquake engineering and socioeconomic considerations for the most cost-effective seismic hazard mitigation. Among others, the following tasks are being carried out:

1. Study seismic damage and develop fragility curves for existing structures.
2. Develop retrofit and strengthening strategies.
3. Develop intelligent structures using high-tech and traditional sensors for on-line and real-time diagnoses of structural integrity under seismic excitation.
4. Improve and promote damage-control design for new structures.
5. Study critical code issues and assist code groups to upgrade seismic design code.
6. Investigate the integrity of nonstructural systems under seismic conditions.

The report develops the methodology for analytically developing damage probability matrices (DPM) for comparison with those proposed by ATC-13 based on expert opinion surveys. Such comparisons are needed to establish a more rational approach to probabilistic damage assessments in order to improve building code provisions and to refine cost estimates of earthquake damage. The proposed methodology is comprehensive in its dealing with the many complex aspects of probabilistic damage assessment required to accomplish the above task. The application of this methodology to common building frames of three heights and therefore frequency ranges provides an important benchmark set of results.

ABSTRACT

This report presents formulations for developing fragility curves and damage probability matrices for reinforced concrete frame structures. Three different classes of reinforced concrete frames, based the story heights, are considered. The development of fragility curves and damage probability matrices requires the characterization of ground motion and the identification of different degrees of structural damage.

The ground motion characterization parameters used in this report are the spectral acceleration and the root mean square acceleration. At a given ground motion parameter, an ensemble of ground motions is required for evaluating the conditional probabilities of the different degrees of damage. Autoregressive moving average (ARMA) models and Gaussian stationary models with modulating functions are used for this purpose.

The identification of the different degrees of structural damage is carried out based on the structural damage models. Models for characterizing the seismic damage to reinforced concrete structures are reviewed in this report. The Park and Ang damage index is used in this report for the development of fragility curves and damage probability matrices.

Constrained Monte Carlo simulation techniques are used for evaluating the fragility curves. The comparison of the damage probability matrices for the three classes of reinforced concrete frames, developed in this study, with those in ATC-13 (1985) shows that the ATC-13 DPM's potentially underestimate the damage, particularly at the high intensity levels. Because the existing definitions of damage to reinforced concrete structures are found to be inadequate, a new technique for identifying different damage states for such structures is presented that considers the crack widths and interstory drift ratios.

ACKNOWLEDGMENT

The authors would like to express their gratitude to Dr. Andrei Reinhorn for providing us with the program IDARC2D. In addition, Dr. J. P. Conte provided input to the ARMA modeling of earthquake ground motions. Their help is gratefully appreciated.

TABLE OF CONTENTS

SECTION	TITLE	PAGE
1	INTRODUCTION AND LITERATURE SURVEY	1-1
1.1	Introduction	1-1
1.1.1	Objectives and Scope	1-1
1.1.2	Organization of the Report	1-2
1.2	Review of Previous Work	1-3
1.2.1	Ground Motion Characterization	1-3
1.2.1.1	Strong Motion Duration	1-4
1.2.1.2	Ground Motion Amplitude	1-5
1.2.1.3	Housner's Spectral Intensity	1-5
1.2.1.4	Arias Intensity	1-6
1.2.1.5	Root Mean Square Acceleration	1-7
1.2.1.6	Response Spectrum	1-7
1.2.1.7	Modified Mercalli Intensity	1-8
1.2.2	Measures of Structural Damage	1-8
1.2.2.1	Local Damage Indices	1-9
1.2.2.2	Global Damage Indices	1-12
2	METHODOLOGY FOR DAMAGE ANALYSIS	2-1
2.1	Identification of Damage States	2-4
2.1.1	Damage States Based on Structural Damage Indices	2-4
2.1.2	Proposed Damage States Based on Crack Width and Interstory Drift ...	2-6
2.2	Damage Analysis	2-8
2.2.1	Structural Modeling in IDARC2D	2-8
3	MODELING PARAMETER RELATIONSHIPS AND RANDOMNESS	3-1
3.1	Modeling of Uncertainties in Structural Capacity	3-1
3.2	Modeling of Uncertainties in Demand Parameters	3-2
3.2.1	Uncertainties in Kanai-Tajimi Parameters	3-2
3.2.2	Uncertainties in Dynamic Amplification Factors	3-3
3.2.3	Uncertainties in Strong Motion Duration	3-4
3.3	Relationship Between MMI and S_a	3-11
3.4	Development of Damage Probability Matrices	3-20
4	MONTE CARLO SIMULATION TECHNIQUE	4-1
4.1	Ground Motion Simulation	4-4
4.1.1	Geophysical Models	4-5
4.1.2	Gaussian Stationary Models with Modulating Functions	4-5
4.1.3	ARMA Models	4-6
4.1.3.1	Simulation of Time Histories with Specified RMS and Duration	4-9
4.2	Damage Simulation	4-13

TABLE OF CONTENTS (Cont'd)

SECTION	TITLE	PAGE
5	IMPLEMENTATION OF THE METHODOLOGY	5-1
5.1	Description of the Two Story Building	5-1
5.1.1	Fragility Curves.....	5-3
5.1.2	Damage Probability Matrix.....	5-8
5.2	Description of the Six Story Building	5-9
5.2.1	Fragility Curves.....	5-9
5.2.2	Damage Probability Matrix.....	5-13
5.3	Description of the Thirteen Story Building.....	5-14
5.3.1	Fragility Curves.....	5-15
5.3.2	Damage Probability Matrix.....	5-19
5.4	Comparison of Results	5-20
5.5	Comments on Damage Measures.....	5-21
6	SUMMARY AND FUTURE WORK.....	6-1
6.1	Summary.....	6-1
6.2	Future Work	6-2
7	REFERENCES.....	7-1
APPENDIX A	BAYESIAN TECHNIQUE.....	A-1

LIST OF ILLUSTRATIONS

FIGURE	TITLE	PAGE
1-1	Definition of δ_m in the Park and Ang (1984) index.....	1-10
1-2	Damage index definitions by Chung et al. (1987).....	1-12
2-1	Steps in the development of fragility curves and damage probability matrices	2-3
2-2	Stiffness degradation in the hysteretic loop	2-9
3-1	Parameters of the dynamic amplification factors for firm sites	3-3
3-2	Correlation between Trifunac and Brady's (1975) strong motion duration and the RMS for firm sites with distances to rupture zones less than 50 km.....	3-8
3-3	Correlation between Trifunac and Brady's (1975) strong motion duration and the RMS for firm sites with distances to rupture zones greater than 50 km	3-8
3-4	Correlation between Trifunac and Brady's (1975) strong motion duration and the average S_a in the period range 0.1-0.45 sec for firm sites.....	3-9
3-5	Correlation between Trifunac and Brady's (1975) strong motion duration and the average S_a in the period range 0.45-0.85 sec for firm sites.....	3-10
3-6	Correlation between Trifunac and Brady's (1975) strong motion duration and the average S_a in the period range 0.85-2.5 sec for firm sites.....	3-10
3-7	Comparison of the observed and the estimated log normal distribution of strong motion duration for firm sites	3-11
3-8	Map showing the MMI contours and the CSMIP station numbers for the Morgan Hill earthquake of April 24, 1984.....	3-13
3-9	Map showing the MMI contours and the CSMIP station numbers for the Whittier Narrows earthquake of October 1, 1987.....	3-14
3-10	Map showing the MMI contours and the CSMIP station numbers for the Loma Prieta earthquake of October 18, 1989.....	3-15
3-11	Map showing the MMI contours and the USGS station numbers for the Loma Prieta earthquake of October 18, 1989.....	3-16
3-12	S_a -MMI correlation and the probability distributions for average spectral acceleration, in the period range 0.1-0.45 sec, conditional on MMI	3-19
3-13	S_a -MMI correlation and the probability distributions for average spectral acceleration, in the period range 0.45-0.85 sec, conditional on MMI	3-19

LIST OF ILLUSTRATIONS (Cont'd)

FIGURE	TITLE	PAGE
3-14	S _a -MMI correlation and the probability distributions for average spectral acceleration, in the period range 0.85-2.5 sec, conditional on MMI	3-20
4-1	Steps in the Monte Carlo simulation technique	4-2
4-2	Steps in the simulation of time histories A and B in figure 4-1.....	4-2
4-3	General probability density function with N intervals used in the Latin Hypercube sampling scheme.....	4-4
5-1	Typical floor plan of the two story building	5-2
5-2	Elevation of frames A and B in the two story building	5-3
5-3	Fragility curves for the two story building for sites with distances to rupture zones less than 50 km.....	5-6
5-4	Fragility curves for the two story building for sites with distances to rupture zones greater than 50 km	5-6
5-5	Fragility curves for the two story building with ground motion characterized by spectral acceleration in the period range 0.1-0.45 sec..	5-7
5-6	Typical floor plan of the six story building	5-10
5-7	Elevation of frames A and B in the six story building	5-11
5-8	Fragility curves for the six story building with ground motion characterized by spectral acceleration in the period range 0.45-0.85 sec	5-13
5-9	Typical floor plan of the thirteen story building.....	5-16
5-10	Elevation of frames A and B in the thirteen story building.....	5-17
5-11	Fragility curves for the thirteen story building with ground motion characterized by spectral acceleration in the period range 0.85-2.5 sec..	5-19
5-12	Relationship between Park-Ang damage index and interstory drift ratio for the two story building	5-22
5-13	Relationship between Park-Ang damage index and interstory drift ratio	5-22
5-14	Relationship between Park-Ang damage index and interstory drift ratio	5-23

LIST OF TABLES

TABLE	TITLE	PAGE
2-I	Park and Ang's (1984) damage index for different damage states as defined by Park et al. (1987).....	2-5
2-II	Chung, Meyer and Shinozuka's (1987) damage index for different damage states as defined by Hatamoto et al. (1990).....	2-5
2-III	Park and Ang's (1984) damage index for different damage states as defined by Gunturi (1992).....	2-5
2-IV	Definitions of damage states based on maximum crack width and maximum interstory drift ratio.....	2-8
3-I	Trifunac and Brady's (1975) strong motion duration and RMS values for Loma Prieta, Whittier Narrows and Morgan Hill earthquakes for sites with distances to rupture zones less than 50 km.....	3-6
3-II	Trifunac and Brady's (1975) strong motion duration and RMS values for Loma Prieta and Whittier Narrows earthquakes for sites with distances to rupture zones greater than 50 km.....	3-7
3-III	Parameters for the estimation of the mean and the variance of the conditional strong motion duration given the RMS.....	3-9
3-IV	Average spectral acceleration and MMI values for the Loma Prieta, Whittier Narrows and Morgan Hill earthquakes.....	3-17
5-I	Properties of beams and columns in the two story building.....	5-2
5-II	Mean and standard deviation of the damage index at the mean value of RMS for the two story building.....	5-4
5-III	Mean and standard deviation of the maximum story damage index for spectral acceleration in the range 0.1-0.45 sec for the two story building.....	5-5
5-IV	Parameters of the lognormal distribution functions in terms of RMS.....	5-7
5-V	Parameters of the lognormal distribution functions in terms of spectral acceleration.....	5-7
5-VI	Damage probability matrix for the two story building.....	5-8
5-VII	Damage probability matrix for low-rise, ductile moment resisting frames.....	5-8
5-VIII	Damage probability matrix for low-rise, non-ductile moment resisting frames.....	5-9
5-IX	Properties of beams and columns in frames A and B in the six story building.....	5-9
5-X	Mean and standard deviation of the maximum story damage index for the six story building.....	5-12
5-XI	Parameters of the lognormal distribution functions.....	5-12
5-XII	Damage probability matrix for the six story building.....	5-14
5-XIII	Damage probability matrix for mid-rise, ductile moment resisting frames.....	5-14

LIST OF TABLES (Cont'd)

TABLE	TITLE	PAGE
5-XIV	Damage probability matrix for mid-rise, non-ductile moment resisting frames	5-14
5-XV	Properties of beams and columns in frames A and B in the thirteen story building	5-15
5-XVI	Mean and standard deviation of the maximum story damage index for the thirteen story building	5-18
5-XVII	Parameters of the lognormal distribution functions.....	5-18
5-XVIII	Damage probability matrix for the thirteen story building.....	5-20
5-XIX	Damage probability matrix for high-rise, ductile moment resisting frames	5-20
5-XX	Damage probability matrix for high-rise, non-ductile moment resisting frames	5-20

LIST OF SYMBOLS

$a(t)$	ground acceleration at time t
A_n	amplitude of n^{th} sinusoid
d	diameter of reinforcing bar
D_T	Park and Ang global damage index
D_g	Chung, Meyer and Shinozuka's global damage index
E_n	normalized dissipated energy
e_k	stationary discrete white-noise process
g	acceleration due to gravity
I_H	Housner's spectral intensity
I	Arias intensity
$I(t)$	envelope function
P_{ik}	probability of reaching damage state d_i at ground motion level y_k
P_{ik}	probability of reaching or exceeding damage state d_i at ground motion level y_k
Q_y	yield strength of an element
S_0	intensity of white noise excitation at bedrock
T_d	total duration of the earthquake
T_s	strong motion duration
T	natural period of a structure
T_0	initial natural period of a structure
T_{\max}	maximum natural period of an equivalent linear system
w_{\max}	maximum crack width
ε_s	strain in tensile reinforcement
ρ	correlation coefficient
ϕ_{\max}	maximum curvature
ϕ_y	yield curvature

LIST OF SYMBOLS (Cont'd)

ϕ_n	Phase angle of n^{th} sinusoid
μ_θ	Rotation ductility
μ_ϕ	Curvature ductility
$\Psi(t)$	Envelope function
σ_0	Root mean square acceleration
θ_{\max}	Maximum rotation
θ_y	Yield rotation
ϕ_1, ϕ_2, θ_1	ARMA parameters
δ_m	Maximum response under earthquake
δ_u	Ultimate deformation capacity under monotonic loading
δ_M	Dipasquale and Cakmak's maximum softening index
ω_g	Predominant ground natural frequency
ω_n	Frequency of n^{th} sinusoid
ξ_g	Effective damping coefficient of the ground
λ_{RMS}	Expected value of $\text{Ln}(\text{RMS})$

SECTION 1

INTRODUCTION AND LITERATURE SURVEY

1.1 Introduction

Earthquakes can have a seriously negative impact on society by causing human suffering and economic losses. Earthquakes affect structures in various ways which include damage to structural elements as well as nonstructural, architectural, electrical and mechanical elements. The main structural components affected are the components of the lateral load resisting system. Nonstructural components include the exterior curtain walls, interior partition walls and mechanical and electrical equipment. Nonstructural damage can occur even at low levels of ground shaking when there is little or no structural damage. This report is, however, confined to evaluating structural damage as a result of earthquakes.

Reliable damage estimation and rehabilitation decisions require sufficient information on the degree of structural damage. Relationships between earthquake ground motion severity and structural damage along with seismic site hazard analysis can be used to assess extensive damage, collapse casualties and subsequent long term economic losses due to earthquakes. The motion-damage relationships obtained in the form of probability distributions of damage at specified ground motion intensities are usually expressed by means of fragility curves and damage probability matrices. The fragility curves and damage probability matrices describe the conditional probabilities of reaching different damage states at specified ground motion levels. Currently available motion-damage relationships, for different types of buildings, are in the form of damage probability matrices (ATC-13, 1985). These matrices are based on expert opinion since actual damage data are not available to develop these functions empirically.

1.1.1 Objectives and Scope

The objective of this project is to develop a methodology for obtaining relationships between ground motion and structural damage to reinforced concrete structures. This involves the formulation of motion-damage relationships based on analytical models, in contrast to the currently available motion-damage relationships which are subjective in nature. This objective can be achieved through the following steps:

- Identification of suitable ground motion parameters;
- Identification of different damage states based on suitable structural response parameters;
- Evaluation of the probability of a concrete structure being in different damage states;

- Parametric study of the motion-damage relationships for different geometric and material property variations;

This study presents the development of motion-damage relationships for reinforced concrete moment resisting frames located on firm soils. Damage due to landslides and liquefaction is not considered. Only damage due to ground motion is included. The methodology presented in this report is illustrated by application to example buildings. Parametric studies are performed to assess the effect of geometric and material variations in the performance of concrete frame structures.

1.1.2 Organization of the Report

The remainder of this section presents a review of previous work on ground motion characterization and damage evaluation for reinforced concrete structures. The various parameters used to quantify ground motion are first reviewed. Various measures of structural damage are then described. Three different classes of reinforced concrete frames, based the story heights, are considered. The period range for each class of buildings is identified and is used to characterize the ground motion in terms of spectral response.

Section 2 presents the methodology for performing damage analysis. Various techniques available for damage analysis are reviewed and the method used in this study is explained in detail. Modified Mercalli intensity, MMI, root mean square acceleration, RMS, and spectral acceleration, S_a , are selected as the parameters to characterize the ground motion. The Park and Ang (1984) damage index and the modified version of this index (Kunnath et al., 1992) are selected to identify the different damage states.

Section 3 describes the modeling of uncertainties in system parameters. The uncertainties in structural demand and capacities are presented. The uncertainty associated with seismic demand is much larger compared to the uncertainties in other loads. Therefore, uncertainties in demand are taken into account by considering the uncertainties associated with the characterization of ground motion. The uncertainties in the ground motion are considered by incorporating the error associated with the Kanai-Tajimi parameters, dynamic amplification factors and the strong motion duration.

The Monte Carlo simulation technique used for evaluating the fragility curves and damage probability matrices is described in Section 4. The direct Monte Carlo technique requires a large

number of simulation cycles to achieve an acceptable level of confidence in the estimated probabilities. The Latin Hypercube sampling technique is used to reduce the number of simulation cycles. At a given ground motion level, an ensemble of ground motion time histories is required for evaluating the conditional probabilities. Due to the paucity of recorded ground motions for the same ground motion level, artificial ground motions are generated. Various techniques for the simulation of artificial ground motion are reviewed. Autoregressive moving average models (ARMA) and Gaussian stationary models with modulating functions are used for this purpose.

An illustration of the methodology is presented in Section 5. Damage analysis is performed for three example buildings. The example buildings include a two-story, a six-story and a thirteen story building corresponding to low-rise, mid-rise and high-rise buildings, respectively. The results of damage analysis are obtained in the form of damage probability matrices and fragility curves.

Section 6 summarizes the main conclusions from this project and discusses the scope of future work.

1.2 Review of Previous Work

Reliable damage estimation and rehabilitation decisions require information on the degree of structural damage. The motion-damage relationships are usually expressed by means of fragility curves and damage probability matrices. Fragility curves and damage probability matrices describe the conditional probability of being in a particular damage state at a given level of ground motion. Ground motion characterization and damage state identification are needed for evaluating these conditional probabilities.

Various ground motion parameters that can be correlated to structural damage are first reviewed. Then, the different indices available to describe structural damage to reinforced concrete structures are discussed. Damage state identification can be carried out based on the structural damage indices.

1.2.1 Ground Motion Characterization

It is difficult to determine a single parameter that best characterizes the ground motion. Recorded time histories, even at the same site, show variations in details. Earthquake ground motion amplitude, frequency content, duration and the number of peaks in the time history above a

certain amplitude are some of the characteristics important for determining structural response and damage. Ground motion amplitude is measured in terms of acceleration, velocity and displacement. Frequency content of an earthquake time history is important in identifying the amount of energy imparted at different frequencies. The strong motion duration of an earthquake time history is the time interval during which most of the energy of that time history is contained. Various measures of strong motion duration are presented in the next section.

Numerous parameters have been used to relate ground motion to the degree of damage sustained by a structure. Peak ground acceleration (PGA) has frequently been used as a parameter to characterize ground motion. Other parameters include Housner's spectral intensity, Arias intensity, root mean square acceleration (RMS), response spectrum and modified Mercalli intensity (MMI).

Root mean square acceleration, response spectrum and MMI are the parameters used to characterize ground motion in this study. Although only these three parameters are used in this study, other parameters are also discussed for the sake of completeness.

1.2.1.1 Strong Motion Duration

Several measures of strong-motion duration have been discussed in the literature. The different definitions of strong-motion duration include those by Bolt (1975), Trifunac and Brady (1975), McCann and Shah (1980), and Vanmarcke and Lai (1980). The Trifunac and Brady (1975) definition of strong motion duration is used in this study as it is based on the concept of cumulative energy. The Trifunac and Brady (1975) strong motion duration is the time interval required to accumulate 90 percent of the total energy.

The times T_1 and T_2 of Trifunac and Brady's definition of strong motion duration can be represented by means of the following two equations:

$$\int_0^{T_1} a^2(t) dt = 0.05 \int_0^{T_d} a^2(t) dt \tag{1.1}$$

and

$$\int_0^{T_2} a^2(t) dt = 0.95 \int_0^{T_d} a^2(t) dt \quad (1.2)$$

where:

T_d = total duration of the earthquake

$a(t)$ = ground acceleration at time t .

Trifunac and Brady's strong motion duration is thus given as:

$$T_s = T_2 - T_1 \quad (1.3)$$

The strong motion duration is needed for evaluating the root mean square acceleration (discussed in Section 1.2.1.5).

1.2.1.2 Ground Motion Amplitude

The parameters used to describe ground motion amplitude include peak ground acceleration, PGA, peak ground velocity, PGV, and peak ground displacement, PGD. As the inertia forces depend directly on acceleration, peak ground acceleration is one of the parameters widely used to describe the intensity and damage potential of an earthquake at a given site. However, PGA is a poor indicator of damage as time histories with the same PGA could be very different in frequency content, strong motion duration and energy level, thus causing varying amounts of damage. Therefore, PGA represents only a single amplitude and does not incorporate any of the other characteristics considered to be important for damage evaluation.

1.2.1.3 Housner's Spectral Intensity

Housner (1952) defined a measure for expressing the relative severity of earthquakes in terms of the area under the pseudo-velocity spectrum between 0.1 and 2.5 seconds. Housner's spectral intensity can be defined by means of the following equation:

$$I_H = \int_{0.1}^{2.5} S_v(T, \xi) dT = \frac{1}{2\pi} \int_{0.1}^{2.5} S_a(T, \xi) T dT \quad (1.4)$$

where:

$S_v(T, \xi)$ = pseudo-velocity at undamped natural period T and damping ratio ξ

$S_a(T, \xi)$ = pseudo-acceleration at undamped natural period T and damping ratio ξ .

Housner's spectral intensity is thus the first moment of the area of S_a ($0.1 \leq T \leq 2.5$ sec) about the S_a axis. This implies that the Housner spectral intensity is larger for ground motions with a significant amount of low frequency content. Thus, ground motions with larger Housner spectral intensity could cause more damage to tall structures. Housner's spectral intensity, however, does not provide information on the strong motion duration.

1.2.1.4 Arias Intensity

Arias (1970) defined the intensity, I , of an earthquake as the sum of the energy dissipated (per unit weight) by all the structures belonging to the entire population. Thus

$$I = \int_0^{\infty} E \, d\omega \quad (1.5)$$

where:

E = energy dissipated per unit weight of a structure as a consequence of the motion induced on it by an earthquake

ω = frequency of the structure

Using Parsevaal's theorem, equation 1.5 can be written as:

$$I = \frac{\pi}{2g} \int_0^{T_d} a^2(t) \, dt \quad (1.6)$$

where:

I = intensity at zero damping

$a(t)$ = ground acceleration at time t

T_d = total duration of earthquake motion

g = acceleration due to gravity

As can be seen from the definition, Arias intensity provides an estimate of the total energy of an earthquake. However, Arias intensity does not incorporate any information on the frequency content and strong motion duration of the earthquake.

1.2.1.5 Root Mean Square Acceleration

The root mean square acceleration (RMS) is a parameter incorporating the total intensity and the strong-motion duration. RMS is defined as

$$\sigma_0 = \left[\frac{1}{T_s} \int_{T_s} a^2(t) dt \right]^{\frac{1}{2}} \quad (1.7)$$

where:

- σ_0 = RMS of strong-motion acceleration
- T_s = strong-motion duration
- $a(t)$ = ground motion acceleration at time t .

Root mean square acceleration is a measure of the average rate of energy input to the structure. However, RMS does not provide any information about the frequency content as it is the sum of input power at all frequencies.

1.2.1.6 Response Spectrum

The linear elastic response spectrum represents the maximum acceleration, maximum relative velocity or maximum relative displacement of a single-degree-of-freedom (SDOF) system subjected to a particular ground motion. The spectral acceleration provides an estimate of the maximum elastic force that can be developed in an elastic SDOF system. The lower bound of the maximum energy input to an elastic SDOF system can be estimated from the spectral velocity as follows:

$$E = \frac{1}{2} M S_v^2(T, \xi) \quad (1.8)$$

where:

- E = maximum input energy
- M = mass of the SDOF system
- S_v = spectral velocity ordinate at the natural period of the SDOF system
- ξ = damping ratio of the SDOF system

In this study, the average spectral acceleration in three period bands is used to characterize the ground motion for the three classes of reinforced concrete frames. The period ranges for different reinforced concrete frame structures are defined as follows:

- (a) $0.1 \leq T \leq 0.45$ sec for low-rise (1-3 stories)
- (b) $0.45 < T \leq 0.85$ sec for mid-rise (4-7 stories)
- (c) $0.85 < T \leq 2.5$ sec for high-rise (>7 stories)

1.2.1.7 Modified Mercalli Intensity

Modified Mercalli intensity (MMI) is based largely on the performance of unreinforced masonry buildings, chimneys and some other older construction. The MMI scale is often used to specify the severity of ground shaking in a given geographic region. It is also used to describe the distribution of damage over a region. The main advantage of the MMI scale is that it has been in use for a long time and is familiar to earthquake practitioners. However, its use is subjective and differences in interpretation are substantial.

1.2.2 Measures of Structural Damage

There are many damage models which characterize the state of reinforced concrete structures after earthquakes. The structural damage in reinforced concrete is frequently represented by means of various local and global damage indices. These damage indices usually employ the concepts of ductility and dissipated energy. Most of the definitions consider damage to individual elements and are based on some form of ductility ratio or dissipated energy. Bannon et al. (1981) provide the definition for normalized dissipated energy and review the definitions of rotation and curvature ductility. The rotation ductility, μ_θ , is the ratio of the maximum rotation, θ_{max} , to the rotation at yielding, θ_y . The rotation ductility is expressed as follows:

$$\mu_\theta = \frac{\theta_{max}}{\theta_y} \quad (1.9)$$

Curvature ductility μ_ϕ is defined in a similar way except that rotation, θ , is replaced by curvature, ϕ . This relationship can be expressed as follows:

$$\mu_\phi = \frac{\phi_{max}}{\phi_y} \quad (1.10)$$

The normalized dissipated energy, E_n , is the ratio of the energy dissipated by inelastic rotation at one end of the member to half of the maximum elastic energy stored in the member in anti-symmetric bending. The normalized dissipated energy is thus given by the following equation:

$$E_n(t) = \frac{\int_0^t M(\tau)\theta d(\tau)}{\frac{1}{2}M_y\theta_y} \quad (1.11)$$

where:

t = time elapsed since the beginning of loading

$\theta(d\tau)$ = the rotation increment of the inelastic spring at one end of the member during the time interval between τ and $\tau + d\tau$

1.2.2.1 Local Damage Indices

These indices are used to express the damage sustained by individual elements. Most of the damage models first consider the damage to individual structural elements. Global damage is then defined as a combination of the damage to individual elements. Two of the definitions of local damage which are more widely used for reinforced concrete elements are those proposed by Park and Ang (1984) and by Chung, Meyer and Shinozuka (1987). Kunnath et al., (1992) have proposed a modified version of the Park-Ang (1984) damage index which is discussed in Section 2.2.1. The Park-Ang (1984) and the Chung, Meyer and Shinozuka (1987) damage indices are discussed in the following two sections.

Park and Ang's Local Damage Index

Park and Ang (1984) proposed a damage index which is a linear combination of the damage caused by excessive deformation and that contributed by repeated cyclic loading effect. The Park and Ang damage index is expressed as follows:

$$D = \frac{\delta_m}{\delta_u} + \frac{\beta}{P_y\delta_u} \int dE \quad (1.12)$$

or

$$D = \frac{\delta_m}{\delta_u} + \beta \int \left(\frac{\delta}{\delta_u} \right)^\alpha \frac{dE}{E_c(\delta)} \quad (1.13)$$

where:

- δ_m = maximum response deformation under an earthquake
- δ_u = ultimate deformation capacity under monotonic loading
- P_y = calculated yield strength
- $E_c(\delta)$ = hysteretic energy per cycle at deformation δ
- α, β = non-negative parameters
- δ = amplitude of deformation in each cycle of oscillation
- dE = incremental dissipated hysteretic energy

The first term in the expression for the damage index (equations 1.12 and 1.13) represents the damage due to maximum deformation experienced during seismic loading, and the second term represents the damage due to cumulative hysteretic energy dissipation. The load deformation terms are shown in figure 1-1, where $\delta_{p1}, \delta_{p2}, \dots, \delta_{pn}$ represent the deformation in each cycle. The parameter δ_m is the maximum of $\delta_{p1}, \delta_{p2}, \dots, \delta_{pn}$ for all the cycles. The deformation at yield under monotonic loading is represented by δ_y . The damage index, D , is zero when there is no damage and is 1.0 for collapse.

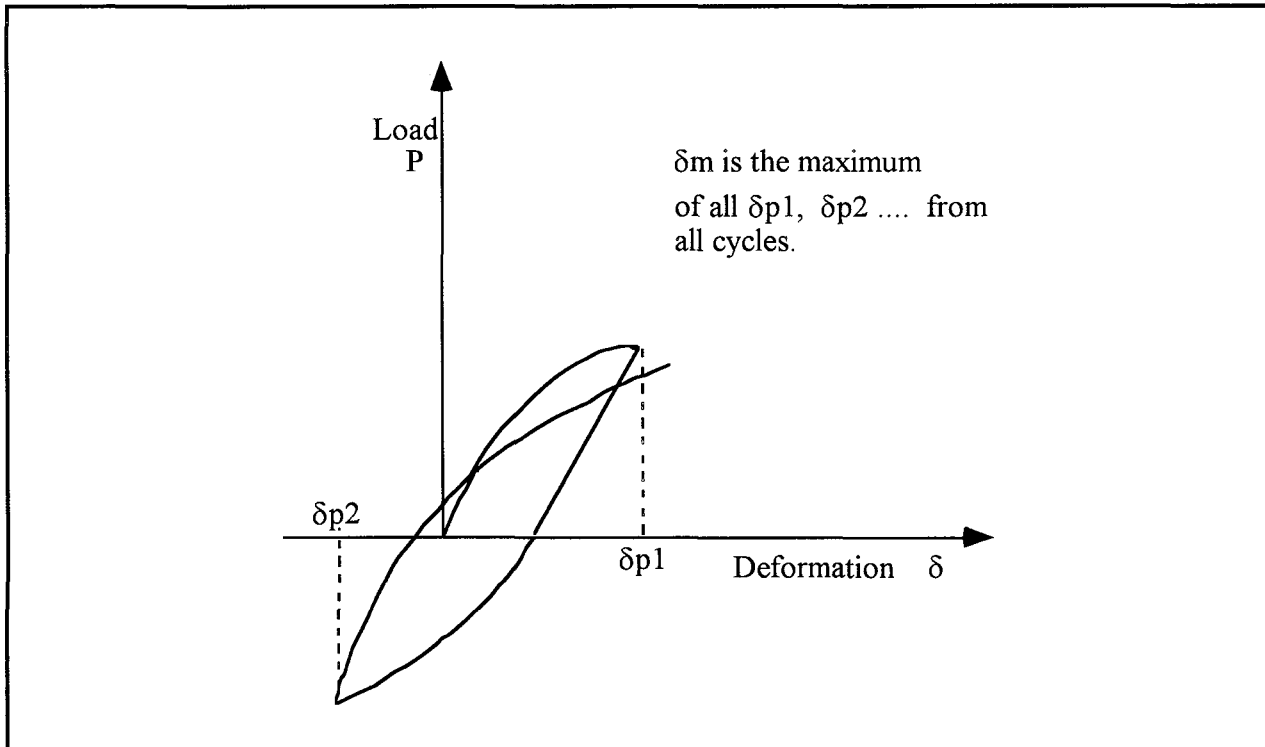


FIGURE 1-1 Definition of δ_m in the Park and Ang (1984) index

The ultimate deformation capacity of a member under monotonic loading, δ_u , is an indicator of the ductility capacity of a member. Reinforced concrete members with about the same level of yield deformation and about the same axial load can have different ultimate deformation values depending on the confinement ratios. The ultimate deformation appears to be more important than the yield deformation in predicting damage.

Chung, Meyer and Shinozuka's Local Damage Index

Chung, Meyer and Shinozuka (1987) proposed a damage index which combines a modified version of Miner's Hypothesis with damage modifiers that reflect the effect of the loading history. This index considers the difference in response of members to positive and negative moments and is evaluated by the following expression:

$$D_e = \sum_i \left(\alpha_i^+ \frac{n_i^+}{N_i^+} + \alpha_i^- \frac{n_i^-}{N_i^-} \right) \quad (1.14)$$

where:

i = indicator of displacement or curvature level

N_i = $\frac{M_i - M_{fi}}{\Delta M_i}$ = number of cycles to cause failure at curvature level i

n_i = number of cycles actually applied at curvature level i

α_i = damage modifier

+, - = loading and unloading respectively

The terms M_i , M_{fi} and ΔM_i are defined in figure 1-2.

The effect of loading history is taken into account by damage modifier, α_i , which for positive moment loading is defined as:

$$\alpha_i^+ = \frac{\sum k_{ij}^+}{n_i^+ k_i^+} \cdot \frac{\phi_i^+ + \phi_{i-1}^+}{2\phi_i^+} \quad (1.15)$$

where:

k_{ij}^+ = $\frac{M_{ij}^+}{\phi_i^+}$ = stiffness during the j^{th} cycle up to load level i

$$\bar{k}_i^+ = \frac{1}{N_i^+} \sum_{j=1}^{N_i^+} k_{ij}^+ = \text{average stiffness during } N_i^+ \text{ cycles up to load level } i$$

$$M_{ij}^+ = M_{i1}^+ - (j-1)\Delta M_i^+ = \text{moment reached after } j \text{ cycles up to load level } i.$$

For negative loading, the damage modifier is defined similarly.

The damage index definition by Chung et al. does not explicitly account for the damage caused by the maximum deformation experienced by the element.

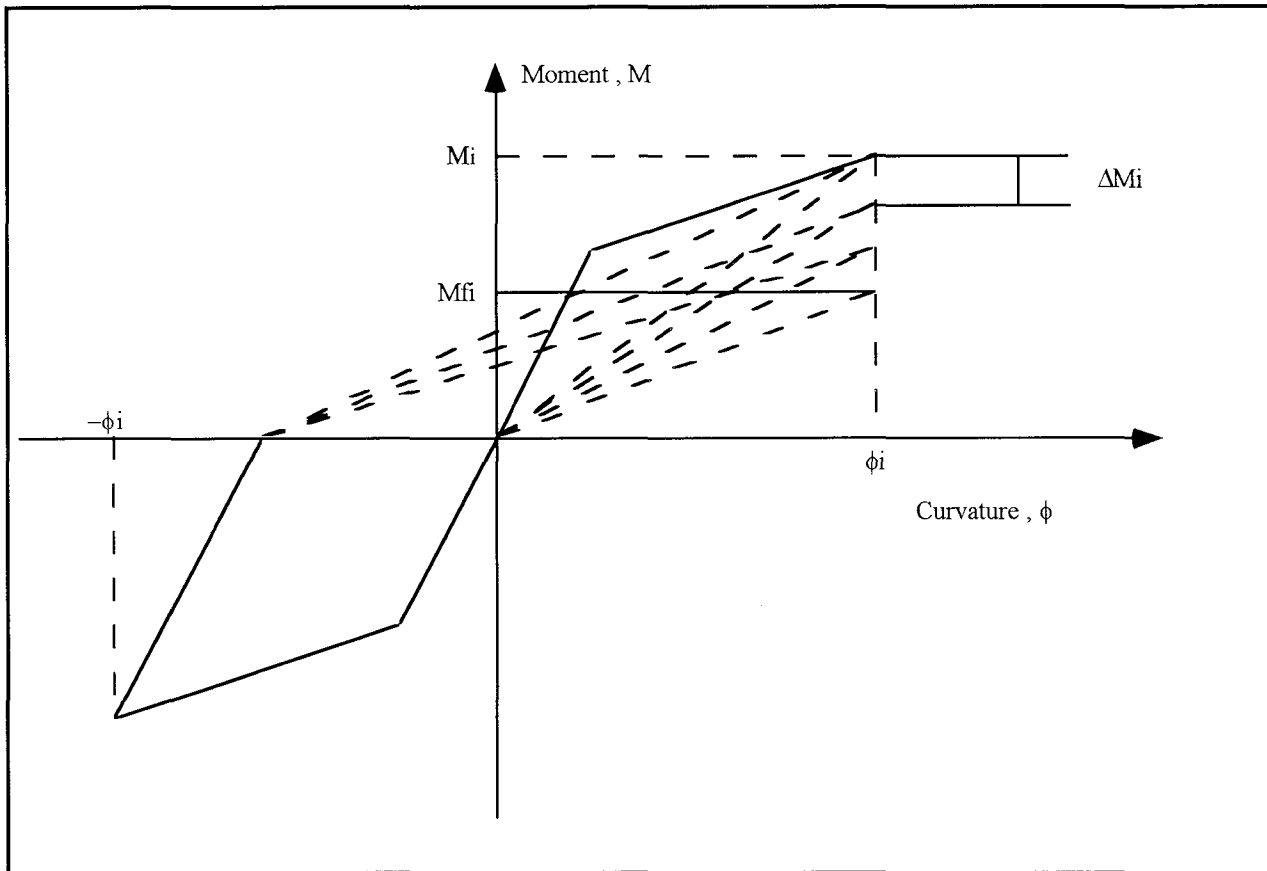


FIGURE 1-2 Damage index definitions by Chung et al. (1987)

1.2.2.2 Global Damage Indices

Global damage indices provide information about the damage to the overall structure. When a structure is statically determinate, local damage at the most damaged member is enough to determine the damage state of the entire structure. However, a global damage index is required for redundant structures. The different types of global damage indices are described in the following sections.

Park and Ang's Global Damage Index

Park and Ang's (1984) and the modified Park-Ang (Kunnath et al, 1992) global damage indices are defined as a weighted average of the local damage indices of each element. The weighting function for each element is proportional to the energy dissipated in the element. The global damage index is thus given by the following equation:

$$\mathbf{D}_T = \sum_{i=1}^N \lambda_i \mathbf{D}_i \quad (1.16)$$

where:

$$\lambda_i = \frac{E_i}{\sum_{i=1}^N E_i}$$

N = number of elements

E_i = energy dissipated in element i

In addition to the overall damage index, story-level damage indices can also be obtained. The story-level damage indices can be used to identify the story with the highest damage.

The global damage index, as defined by equation 1.16, does not properly account for the local concentration of damage. It is possible for a few structural members of the building to have undergone severe damage without the global index reflecting it.

Chung, Meyer and Shinozuka's Global Damage Index

Chung et al. (1987) used the damage index from each story to define the global damage index. The story damage index is obtained as a weighted average of the local damage indices of all elements in the story, with the energy dissipated in the member as the weighting function. The story damage index is obtained by the following equation:

$$\mathbf{D}_{s_k} = \frac{\sum_{i=1}^n \mathbf{D}_i^k \mathbf{E}_i^k}{\sum_{i=1}^n \mathbf{E}_i^k} \quad (1.17)$$

where:

- D_i^k = local damage at location i on story k
- E_i^k = energy dissipated at location i on story k
- n = number of locations at which the local damage is computed for story k.

This definition of the story damage index is similar to the definition of the Park and Ang global damage index provided by equation 1.16. However, the local damage indices D_i and D_i^k in equations 1.16 and 1.17 are different and are evaluated using equations 1.12 and 1.14 respectively.

The global damage index is obtained as weighted average of the story damage indices using a triangular weighting function with the maximum at the base. Thus, the global damage index is given by the following equation:

$$D_g = \sum_{k=1}^N D_{s_k} I_k \quad (1.18)$$

where:

$$I_k = \frac{N+1-k}{N} = \text{weighting factor for story } k$$

N = number of stories

DiPasquale and Cakmak's Damage Index

DiPasquale and Cakmak (1990) proposed a damage index which is based on the predominant period of the structure. This damage index does not require the averaging of the local damage indices. Their index, named *Maximum Softening* index is given by the following equation:

$$\delta_M = 1 - \frac{T_0}{T_{max}} \quad (1.19)$$

where:

T_0 = initial natural period

T_{max} = maximum natural period of an equivalent linear system

The Maximum Softening index depends on a combined effect of stiffness degradation and plastic deformations. For computing the Maximum Softening index, the response of the structure to

input ground motion must be known. Thus, it is necessary to specify the ground acceleration time history and the structural response at various locations of the structure.

The computation of the Maximum Softening index does not explicitly account for the dissipated hysteretic energy and strength degradation. Also, the Maximum Softening index does not provide information about the extent of local damage sustained by different members.

In this study, the Park and Ang damage index is adopted to represent the structural damage. The ground motion is chosen to be characterized by root mean square acceleration, spectral acceleration and modified Mercalli intensity. Work is currently under way at Princeton University to obtain the fragility curves using the Maximum Softening index.

SECTION 2

METHODOLOGY FOR DAMAGE ANALYSIS

This section presents the methodology for the development of motion-damage relationships for reinforced concrete frame structures. Currently available motion-damage relationships are in the form of damage probability matrices (ATC-13, 1985). These matrices are based on expert opinion since actual damage data are not available to develop them empirically. In this study, a method for developing motion-damage relationships based on mechanistic models that relate loading to structural damage is formulated. The motion-damage relationships are represented as damage probability matrices and fragility curves.

The fragility curves and damage probability matrices describe the conditional probabilities of being in different damage states at specified levels of ground motion. A fragility curve for a particular damage state is obtained by computing the conditional probabilities of being in that damage state at various levels of ground motion. A plot of the computed conditional probabilities versus the ground motion parameter gives the fragility curve for that damage state. The conditional probabilities are given as follows:

$$p_{ik} = P[\mathbf{D} = \mathbf{d}_i \mid \mathbf{Y} = \mathbf{y}_k] \quad (2.1)$$

where:

p_{ik} = probability of being in damage state d_i given the ground motion is y_k

\mathbf{D} = damage random variable defined on the damage state vector $\mathbf{D} = \{d_0, d_1, \dots, d_n\}$

\mathbf{Y} = ground motion random variable

The identification of the different damage states based on structural response parameters will be discussed in Section 2.1. Three ground motion parameters will be used to characterize the variable \mathbf{Y} . These are the root mean square acceleration, RMS, spectral acceleration, S_a , and the modified Mercalli intensity, MMI. The motivation for selecting these parameters was discussed in Section 1.

An alternate representation of fragilities is given by the probabilities of reaching or exceeding a specified damage state given a ground motion level. This definition of fragility can be evaluated as follows:

$$P_{ik} = P[D \geq d_i | Y = y_k] = \sum_{j=i}^n P_{jk} \quad (2.2)$$

The overall methodology for the development of fragility curves and damage probability matrices is presented in figure 2-1. The various models for incorporating the uncertainties in structural parameters and imposed loads first need to be identified. In this study, the compressive strength of concrete and the yield strength of steel are the only parameters treated as the random variables affecting the capacity of a structure. The uncertainty associated with dead and live loads is considerably smaller compared to the uncertainty in seismic load. In this study, only the earthquake load represented through ground motion is modeled as a stochastic Gaussian process. The ground motion is assumed to have Kanai-Tajimi (Tajimi, 1960) power spectral density when generating ground motions corresponding to a particular RMS. When generating time histories for a particular value of spectral acceleration, the dynamic amplification factors are used to obtain an ensemble of response spectra corresponding to the given average spectral acceleration. Earthquake time histories are then generated corresponding to these response spectra. A detailed treatment of the uncertainty in system parameters is presented in Section 3.

The fragility formulations defined in equations 2.1 and 2.2 are determined by Monte Carlo simulation. A large number of simulation cycles are needed to achieve an acceptable level of confidence in the estimated probabilities. The Latin Hypercube sampling technique is used to reduce the number of simulation cycles. A detailed description of the Monte Carlo simulation technique is presented in Section 4.

Artificial ground motions are generated to obtain an ensemble of time histories for the development of the fragility curves and damage probability matrices. Various techniques for the generation of artificial time histories are presented in Section 4. Autoregressive moving average (ARMA) models are used for the generation of artificial time histories when the ground motion is characterized by root mean square acceleration. Gaussian stationary models with modulating functions are used for the generation of time histories when spectral acceleration is used to characterize the ground motion. Damage analysis is carried out for each generated time history.

Nonlinear dynamic analysis is then carried out to obtain the sample statistics for the ensemble of structural response parameters. Nonlinear dynamic analysis is carried out for each generated time history. Thus, for an ensemble of artificial time histories, the mean and variance of the structural

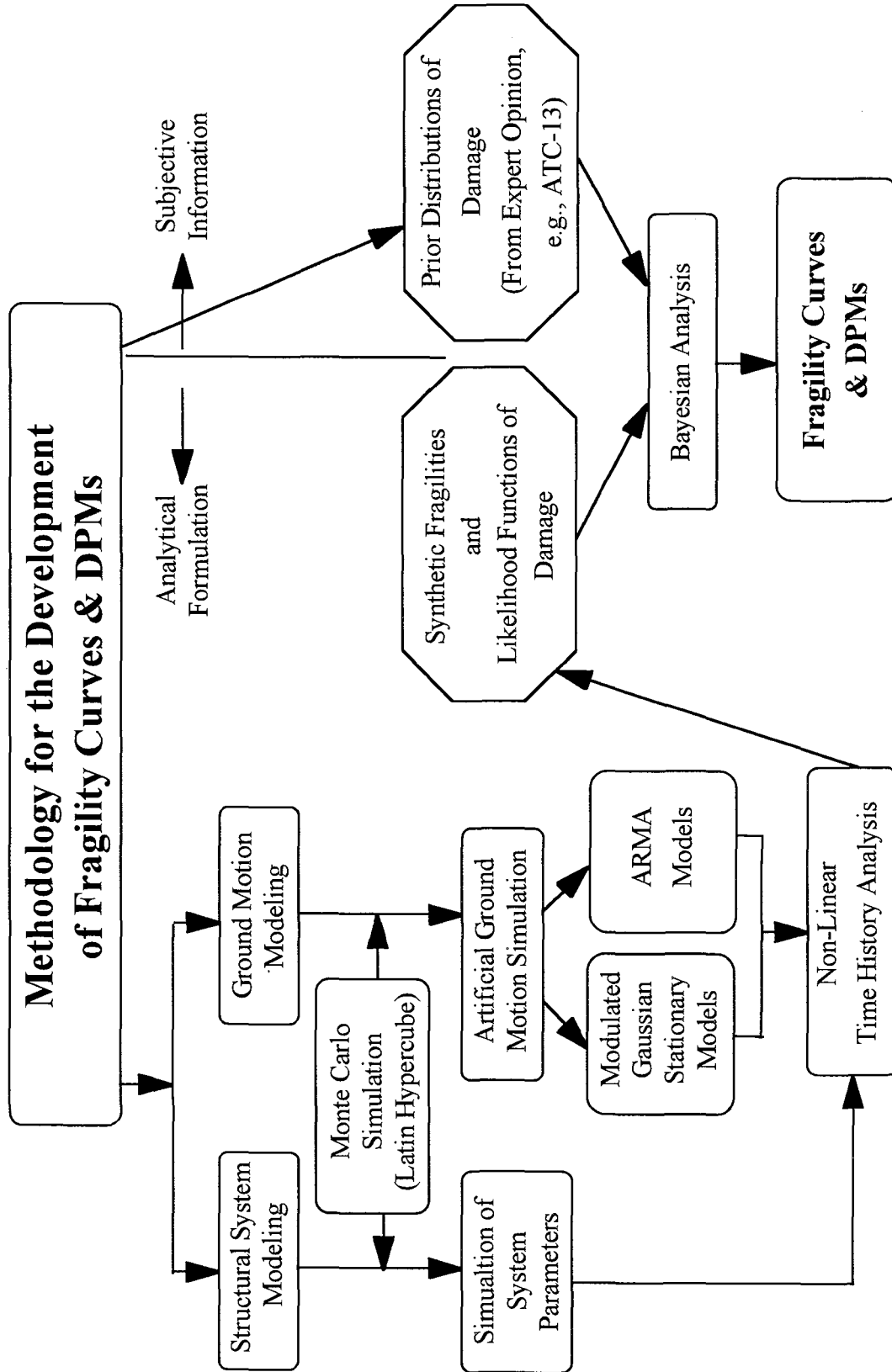


FIGURE 2-1 Steps in the development of fragility curves and damage probability matrices

response parameters are computed. These statistics are used for computing the probabilities of the different damage states at a given ground motion level. The structural response parameters that can be used include the damage measures discussed in Section 1. In addition, response measures like interstory drift ratio and crack width are being investigated. The different response measures for identifying the damage states are discussed in Section 2.1.

A Bayesian approach can be used to update the parameters of the probability distributions of damage. The analytical fragility curve parameters can be used to model the likelihood function for damage states. The parameters of the prior probability distributions can be obtained from subjective information such as that provided in ATC-13 (1985). The likelihood functions and prior distributions can be combined to obtain the posterior distributions of damage. The Bayesian formulation of fragility curves will be fully developed in a subsequent study.

2.1 Identification of Damage States

The analytical development of fragility curves and damage probability matrices requires the identification of different damage states based on the structural response parameters. It should be possible to relate the different damage to the dollar-loss ratio expressed as proportion of replacement value required to repair the building. The dollar-loss ratio can be used to estimate the economic loss due to earthquakes. Various studies have been carried out to relate the different measures of structural damage discussed in Section 1 to different damage states (Park et al., 1987, Hatamoto et al., 1990, Gunturi, 1992, and Nielsen et al., 1992). However, these studies do not provide any relationship between the dollar-loss ratio and the different damage states. In this study, the identification of the different damage states is carried out based on the Park-Ang (1984) and the modified (Kunnath et al., 1992) damage indices. Studies are currently under way to identify damage states based on some other response measures which can be related to the dollar-loss ratio.

2.1.1 Damage States Based on Structural Damage Indices

The different damage states of a building can be identified based on the global damage indices of the overall structure discussed as in Section 1. Park et al. (1987) provide the ranges of the Park and Ang (1984) global damage index for three different damage states: *Moderate*, *Severe* and *Collapse*. These ranges are shown in table 2-I. Hatamoto et al. (1990) define four damage states based on the Chung, Meyer and Shinozuka (1987) damage index. The four damage states that

they consider are: *Minor*, *Repairable*, *Irrepairable* and *Unsafe*. The ranges of the damage index for these four damage states are presented in table 2-II.

Gunturi (1992) reviews the ranges of the Park and Ang (1984) global damage index for four different damage states. The four damage states that are considered are: *Minor*, *Repairable*, *Irrepairable* and *Collapse*. The ranges of the Park and Ang damage index for different damage states are presented in table 2-III. Nielsen et al. (1992) provide the conditional probabilities of different damage states given the Dipeasquale and Cakmak (1987) *Maximum Softening* index. In this study, *Minor* damage is assumed to have a range of Park and Ang (1984) damage index from 0.1 to 0.2. The other damage states have the ranges as suggested by Gunturi.

TABLE 2-I Park and Ang's (1984) damage index for different damage states as defined by Park et al. (1987)

Damage State	Range of the Park and Ang (1984) index
Moderate	< 0.4
Severe	0.4 - 1.0
Collapse	> 1.0

TABLE 2-II Chung, Meyer and Shinozuka's (1987) damage index for different damage states as defined by Hatamoto et al. (1990)

Damage State	Range of the damage index
Minor	0.0 - 0.2
Repairable	0.2 - 0.5
Irrepairable	0.5 - 1.0
Structure Unsafe	≥ 1.0

TABLE 2-III Park and Ang's (1984) damage index for different damage states as defined by Gunturi (1992)

Damage State	Range of the Park and Ang (1984) index
Minor	0.0 - 0.2
Repairable	0.2 - 0.4
Irrepairable	0.4 - 1.0
Collapse	> 1.0

The Park-Ang damage index as expressed by equations 1.12 and 2.5 represents a linear combination of damage due to maximum deformation and dissipated hysteretic energy. In the course of developing the fragility curves, it was found that the dissipated hysteretic energy portion of the index is captured by the interstory drift. This aspect is illustrated in Section 5.

2.1.2 Proposed Damage States Based on Crack Widths and Interstory Drift

Four damage states are considered to describe the damage to reinforced concrete frame structures. These are *Minor*, *Moderate*, *Severe* and *Collapse*. The method for the identification of the *Minor* and *Moderate* damage states currently investigated by the authors is based on crack width in the elements. The interstory drift ratio can be used for the identification of the *Severe* and *Collapse* damage states. The *Minor* and *Moderate* damage states based on crack widths can then be directly related to the dollar-loss ratio. The dollar-loss ratio for the *Collapse* damage state has to equal unity.

Various techniques for estimating crack width in concrete members are available. Some are based on empirical relationships (e.g., Gergely and Lutz, 1968) while others (e.g., Bazant and Oh, 1983a and 1983b) are based on analytical formulations using the concept of fracture energy. The prediction of crack width based on the formulation presented by Oh and Kang (1987) is currently being investigated.

The formulas for the prediction of crack width proposed by Oh and Kang are based on the cracking theory developed by Bazant and Oh (1983). Tests on reinforced concrete beams were also carried out by Oh and Kang to check the validity of the proposed formulas. The equation that gives the best prediction of the maximum crack width in a member is given as:

$$\frac{w_{\max}}{d} = a_0(\varepsilon_s - 0.0002) R \quad (2.3)$$

where:

- w_{\max} = maximum crack width
- d = diameter of reinforcing bar
- ε_s = strain in tensile reinforcement
- R = h_2/h_3

$$a_0 = 159 \left(\frac{t_b}{h_2} \right)^{4.5} + 2.83 \left(\frac{A_1}{A_{s1}} \right)^{1/3}$$

A_1 = effective area of concrete surrounding one reinforcing bar

A_{s1} = average area of one tensile reinforcing bar

t_b = concrete cover for tensile reinforcement

h_2 = distance from extreme tension fiber to the neutral axis

h_3 = distance from the centroid of steel to the neutral axis

The effect on dynamic loading on the crack widths will be investigated next. Beshara (1993) provides a relationship between the dynamic cracking strain and the static cracking strain as a function of effective strain rate. In general, the crack widths can be computed based on the residual strain in the member after dynamic analysis.

In the Manual for Repair Methods of Civil Engineering Structures Damaged by Earthquakes (1987), it is suggested that cracks with widths in the range of 0.5 mm - 0.8 mm can be repaired with epoxy injection. It is also suggested in that manual that cracks with widths greater than 0.8 mm require V-cut before repair. Thus, if the maximum crack width anywhere in the structure is in the range 0.5 mm - 0.8 mm, it can be said to be in *Minor* damage state. This definition of Minor damage state implies that the damage can be repaired by epoxy injection. A crack width larger than 0.8 mm can be defined to be the lower bound of the *Moderate* damage state.

The identification of upper and lower bounds of *Severe* and *Collapse* damage states and upper bound of the *Moderate* damage state can be carried out based on the interstory drift ratio. Shahrooz and Moehle (1990) use the drift limit suggested in ATC 3-06 (1978) for comparing the results obtained for their test structure. ATC 3-06 suggests that interstory ratio of 0.015 would probably cause extensive nonstructural damage but ductile concrete elements might be expected to be damaged but structurally intact. Ogawa, Elms and Paulay (1988) suggest an interstory drift ratio of 0.025 for collapse. These bounds on the interstory drift ratios can be used for identifying the upper and lower bounds of *Severe* and *Collapse* damage states, and the upper bound on the *Moderate* damage state. The effectiveness of the interstory drift ratio as a response measure for identifying the damage states for high-rise structures still needs to be investigated. For high-rise structures, interstory drift may also be due to cumulative rotations of elements in lower stories than due to the deformation of the elements in that particular story. The bounds of crack widths and interstory drift ratios are summarized in table 2-IV.

**TABLE 2-IV Definitions of damage states based on maximum crack width
and maximum interstory drift ratio**

Damage State	Range of the response parameter
Minor	$0.5 \text{ mm} \leq \text{max. crack width} \leq 0.8 \text{ mm}$
Moderate	$0.8 \text{ mm} \leq \text{max. crack width}$ $\text{max. interstory drift ratio} \leq 0.015$
Severe	$0.015 \leq \text{max. interstory drift ratio} \leq 0.025$
Collapse	$0.025 \leq \text{max. interstory drift ratio}$

2.2 Damage Analysis

Several computer programs are available for performing nonlinear dynamic analysis of reinforced concrete structures. These include IDARC2D (Park et al., 1987, Kunnath and Reinhorn, 1994) and DRAIN-2DX (Prakash and Powell, 1992). These programs are currently limited to the analysis of two dimensional structural systems. DRAIN-2DX considers only the development of concentrated plasticity at the ends of an element, whereas, IDARC2D is capable of incorporating distributed plasticity. In this study, the program IDARC2D is used to perform inelastic dynamic analysis. This program also provides the original (1984) or the modified (Kunnath et al., 1992) Park-Ang damage indices at the member level and also for the overall structure. Computer programs for nonlinear, three dimensional analysis of structural systems are being developed (e.g., DRAIN3D, IDARC3D), but were not available in time for use in this study.

2.2.1 Structural Modeling in IDARC2D

In the computer program, IDARC2D, a building is idealized as a series of plane frames linked together by transverse beams and rigid links. As only plane frame analysis is performed, the torsional moment arising due to the eccentricity between the center of mass and the center of rigidity is ignored.

A frame is modeled using beam, column and transverse beam elements. Beams and columns are modeled as continuous equivalent shear-flexure springs. Transverse elements are assumed to influence the vertical and rotational deformation of the main beams to which they are attached. Transverse elements are modeled using elastic linear and rotational springs. The axial deformation in the columns is considered but its interaction with bending moment is not included.

IDARC2D (Park et al., 1987, Kunnath and Reinhorn, 1994) uses a three parameter (α , β and γ) model to describe the hysteretic behavior of the structural components. These parameters determine the stiffness degradation (α), strength deterioration (β) and pinching (γ) for a reinforced concrete component. Stiffness degradation is taken into account by setting a point on the extrapolated initial stiffness line and assuming that unloading lines target this point until they reach the x-axis after which the previous maximum and minimum points are aimed. The location of the point depends on the yield strength of the element and the parameter α (figure 2-2).

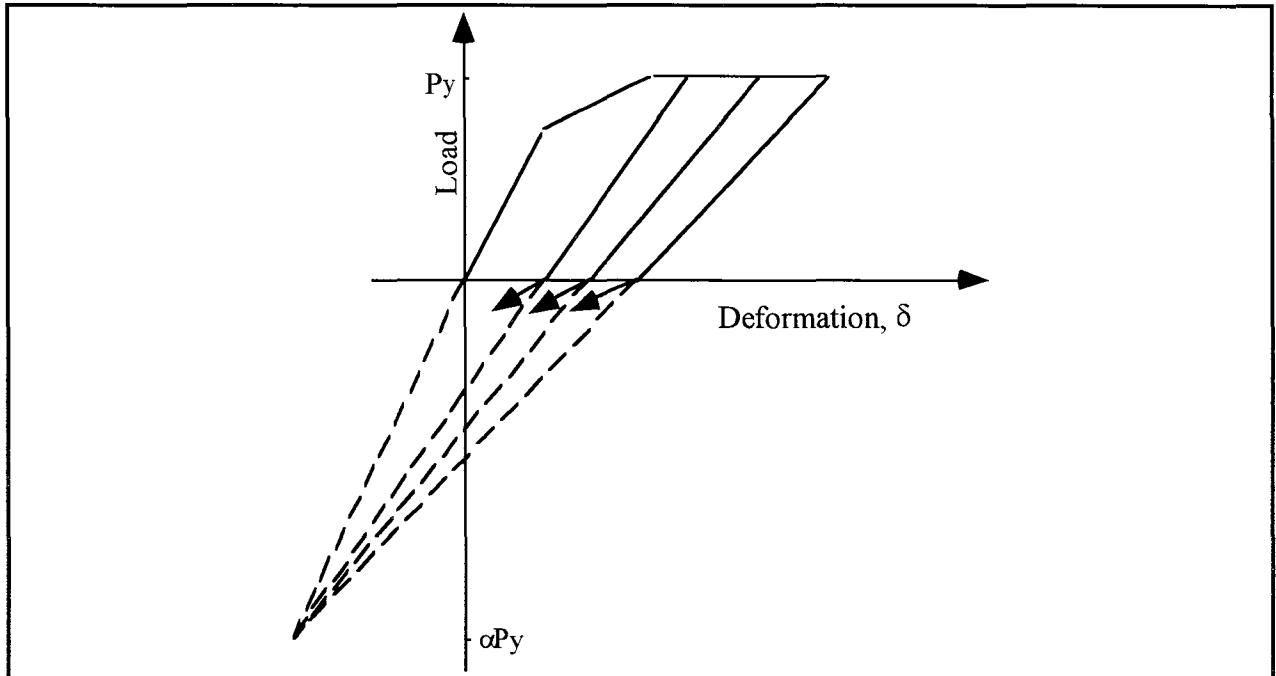


FIGURE 2-2 Stiffness degradation in the hysteretic loop

The rate of strength degradation is specified by the parameter β defined as the ratio of the incremental damage caused by the increase of the maximum response to the normalized incremental hysteretic energy, dE . Thus β is defined by the following equation:

$$\beta = \frac{d\delta_m}{\delta_u} \div \frac{dE}{\delta_u P_y} = \frac{d\delta_m P_y}{dE} \quad (2.4)$$

where:

$d\delta_m$ = incremental maximum response displacement

The remaining symbols represent the same quantities as in equations 1.12 and 1.13

The modified Takeda's hysteretic model is used in this study. The parameters of the modified Takeda's model are $\alpha = 2.0$, $\beta = 0.1$ and γ is equal to infinity (no pinching).

IDARC2D (Kunnath and Reinhorn, 1994) uses a modified version of the original Park and Ang (1984) damage index defined by equations 1.12 and 1.13. The modified form of the damage index (Kunnath et al., 1992) is expressed by the following equation:

$$D = \frac{\theta_m - \theta_r}{\theta_u - \theta_r} + \frac{\beta}{M_y \theta_u} E_T \quad (2.5)$$

where:

θ_m = maximum rotation attained during load history

θ_u = ultimate rotation capacity of section

θ_r = recoverable rotation at unloading

β = strength degrading parameter

M_y = yield moment of section

E_T = dissipated hysteretic energy

The global damage indices are computed using weighting factors based on dissipated hysteretic energy as defined in equation 1.16. It is assumed that the ranges of the modified Park and Ang damage index for the different damage states are the same as those of the Park and Ang (1984) damage index defined in Section 2.1.1.

SECTION 3

MODELING PARAMETER RELATIONSHIPS AND RANDOMNESS

This section presents the various models for incorporating the uncertainties in structural capacities and demands. Structural capacities and demands can be characterized by a number of parameters which have an important effect on the response statistics and the overall reliability of the system. In this study, the uncertainties associated with the structural capacities and the demands on the structure are treated independently. The modeling of these uncertainties is presented in the following sections. In addition, the relationship between modified Mercalli intensity (MMI) and spectral acceleration (S_a) is investigated. Such a relationship will be needed in order to combine the heuristic damage probability matrices of ATC-13 (1985), for example, with the analytical fragility curves developed in this study.

3.1 Modeling of Uncertainties in Structural Capacity

The different parameters which affect the capacity of a structure include the compressive strength of concrete, the yield strength of reinforcing steel, the hysteretic behavior, the damping ratio, the physical dimensions of the different components and the amount of reinforcing steel. In this study, it is assumed that there is good quality control during construction so that the uncertainty associated with the physical dimensions of the different structural components and the amount of reinforcing steel is very small. The effect of the uncertainty in the hysteretic behavior will be incorporated by considering different hysteretic models in a subsequent study. In this study, the compressive strength of concrete and the yield strength of steel are the only parameters treated as the random variables affecting the capacity of a structure. Uncertainties associated with other parameters such as the placement of reinforcing steel and the compaction of concrete are not considered explicitly. These uncertainties arise due to construction errors. The treatment of construction errors is being investigated at present.

The probability distributions for the concrete and steel strengths suggested by Galambos et al. (1982) are used in this study. They suggest a normal probability distribution for the concrete strength and a lognormal probability distribution for steel strength. Concrete strength is estimated to have a mean of 1.14 times the nominal concrete strength and a coefficient of variation of 0.14. The mean strength of steel is taken to be 1.05 times the nominal strength with a coefficient of variation of 0.11. For the example buildings considered in this study, the nominal strength of steel is 60 ksi. The nominal concrete strength is 4000 psi for the two-story example building, 5000 psi for the six-story building, and 3750 psi for the thirteen story building.

3.2 Modeling of Uncertainties in Demand Parameters

The uncertainty associated with dead and live loads is considerably smaller compared to the uncertainty in seismic load. In this study, only the earthquake load and consequently the ground motion is modeled as a stochastic Gaussian process. The ground motion is assumed to have Kanai-Tajimi (Tajimi, 1960) power spectral density when generating ground motions corresponding to a particular RMS. The ground motion is characterized by dynamic amplification factors when generating time histories for a particular value of the spectral ordinate. The ground motion can have different strong motion durations for a particular value of root mean square acceleration and spectral acceleration. Thus, the strong motion duration is also considered to be a random variable.

3.2.1 Uncertainties in Kanai-Tajimi Parameters

The Kanai-Tajimi power spectral density is defined by the following equation:

$$S(\omega) = \frac{1 + 4\xi_g^2 \left(\frac{\omega}{\omega_g}\right)^2}{\left[1 - \left(\frac{\omega}{\omega_g}\right)^2\right]^2 + 4\xi_g^2 \left(\frac{\omega}{\omega_g}\right)^2} \cdot S_0 \quad (3.1)$$

where:

S_0 = intensity of the ideal white noise excitation at the bedrock level

ω_g = predominant ground natural frequency

ξ_g = effective damping coefficient of the ground

The Kanai-Tajimi power spectral density is defined by two random variables ω_g and ξ_g . Lai (1982) proposed a gamma probability density function for ξ_g and a lognormal probability density function for ω_g . He used 22 rock site records to arrive at the means and standard deviations of ω_g and ξ_g . He obtained the mean and standard deviation of ω_g as 26.7 rad/sec and 10.6 rad/sec, respectively. He also obtained the mean and standard deviation of ξ_g as 0.35 and 0.14, respectively. These distributions are used in this study when generating time histories for a given RMS.

3.2.2 Uncertainties in Dynamic Amplification Factors

The dynamic amplification factors represent the normalized spectral values at specified damping. The dynamic amplification factors are obtained as a ratio of the spectral acceleration to the peak ground acceleration. In this study, the dynamic amplification factors are obtained at a damping ratio of 5 percent of the critical damping. The dynamic amplification factors are used to obtain an ensemble of response spectra corresponding to a given average ordinate of spectral acceleration in the period range corresponding to each structure class (for example, $0.1 \leq T \leq 0.45$ sec for low rise reinforced concrete frames). Earthquake time histories are then generated corresponding to the response spectra. The procedure for generating time histories for a target response spectrum is discussed in Section 4. The firm site records of Loma Prieta, Morgan Hill and Whittier Narrows earthquakes are used for obtaining the parameters of the lognormal distributions of the dynamic amplification factors at different periods. The computed mean and standard deviations of the dynamic amplification factors are shown in figure 3-1.

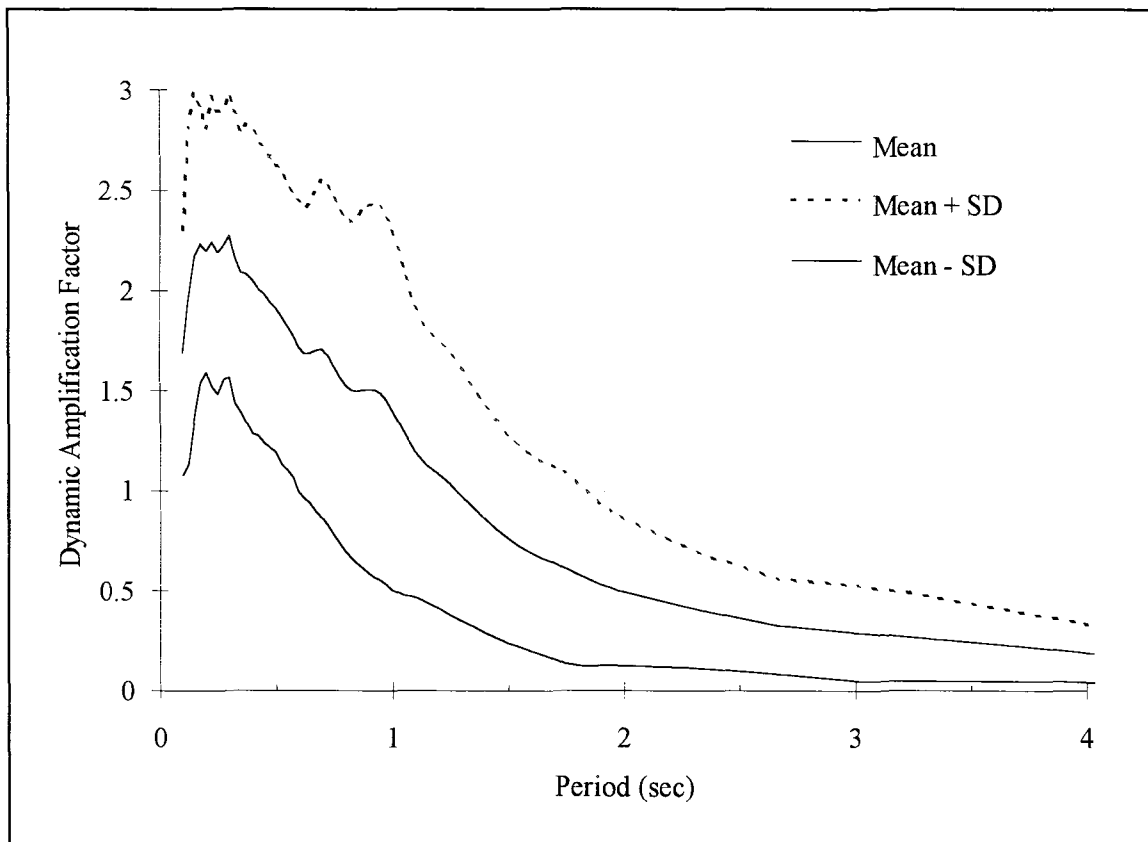


FIGURE 3-1 Parameters of the dynamic amplification factors for firm sites

3.2.3 Uncertainties in Strong Motion Duration

Trifunac and Brady's (1975) definition of strong motion duration, given by equations 1.1 through 1.3, is used in this study. The probability distributions of the strong motion duration T_s for firm sites given the RMS, $f_{T_s|RMS}(t_s|RMS)$, are derived using the firm site data from Loma Prieta, Morgan Hill and Whittier Narrows earthquakes. Only the free-field records are considered in this study to avoid possible soil-structure interaction effects. The conditional probability distributions of strong motion duration at given RMS are obtained by assuming the RMS and the strong motion duration to be jointly lognormally distributed. The distributions of the strong motion duration given the RMS are therefore lognormal with parameters λ'_{T_s} and $\xi'^2_{T_s}$, defined by the following two expressions:

$$\lambda'_{T_s} = E[\ln(T_s)|RMS = r] = \lambda_{T_s} + \rho \frac{\xi_{T_s}}{\xi_{RMS}} (\ln(RMS) - \lambda_{RMS}) \quad (3.2)$$

$$\xi'^2_{T_s} = (1 - \rho^2) \xi^2_{T_s} \quad (3.3)$$

where:

- T_s = strong motion duration
- λ_{RMS} = expected value of \ln RMS
- T_s = strong motion duration
- λ_{T_s} = expected value of \ln strong motion duration
- ξ^2_{RMS} = variance of \ln RMS
- $\xi^2_{T_s}$ = variance of \ln strong motion duration
- ρ = correlation coefficient of \ln RMS and \ln strong motion duration

The expected value of the strong motion duration, T_s , given the RMS can thus be written as:

$$\begin{aligned} E[T_s|RMS = r] &= \exp\left(\lambda'_{T_s} + \frac{1}{2} \xi'^2_{T_s}\right) \\ &= r^{\rho \frac{\xi_{T_s}}{\xi_{RMS}}} \exp\left[\frac{1}{2} (1 - \rho^2) \xi^2_{T_s} + \lambda_{T_s} - \rho \lambda_{RMS} \frac{\xi_{T_s}}{\xi_{RMS}}\right] \end{aligned} \quad (3.4)$$

and the variance of T_s , given the RMS, can be written as:

$$\text{var}(T_s | \text{RMS} = r) = \omega(\omega - 1)r^{2\rho \frac{\xi_{T_s}}{\xi_{\text{RMS}}}} \exp \left[2 \left(\lambda_{\text{RMS}} - \rho \lambda_{\text{RMS}} \frac{\xi_{T_s}}{\xi_{\text{RMS}}} \right) \right] \quad (3.5)$$

where:

$$\omega = \exp \left[(1 - \rho^2) \xi_{T_s}^2 \right] \quad (3.6)$$

The dependence of the parameters of the distributions on the distance from the rupture zone is taken into account by dividing the recording stations into two groups: one with distance to the rupture zone less than 50 km and the other with distance greater than 50 km. Due to the limited amount of data available for each group, further subdivision into more groups based on the distance from the rupture zone will result in a very small data set and consequently the parameters determined from each group will be quite unreliable. Moreover, further subdivision would require more simulations which would be economically prohibitive. The data considered for computing the parameters for the distributions are presented in tables 3-I and 3-II. These tables show the different recording stations located on firm sites for Loma Prieta, Whittier Narrows and Morgan Hill earthquakes. These tables also show the Trifunac and Brady strong motion duration and the corresponding RMS values for the two directions of recorded ground motion at each recording station.

The parameters of the distributions are determined using the method of maximum likelihood. For RMS, the parameters are determined using the following two equations:

$$\lambda_{\text{RMS}} = \frac{\sum_{i=1}^n \ln(\text{rms}_i)}{n} \quad (3.7)$$

and

$$\xi_{\text{RMS}}^2 = \frac{1}{n} \sum_{i=1}^n (\ln(\text{rms}_i) - \lambda_{\text{RMS}})^2 \quad (3.8)$$

where:

n = number of samples in the data

The parameters λ_{T_s} and ξ_{T_s} are computed in a similar manner. Figures 3-2 and 3-3 show the plot of the data. As can be seen from these figures, there is a strong negative correlation between

TABLE 3-I Trifunac and Brady's (1975) strong motion duration and RMS values for Loma Prieta, Whittier Narrows and Morgan Hill earthquakes for sites with distances to rupture zones less than 50 km.

SITE NAME AND NUMBER	EARTHQUAKE	AZIMUTH	DURATION (sec)	RMS (cm/sec ²)
Corralitos - Eureka Canyon 57007	Loma Prieta	360	6.86	163.240
		90	7.98	134.521
Crystal Springs - Pulgas 58378	Loma Prieta	0	15.12	32.871
		90	16.10	24.841
Crystal Springs - Skyline 58373	Loma Prieta	0	16.76	26.600
		90	15.98	30.071
Gilroy #1 - G.C. Water Tank 47379	Loma Prieta	360	3.70	159.600
		90	6.64	94.680
Gilroy #6 - San Ysidro 57383	Loma Prieta	90	12.66	44.473
		360	12.98	31.244
Monterey City Hall 47377	Loma Prieta	0	13.28	18.542
		90	11.96	16.448
SAGO South 47189	Loma Prieta	261	14.80	18.065
		351	18.84	16.979
Santa Cruz - UCSC 58135	Loma Prieta	360	9.50	125.522
		90	9.70	108.757
Saratoga - Aloha Ave. 58065	Loma Prieta	360	9.40	93.345
		90	8.26	86.349
Stanford Linear Accelerator 1601	Loma Prieta	360	11.62	66.926
		270	12.56	50.524
Woodside - Fire Station 58127	Loma Prieta	90	15.90	21.274
		0	18.06	18.468
Mt. Wilson 24399	Whittier Narrows	90	8.40	41.208
		0	10.08	27.014
LA-Hollywood Storage 24303	Whittier Narrows	90	13.58	25.674
		0	11.62	35.238
Inglewood 14196	Whittier Narrows	90	11.24	41.040
		0	7.84	59.742
LA-116th St. School 14403	Whittier Narrows	360	6.58	86.373
		270	9.52	52.197
LA - Baldwin Hills 24157	Whittier Narrows	90	14.42	32.247
		0	13.62	30.604
Long Beach Park (14241)	Whittier Narrows	90	23.18	10.467
Pacoima (24088)	Whittier Narrows	90	9.90	32.824
Ranchoff (23497)	Whittier Narrows	90	14.96	12.045
Corralitos - Eureka Canyon 57007	Morgan Hill	310	10.30	22.842
		220	11.52	17.988
Gilroy #1 - G.C. Water Tank 47379	Morgan Hill	320	9.10	19.161
		230	9.80	17.442
Gilroy #6 - San Ysidro 57383	Morgan Hill	90	6.50	86.931
		0	7.30	54.609
Gilroy Gavilan College 47006	Morgan Hill	67	8.60	19.364
		337	8.54	18.971

TABLE 3-II Trifunac and Brady's (1975) strong motion duration and RMS values for Loma Prieta and Whittier Narrows earthquakes for sites with distances to rupture zones greater than 50 km.

SITE NAME AND NUMBER	EARTHQUAKE	AZIMUTH	DURATION (sec)	RMS (cm/sec ²)
Berkeley - LB Lab 58471	Loma Prieta	90	8.16	32.149
		0	18.22	14.115
Hayward - CSUH Stadium 58219	Loma Prieta	90	19.30	17.421
		0	19.06	15.371
Piedmont Jr. High School 58338	Loma Prieta	45	11.98	15.043
		315	11.72	15.667
Point Bonita 58043	Loma Prieta	297	8.34	24.743
		207	10.08	18.947
S.F. - Cliff House 58132	Loma Prieta	90	7.26	32.441
		360	10.28	22.420
S.F. - Diamond Heights 58130	Loma Prieta	90	9.42	25.080
		360	8.78	29.915
S.F. - Pacific Heights 58131	Loma Prieta	270	11.10	16.557
		360	12.40	13.467
S.F. - Presidio 58222	Loma Prieta	90	8.56	41.682
		360	10.54	28.719
S.F. - Rincon Hill 58181	Loma Prieta	90	11.52	18.173
		360	13.88	14.943
S.F. - Telegraph Hill 58133	Loma Prieta	90	9.48	16.586
		360	11.46	11.312
S.S.F. Siera Point 58539	Loma Prieta	205	9.48	21.470
		115	11.68	15.039
Yerba Buena Island 58163	Loma Prieta	90	8.32	16.986
		360	21.66	6.509
Vasqpark (24047)	Whittier Narrows	0	9.22	12.877

natural log of RMS and natural log of strong motion duration, T_s . The values of the parameters of the distributions are presented in table 3-III.

The spectral acceleration appears to be poorly related to strong motion duration. Figures 3-4 through 3-6 show the plot of the data and the correlation between the strong motion duration and the spectral acceleration in the three period bands. The correlation coefficient between the natural logarithm of average spectral acceleration and the natural logarithm of strong motion duration is as follows:

- (a) $\rho = -0.5510$ for $0.1 \leq T \leq 0.45$
- (b) $\rho = -0.3067$ for $0.45 < T \leq 0.85$
- (c) $\rho = -0.1885$ for $0.85 < T \leq 2.5$

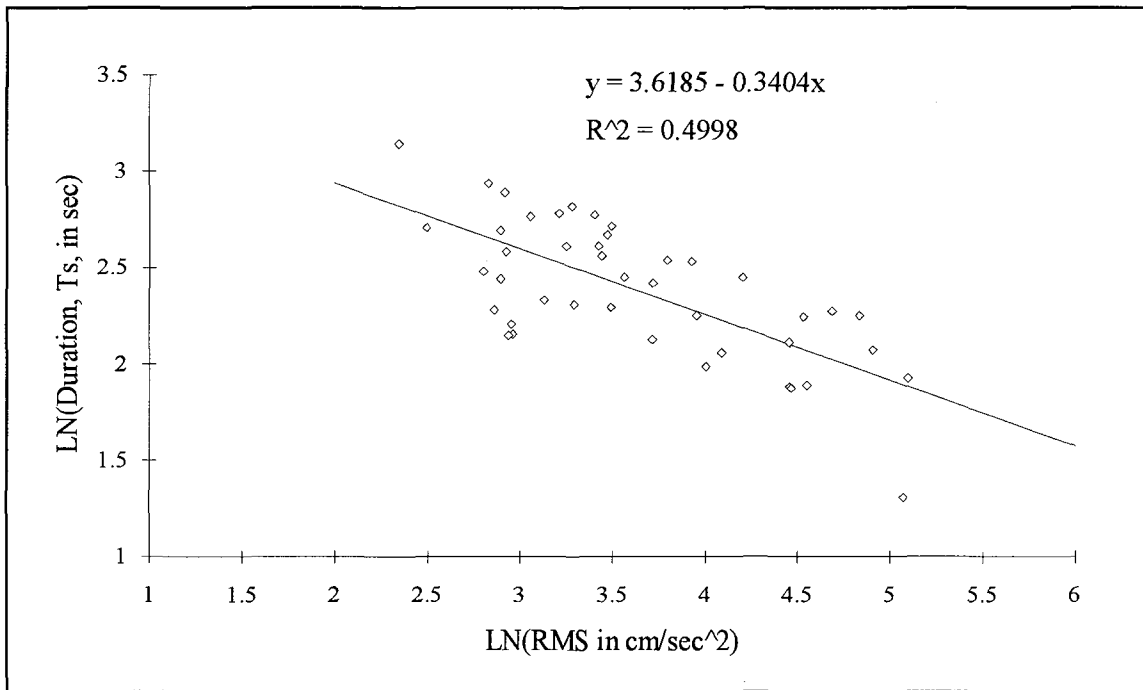


FIGURE 3-2 Correlation between Trifunac and Brady's (1975) strong motion duration and the RMS for firm sites with distances to rupture zones less than 50 km.

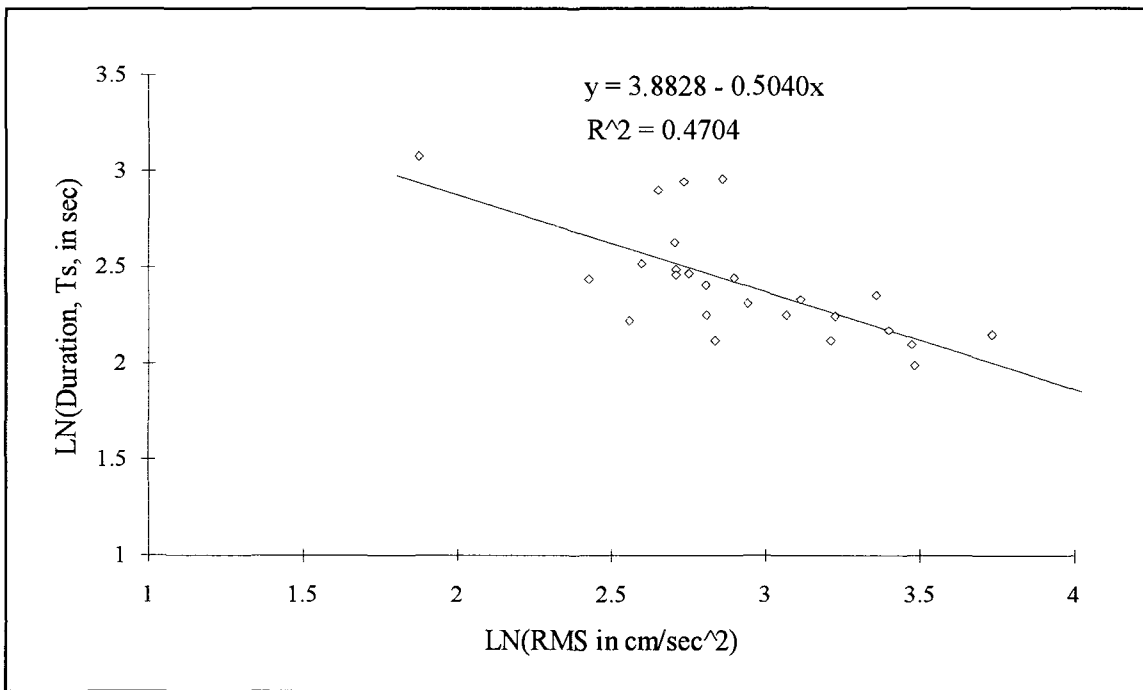


FIGURE 3-3 Correlation between Trifunac and Brady's (1975) strong motion duration and the RMS for firm sites with distances to rupture zones greater than 50 km.

TABLE 3-III Parameters for the estimation of the mean and the variance of the conditional strong motion duration given the RMS

Parameters	Distance less than 50 km.	Distance greater than 50 km.
λ_{RMS}	3.6226	2.9161
ξ_{RMS}	0.7358	0.3984
λ_{T_s}	2.3853	2.413
ξ_{T_s}	0.3543	0.2928
Correl. coeff. $\rho_{\ln T_s, \ln RMS}$	-0.7070	-0.6859

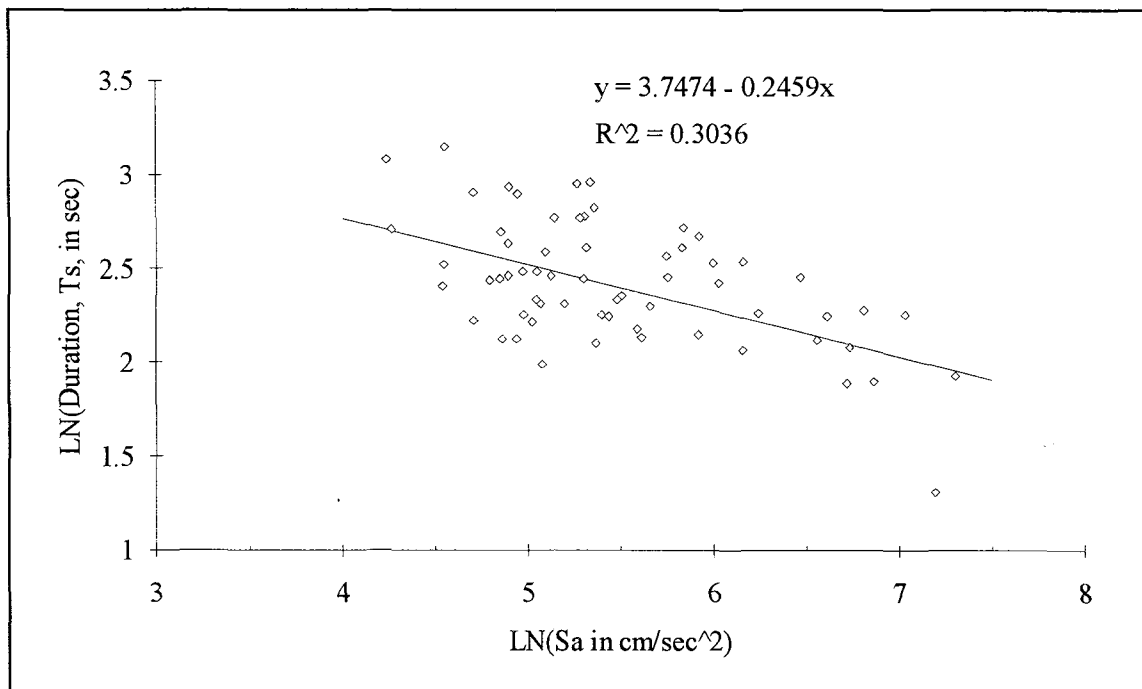


FIGURE 3-4 Correlation between Trifunac and Brady's (1975) strong motion duration and the average S_a in the period range 0.1-0.45 sec for firm sites

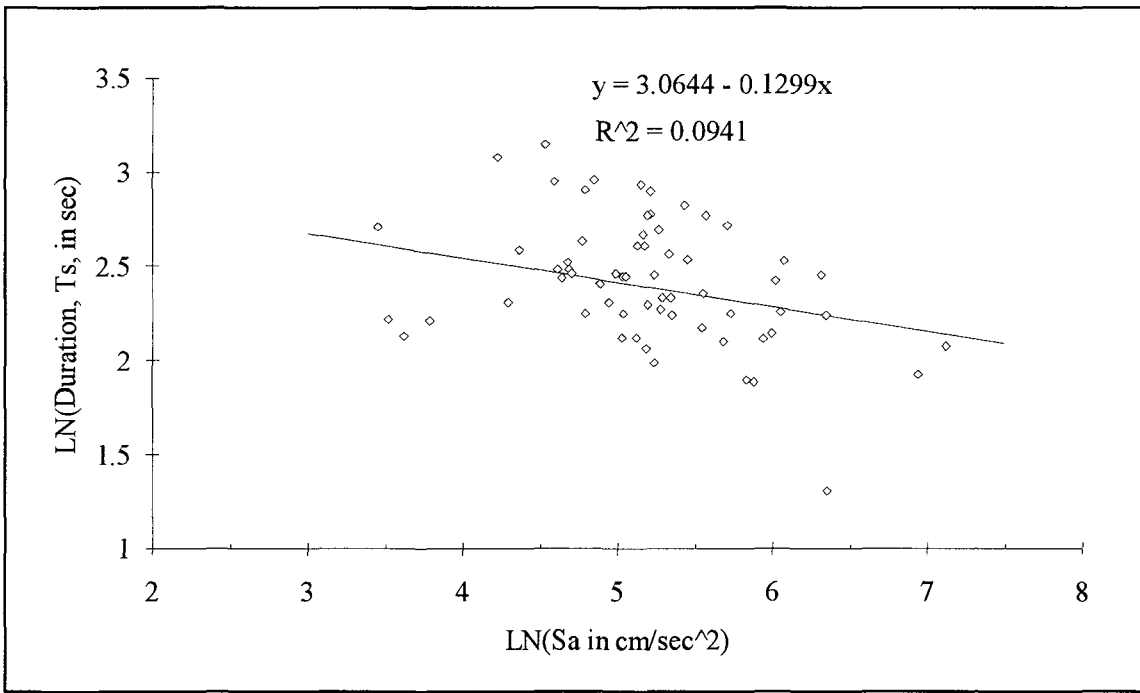


FIGURE 3-5 Correlation between Trifunac and Brady's (1975) strong motion duration and the average S_a in the period range 0.45-0.85 sec for firm sites

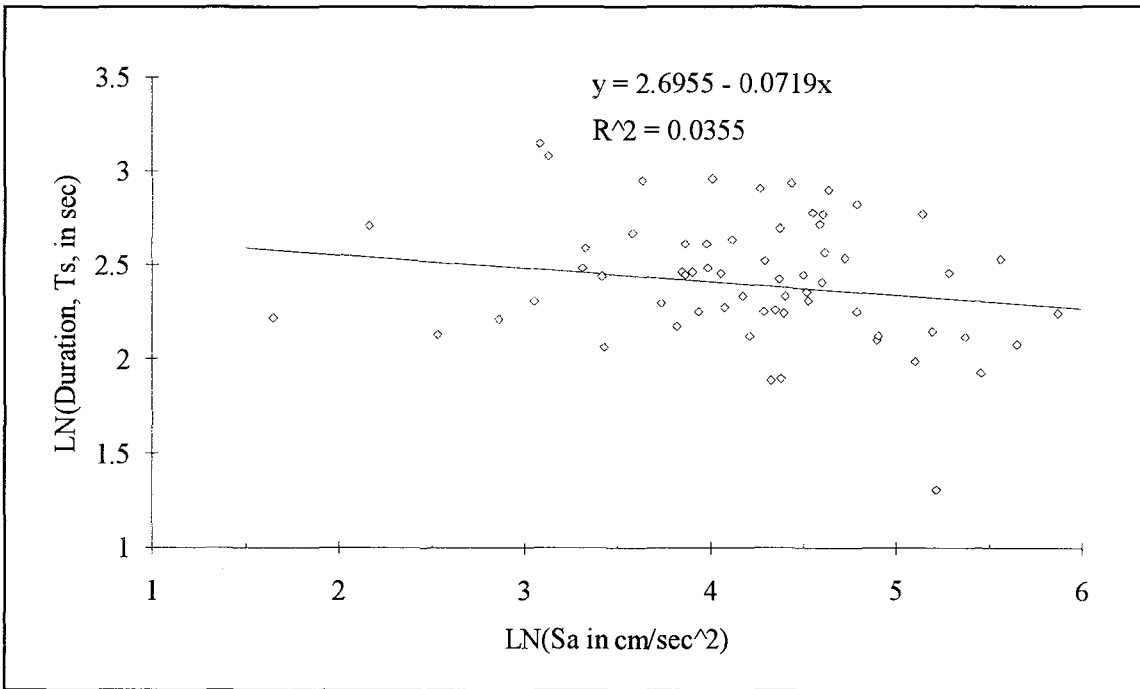


FIGURE 3-6 Correlation between Trifunac and Brady's (1975) strong motion duration and the average S_a in the period range 0.85-2.5 sec for firm sites

A lognormal probability density independent of the spectral acceleration is assumed for the strong motion duration when generating time histories for a given spectral acceleration. The parameters of the distribution are $\lambda_{T_s} = 2.396$ and $\xi_{T_s} = 0.331$. The comparison of the lognormal distribution with these parameters and the observed distribution is presented in figure 3-7.

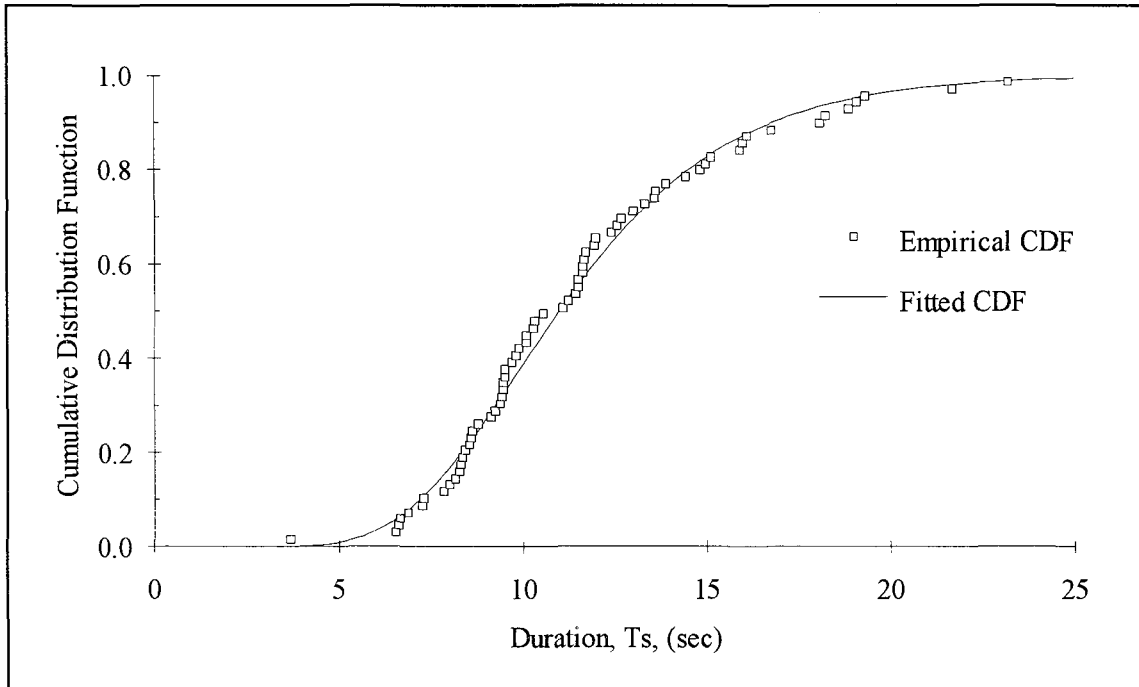


FIGURE 3-7 Comparison of the observed and the estimated log normal distribution ($\lambda_{T_s} = 2.396$ and $\xi_{T_s} = 0.331$) of strong motion duration for firm sites.

3.3 Relationship Between MMI and Spectral Acceleration

The relationship between the modified Mercalli intensity and the average spectral acceleration in each period band is investigated in order to combine the heuristic damage probability matrices of ATC-13 (1985), for example, with the analytically obtained fragility curves and damage probability matrices using the formulation presented in this study. The relationships between MMI and average spectral acceleration for firm sites are developed using the same data as those used to develop the ground motion duration probability distribution parameters. The average spectral acceleration values of the ground motions recorded on firm sites and the MMI values from these earthquakes at the respective recording stations are used to develop these relationships.

The MMI contours along with the station numbers of the recording stations for all four earthquakes are shown in figures 3-8 through 3-11. The contours are rather approximate having been obtained by overlaying the maps with station numbers on the maps with the MMI contours and then tracing out the contours. The data used for regression analysis are presented in table 3-IV. The average spectral acceleration for the larger of the two horizontal components is used in the analysis.

The average spectral acceleration, in each period range, is assumed to have a conditional lognormal probability density function at given values of MMI. Regression analysis is performed between the natural logarithm of the mean of the average spectral acceleration and MMI. Similar regression analysis is performed between the standard deviation of the average spectral acceleration and MMI. The regression curves so obtained are used to predict the means and standard deviations of the average spectral acceleration at higher MMI values for which observed data are not available. The regression curves for the mean and standard deviation of the average spectral acceleration, expressed in cm/sec^2 in each period band, are given by the following equations:

$$\mu_{S_a|MMI} = 8.273 e^{0.581 \text{ MMI}} \quad \text{for } 0.10 \leq T \leq 0.45 \quad (3.9)$$

$$\sigma_{S_a|MMI} = 18.703 e^{0.388 \text{ MMI}} \quad \text{for } 0.10 \leq T \leq 0.45 \quad (3.10)$$

$$\mu_{S_a|MMI} = 3.098 e^{0.665 \text{ MMI}} \quad \text{for } 0.45 \leq T \leq 0.85 \quad (3.11)$$

$$\sigma_{S_a|MMI} = 6.201 e^{0.513 \text{ MMI}} \quad \text{for } 0.45 \leq T \leq 0.85 \quad (3.12)$$

$$\mu_{S_a|MMI} = 0.352 e^{0.835 \text{ MMI}} \quad \text{for } 0.85 \leq T \leq 2.50 \quad (3.13)$$

$$\sigma_{S_a|MMI} = 1.803 e^{0.526 \text{ MMI}} \quad \text{for } 0.85 \leq T \leq 2.50 \quad (3.14)$$

The curves representing the median values of spectral acceleration at specified values of MMI are shown in figures 3-12 through 3-14. These figures also show the conditional distributions for spectral acceleration, with MMI in the range 5 to 8.

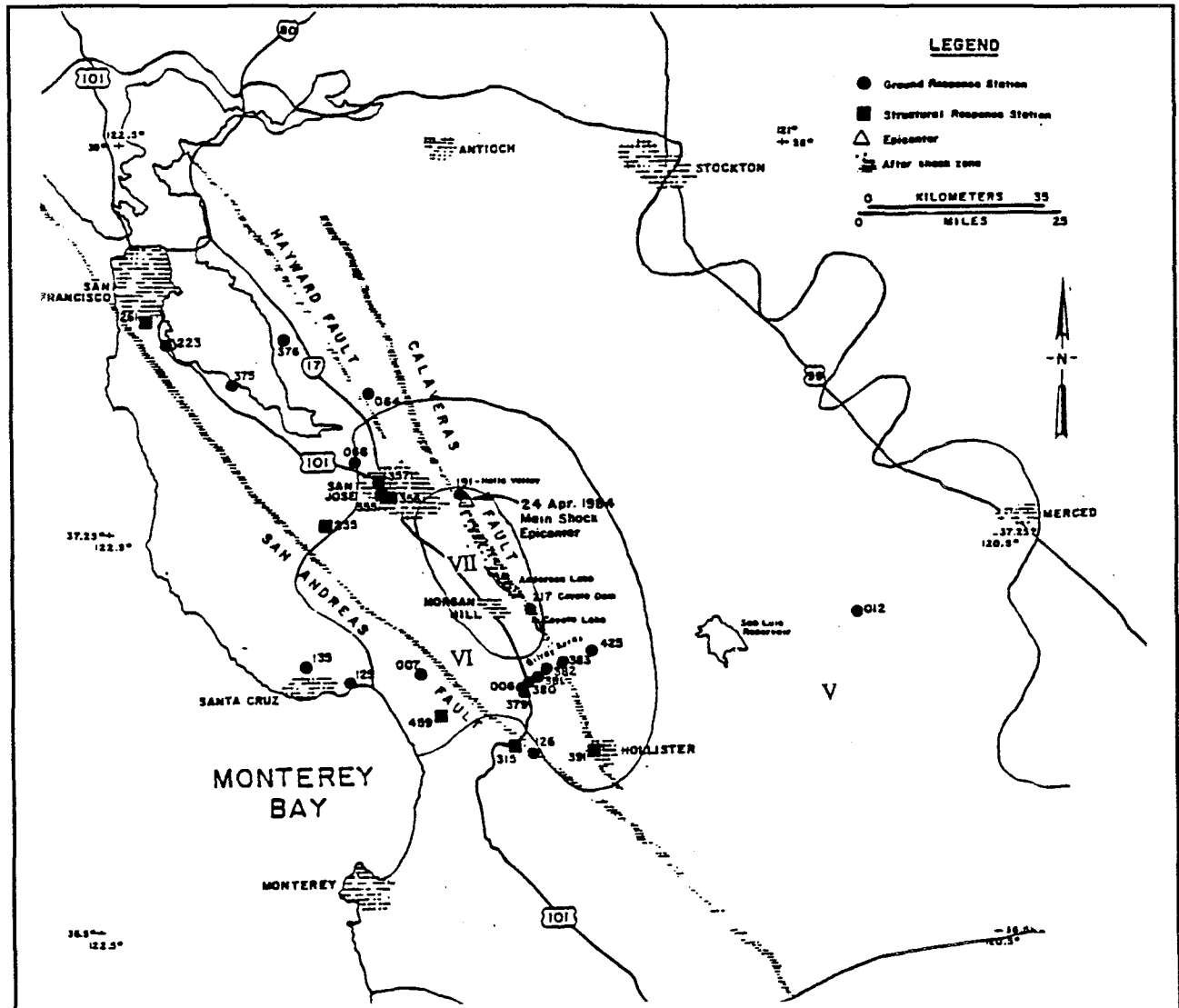


FIGURE 3-8 Map showing the MMI contours and the California Strong Motion Instrumentation Program (CSMIP) station numbers for the Morgan Hill earthquake of April 24, 1984 (M_L of 6.2), (Huang et al. 1985)

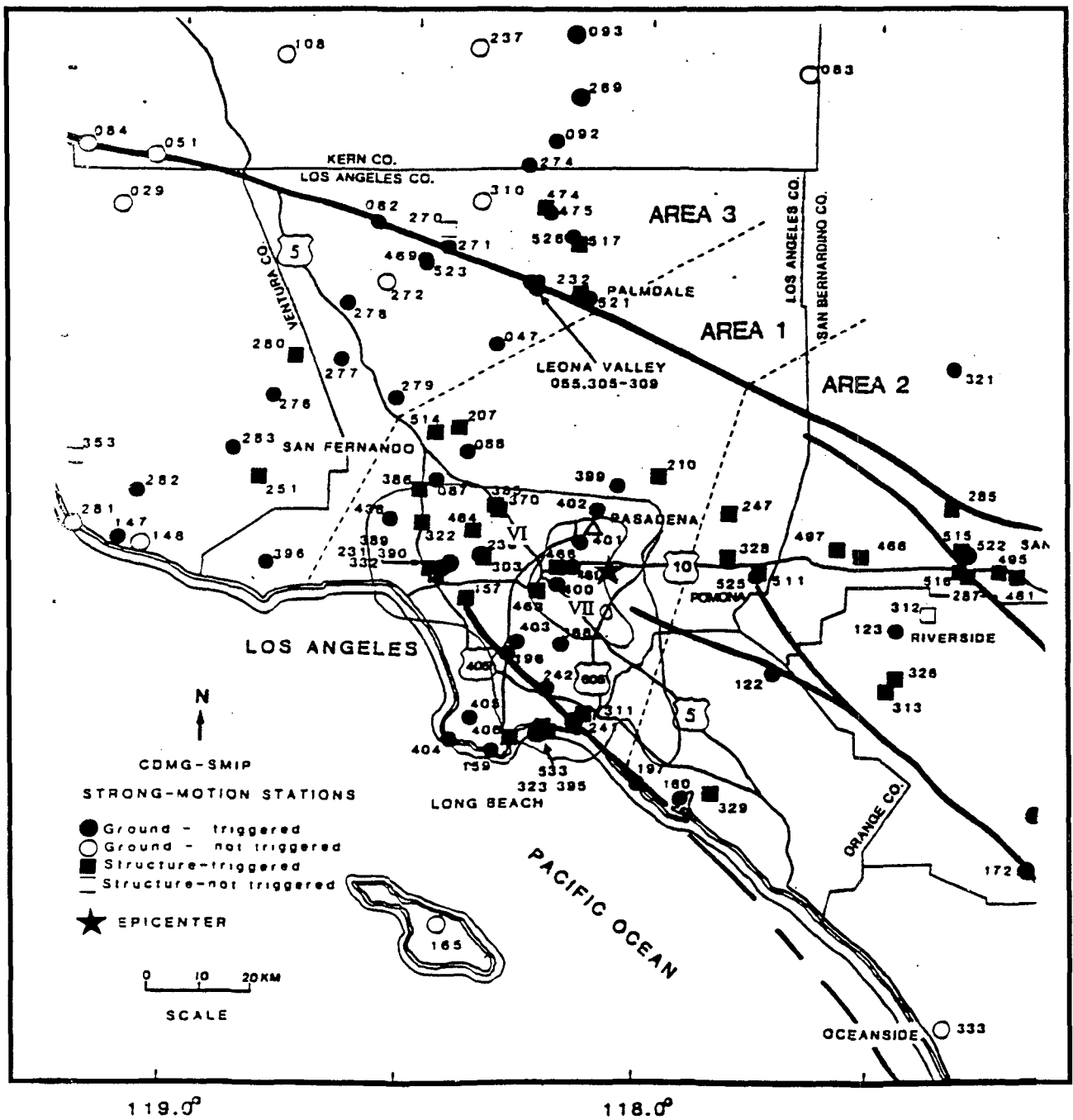


FIGURE 3-9 Map showing the MMI contours and the CSMIP station numbers for the Whittier Narrows earthquake of October 1, 1987 (M_L of 6.1), (Huang et al., 1989)

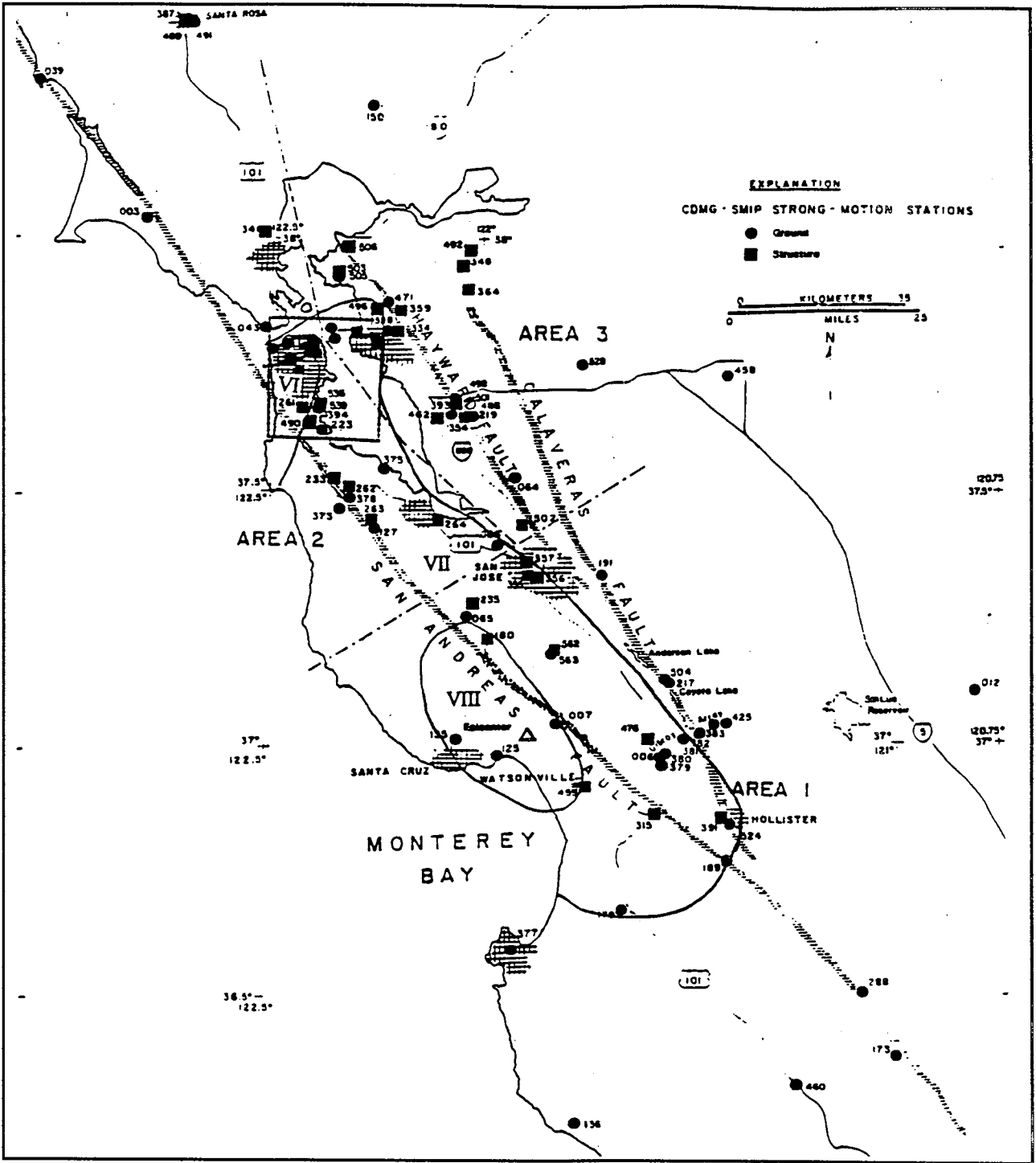


FIGURE 3-10 Map showing the MMI contours and the CSMIP station numbers for the Loma Prieta earthquake of October 18, 1989 (M_L of 7.0 and M_S of 7.1), (Shakal et al., 1989)

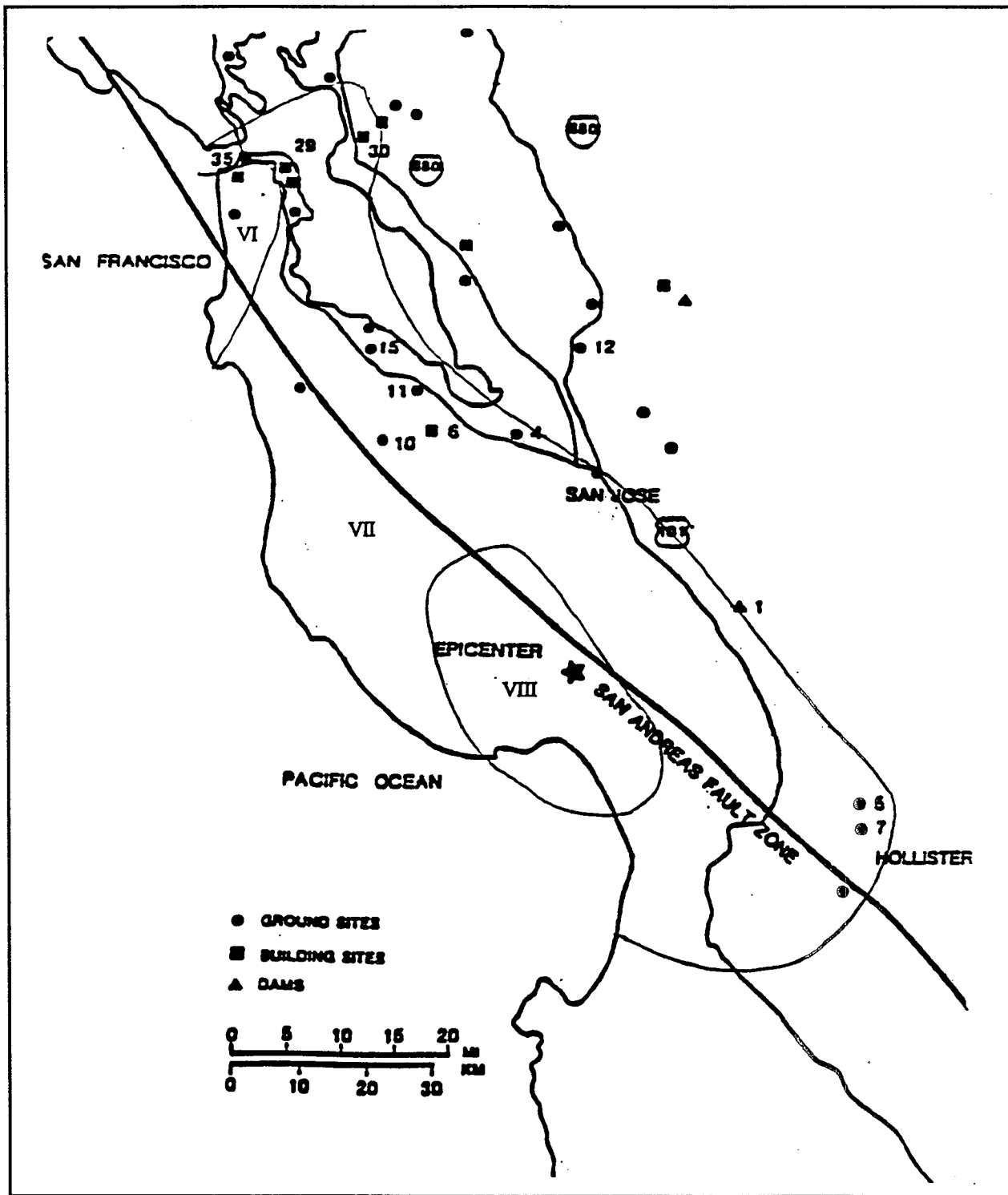


FIGURE 3-11 Map showing the MMI contours and the United States Geological Survey (USGS) station numbers for the Loma Prieta earthquake of October 18, 1989, (M_L of 7.0 and M_S of 7.1), (Maley et al., 1989)

**TABLE 3-IV Average spectral acceleration and MMI values for the Loma Prieta,
Whittier Narrows and Morgan Hill earthquakes**

SITE NAME AND NUMBER	EARTHQUAKE	MMI	Spectral Accel. (0.1≤T≤0.45) (g)	Spectral Accel. (0.45<T≤0.85) (g)	Spectral Accel. (0.85<T≤2.5) (g)
Berkeley - LB Lab 58471	Loma Prieta	7	0.218	0.298	0.136
			0.113	0.122	0.073
Corralitos - Eureka Canyon 57007	Loma Prieta	8	1.509	1.055	0.238
			0.859	1.257	0.290
Crystal Springs - Pulgas 58378	Loma Prieta	7	0.348	0.307	0.100
			0.205	0.186	0.097
Crystal Springs - Skyline 58373	Loma Prieta	7	0.217	0.233	0.122
			0.200	0.267	0.174
Gilroy #1 - G.C. Water Tank 47379	Loma Prieta	7	1.363	0.587	0.188
			0.978	0.349	0.082
Gilroy #6 - San Ysidro 57383	Loma Prieta	6	0.483	0.237	0.115
			0.318	0.211	0.103
Hayward - CSUH Stadium 58219	Loma Prieta	6	0.212	0.131	0.056
			0.198	0.101	0.039
Monterey City Hall 47377	Loma Prieta	6	0.165	0.080	0.028
			0.158	0.102	0.028
Piedmont Jr. High School 58338	Loma Prieta	7	0.147	0.110	0.055
			0.170	0.150	0.051
Point Bonita 58043	Loma Prieta	6	0.142	0.171	0.137
			0.162	0.142	0.094
SAGO South 47189	Loma Prieta	7	0.130	0.196	0.081
			0.136	0.176	0.086
Santa Cruz - UCSC 58135	Loma Prieta	8	1.157	0.311	0.122
			0.927	0.199	0.060
Saratoga - Aloha Ave. 58065	Loma Prieta	8	0.756	0.577	0.361
			0.719	0.387	0.219
S.F. - Cliff House 58132	Loma Prieta	7	0.164	0.192	0.167
			0.158	0.200	0.083
S.F. - Diamond Heights 58130	Loma Prieta	6	0.233	0.215	0.083
			0.272	0.259	0.047
S.F. - Pacific Heights 58131	Loma Prieta	7	0.095	0.136	0.101
			0.096	0.109	0.075
S.F. - Presidio 58222	Loma Prieta	7	0.380	0.407	0.184
			0.251	0.263	0.094

TABLE 3-IV (cont' d) Average spectral acceleration and MMI values for the Loma Prieta, Whittier Narrows and Morgan Hill earthquakes

SITE NAME AND NUMBER	EARTHQUAKE	MMI	Spectral Accel. (0.1≤T≤0.45) (g)	Spectral Accel. (0.45<T≤0.85) (g)	Spectral Accel. (0.85<T≤2.5) (g)
S.F. - Rincon Hill 58181	Loma Prieta	7	0.130	0.157	0.092
			0.136	0.120	0.063
S.F. - Telegraph Hill 58133	Loma Prieta	7	0.148	0.122	0.074
			0.123	0.106	0.031
S.S.F. Siera Point 58539	Loma Prieta	7	0.226	0.156	0.052
			0.135	0.112	0.048
Stanford Linear Accelerator 1601	Loma Prieta	7	0.653	0.561	0.202
			0.409	0.443	0.265
Woodside - Fire Station 58127	Loma Prieta	7	0.175	0.184	0.102
			0.144	0.186	0.105
Yerba Buena Island 58163	Loma Prieta	7	0.131	0.156	0.069
			0.071	0.070	0.023
Mt. Wilson 24399	Whittier Narrows	6	0.279	0.038	0.013
			0.184	0.074	0.022
LA-Hollywood Storage 24303	Whittier Narrows	6	0.207	0.180	0.054
			0.320	0.193	0.059
Inglewood 14196	Whittier Narrows	6	0.422	0.419	0.081
			0.480	0.182	0.031
LA-116th St. School 14403	Whittier Narrows	6	0.842	0.365	0.077
			0.524	0.431	0.079
LA - Baldwin Hills 24157	Whittier Narrows	6	0.379	0.178	0.037
			0.347	0.171	0.049
Long Beach Park (14241)	Whittier Narrows	6	0.097	0.095	0.022
Pacoima (24088)	Whittier Narrows	5	0.294	0.184	0.043
Ranchoff (23497)	Whittier Narrows	5	0.073	0.032	0.009
Vasqpark (24047)	Whittier Narrows	5	0.113	0.034	0.005
Corralitos - Eureka Canyon 57007	Morgan Hill	6	0.245	0.212	0.066
			0.204	0.160	0.049
Gilroy #1 - G.C. Water Tank 47379	Morgan Hill	6	0.154	0.045	0.018
			0.124	0.034	0.016
Gilroy #6 - San Ysidro 57383	Morgan Hill	6	0.743	0.584	0.273
			0.535	0.264	0.066
Gilroy Gavilan College 47006	Morgan Hill	6	0.125	0.039	0.019
			0.146	0.041	0.014

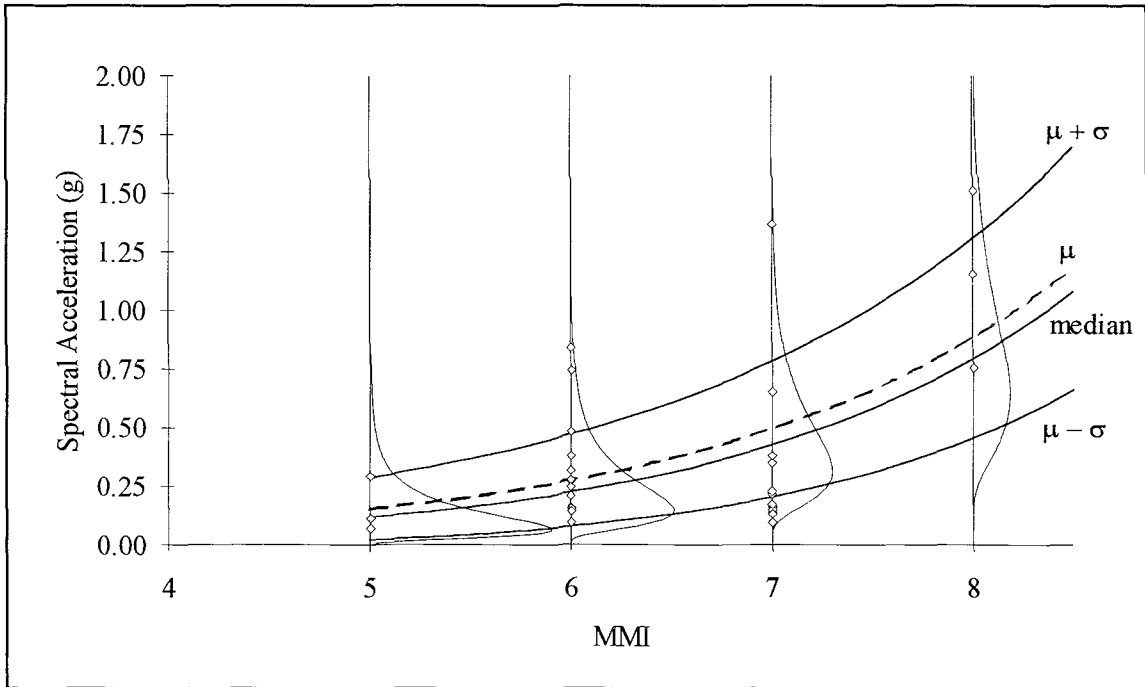


FIGURE 3-12 S_a -MMI correlation and the probability distributions for spectral acceleration averaged over the period range 0.1-0.45 sec, conditional on MMI

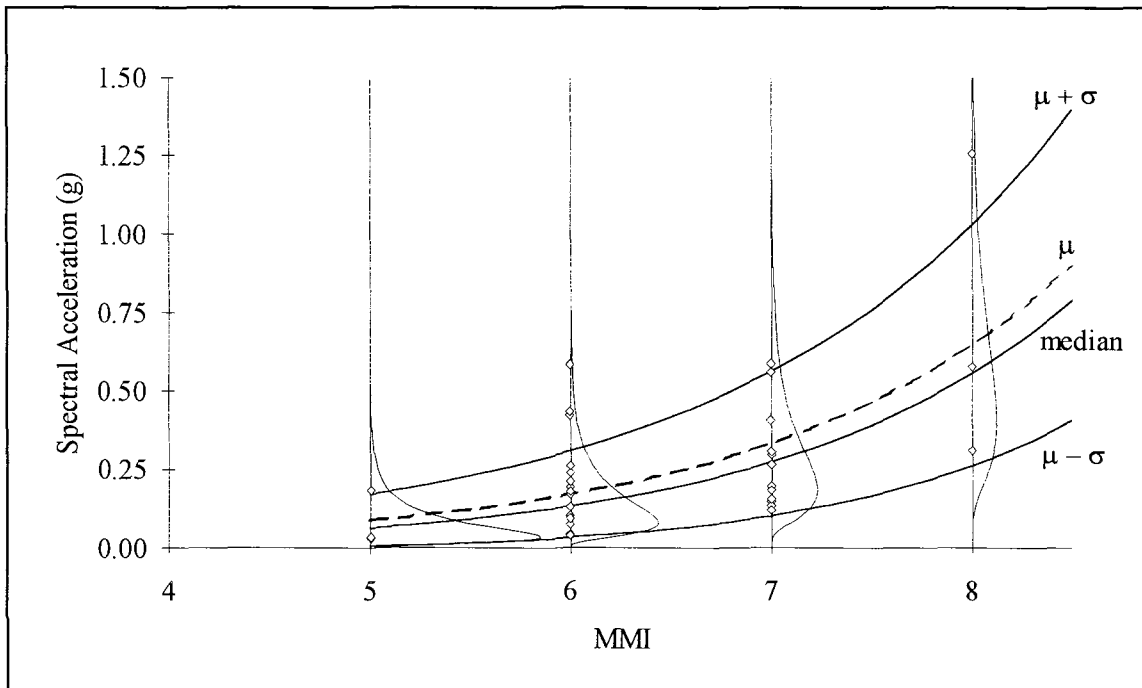


FIGURE 3-13 S_a -MMI correlation and the probability distributions for spectral acceleration averaged over the period range 0.45-0.85 sec, conditional on MMI

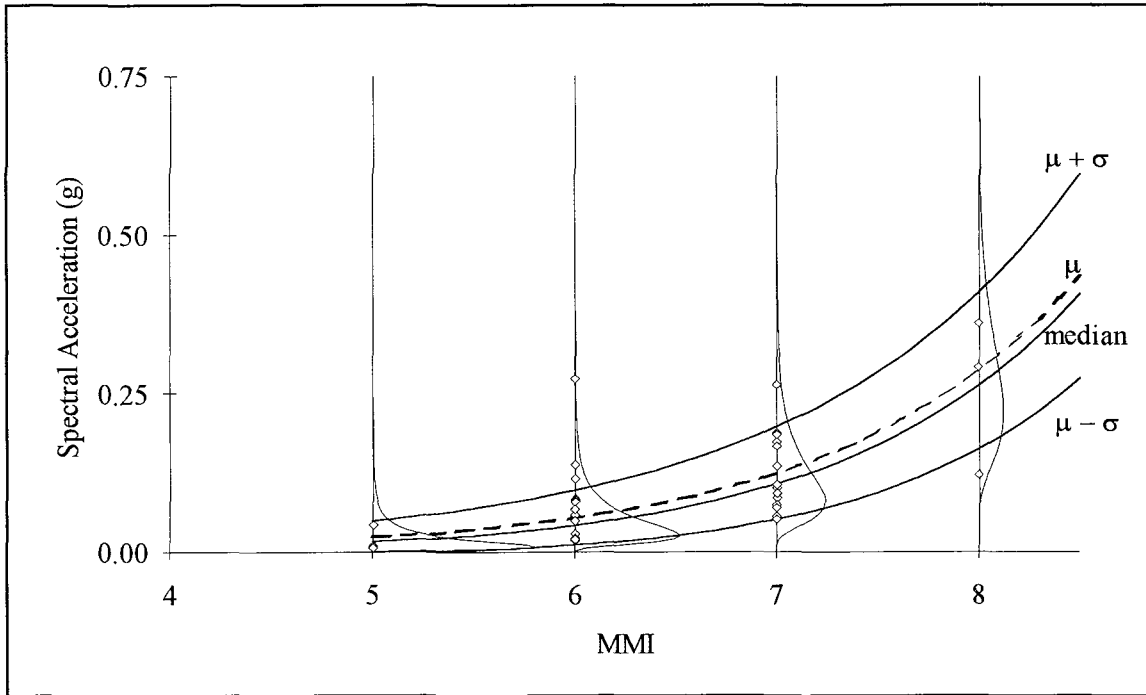


FIGURE 3-14 S_a -MMI correlation and the probability distributions for spectral acceleration averaged over the period range 0.85-2.5 sec, conditional on MMI

3.4 Development of Damage Probability Matrices

The fragility curves for the three example buildings are presented in terms of the spectral acceleration in Section 5. The relationships between spectral acceleration, in the period range relevant period band, and modified Mercalli intensity are used to obtain the damage probability matrices from the fragility curves. The formulation for obtaining the damage probability matrices is shown as follows:

$$P_{D|MMI}[d|MMI] = \int_{S_a} P_{D|MMI,S_a}[d|MMI, S_a] \cdot f_{S_a|MMI}[s_a|MMI] ds_a \quad (3.15)$$

where:

$P_{D|MMI}[d|MMI]$ = probability of being in or exceeding a given damage state at a specified MMI

$P_{D|MMI,S_a}[d|MMI, S_a]$ = probability of being in or exceeding a given damage state at specified MMI and spectral acceleration

$f_{S_a|MMI}[s_a|MMI]$ = conditional probability distribution of spectral acceleration at specified MMI, obtained by assuming this distribution to be lognormal with parameters specified by equations 3.9 through 3.14 for the three period bands

In developing the damage probability matrices, it has been assumed that the probability of being in or exceeding a given damage state at specified MMI and spectral acceleration is same as the probability of being in or exceeding a given damage state at specified spectral acceleration. Thus, equation 3.15 can be simplified as

$$P_{D|MMI}[d|MMI] = \int_{S_a} P_{D|S_a}[d|S_a] \cdot f_{S_a|MMI}[s_a|MMI] ds_a \quad (3.16)$$

The integral in equation 3.16 is evaluated numerically by assuming the probability of being in or exceeding a particular damage state, at a specified spectral acceleration, is constant during a small interval of spectral acceleration. An interval of 0.02 cm/sec² is used in this study. The probability of being in a particular damage state, at a specified MMI, is evaluated from the probabilities evaluated using equation 3.16.

SECTION 4

MONTE CARLO SIMULATION TECHNIQUE

The Monte Carlo simulation technique is used for the computation of the fragility curves and damage probability matrices defined by equations 2.1 and 2.2. This technique involves the generation of artificial ground motion and the simulation of damage to a structure. The overview of the Monte Carlo simulation technique is presented in figure 4-1. The direct Monte Carlo technique requires a large number of simulation cycles to achieve an acceptable level of confidence in the estimated probabilities. The Latin Hypercube technique is used to reduce the number of simulation cycles by employing constrained sampling instead of random sampling required in the direct Monte Carlo method.

The first step in the Monte Carlo technique involves the simulation of artificial time histories and structural parameters. The probability distributions discussed in Section 3.1 are used for the generation of random variables for the structural parameters. The procedure for the generation of artificial time histories is shown in figure 4-2. This involves the generation of an ensemble of Kanai-Tajimi power spectra for a given RMS. Alternatively, an ensemble of response spectra with the same average spectral acceleration, in a prescribed period range, is required. The ensemble of Kanai-Tajimi power spectra is obtained by generating random values for the parameters ω_g and ξ_g in equation 3.1. The modeling of uncertainties in these parameters was discussed in Section 3.2.1. The ensemble of response spectra with the same average spectral acceleration is obtained from an ensemble of dynamic amplification factors. The dynamic amplification factors are scaled to match the given spectral acceleration. In addition, the random variables for the strong motion duration are also generated. The modeling of uncertainties in strong motion duration was discussed in Section 3.2.3. Auto Regressive Moving Average (ARMA) models are used for simulating time histories with a given RMS value. Gaussian stationary models with modulating functions are used for generating time histories with a specified spectral acceleration. The simulation of artificial ground motion is discussed in detail in Section 4.1.

The next step in the Monte Carlo simulation technique involves the random permutations of the generated random variables. Non-linear dynamic analysis is then carried out to obtain the sample statistics for the fragility curves.

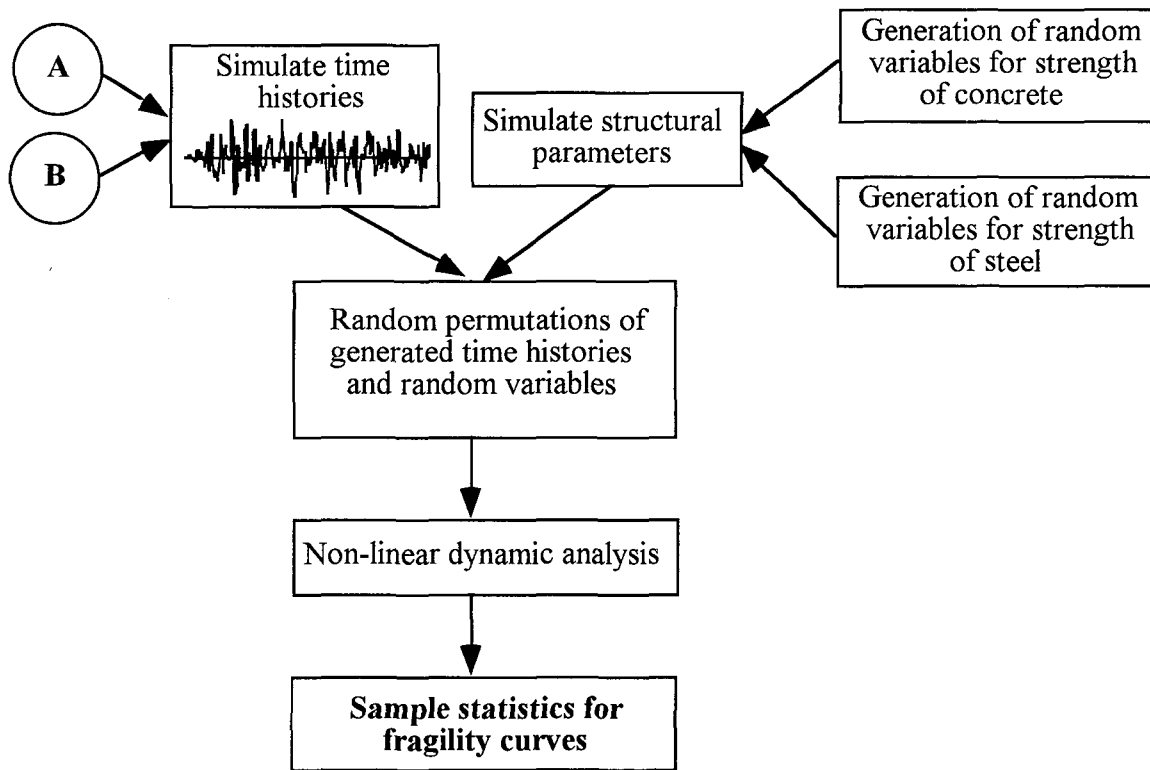


FIGURE 4-1 Steps in the Monte Carlo simulation technique

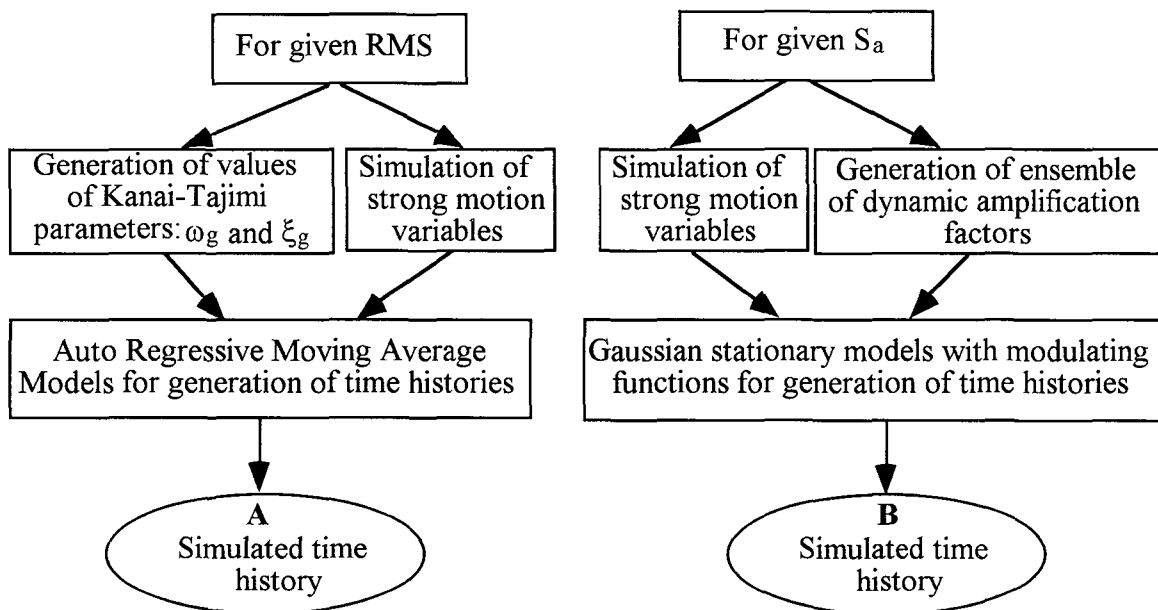


FIGURE 4-2 Steps in the simulation of time histories A and B in figure 4-1

The generation and the random permutations of the random variables is carried out using the Latin Hypercube sampling scheme. The Latin Hypercube sampling scheme involves the selection of N non-overlapping intervals, corresponding to N simulation cycles, such that all intervals have the same probability of occurrence. The intervals for a general probability density function are shown in figure 4-3. N different values for each random variable in each of the N non-overlapping intervals are then randomly selected. This is accomplished by generating N uniform random numbers between 0 and 1 which are transformed to the random numbers in the non-overlapping intervals using the following equation:

$$U_m = \frac{U}{N} + \frac{m-1}{N} \tag{4.1}$$

where:

m = interval number

U = uniform random number in the range (0,1)

U_m = random number in the m^{th} interval

Only one generated value falls within each interval because $\frac{m-1}{N} < U_m < \frac{m}{N}$. The random variables are generated by evaluating the inverse of the cumulative distribution functions at the generated values (given by equation 4.1). This inverse transformation can be expressed as follows:

$$x_m = F_X^{-1}(U_m) \tag{4.2}$$

where:

x_m = m^{th} generated value for variable X

F_X^{-1} = inverse of the cumulative distribution function for variable X

The samples are obtained by random permutation of the generated values of all the random variables. A procedure for obtaining a random sequence of the generated values of a random variable is illustrated by the following shuffling algorithm.

Let $\{x_1, x_2, \dots, x_N\}$ be the initial order of the values generated for random variable X . The random sequence r_1, r_2, \dots, r_N is produced by the following steps:

1. Set $r_1 = x_1, r_2 = x_2, \dots, r_N = x_N$ and $m = N$.

2. Generate an integer I uniformly distributed between 1 and m . Interchange r_I and r_N .
3. Set $m = m-1$. If $m = 1$, return r_1, r_2, \dots, r_N and exit. Otherwise go to 2.

The generated values of all the variables are placed in a random sequence. The n^{th} sample is now obtained by selecting the n^{th} value of all the random variables. The Latin Hypercube sampling technique will be used in this study because of the increase in the efficiency due to the smaller number of samples required for obtaining the same accuracy in the simulation results.

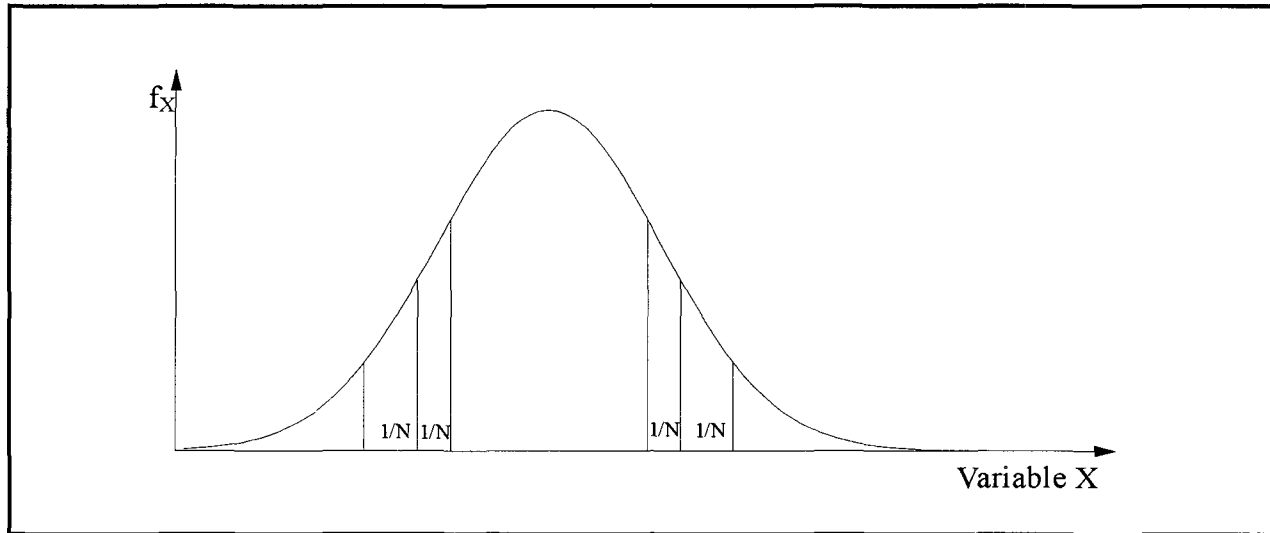


FIGURE 4-3 General probability density function with N intervals used in the Latin Hypercube sampling scheme

4.1 Ground Motion Simulation

The development of the fragility curves and damage probability matrices requires that ensembles of time histories be available at various levels of the ground motion parameters (RMS, S_a or MMI). However, there are only a few recorded time histories with the same ground motion parameter. Thus, the alternative is to simulate artificial time histories to provide such ensembles of ground motion. Several procedures are available for the generation of artificial time histories. These include geophysical models, Gaussian stationary models with modulating functions and autoregressive moving average (ARMA) models. These models are briefly described in the following sections.

In this study, Gaussian stationary models with modulating functions are used for the generation of artificial time histories when spectral acceleration is used to characterize the ground motion.

ARMA models are used for the generation of time histories when the ground motion is characterized by root mean square acceleration.

4.1.1 Geophysical Models

Several techniques using geophysical models are available for the simulation of earthquake ground motions. These include the ray tracing techniques, Green's function techniques and normal mode method (Suzuki and Kiremidjian, 1989). It is difficult to simulate long duration and wide-band frequency waves with the ray tracing methods. Green's function methods become difficult to apply when multilayered earth structure is considered. When the normal mode method is used, it is difficult to generate high frequency waves at intermediate and far distances unless large number of modes are used. The major difficulty with the normal mode method is the enormous computational effort involved in obtaining the normal modes for the earth.

The geophysical models are thus too complex, computationally involved and regionally dependent, thus making it difficult to implement them in this study.

4.1.2 Gaussian Stationary Models with Modulating Functions

Gaussian stationary models with modulating functions have been proposed, among others, by Shinozuka and Sato (1967), Liu (1970), and Shinozuka and Deodatis, (1991). In Gaussian stationary models with modulating functions, the ground motion is expressed as follows:

$$\mathbf{X}(t) = \mathbf{I}(t) \sum_n \mathbf{A}_n \text{Sin}(\omega_n t + \phi_n) \quad (4.3)$$

where:

- \mathbf{A}_n = amplitude of the n^{th} sinusoid
- ω_n = frequency of the n^{th} sinusoid
- ϕ_n = phase angle of the n^{th} sinusoid
- $\mathbf{I}(t)$ = envelope function

The amplitudes are determined from the power spectral density as follows:

$$\frac{A_n^2}{2} = \mathbf{G}(\omega_n) \Delta\omega \quad (4.4)$$

where:

$G(\omega)$ = one sided power spectral density

$G(\omega_n)\Delta\omega$ can be thought of as the contribution of the sinusoid with frequency ω_n to the total power. The nonstationarity is introduced by using an envelope function $I(t)$. SIMQKE (1977) is one of the programs which uses this procedure.

In this study, SIMQKE is used to generate time histories corresponding to a given response spectra. The dynamic amplification factors discussed later are used to obtain an ensemble of time histories corresponding to a given spectral ordinate. The trapezoidal envelope function is used in SIMQKE. The parameters of the envelope function are chosen to satisfy the strong motion duration discussed in Section 3.1.2.3.

4.1.3 ARMA Models

Autoregressive moving average (ARMA) models are often applied for the generation of artificial time histories (e.g., Polhemus and Cakmak, 1981 and Conte et al., 1990). ARMA models consist of a discrete stationary linear transfer function applied to a white noise process. A white noise process is a random process in which all frequencies contribute equally to the mean square value of the process. A white noise process has an infinite variance due to the contribution of all frequencies and is therefore not physically realizable. The autocorrelation and power spectral density functions of white noise process $W(t)$ are expressed mathematically by means of the following two equations:

$$R_{WW}(\tau) = 2\pi\phi_0\delta(\tau) \quad (4.5)$$

and

$$\phi_{WW}(\omega) = \phi_0 \quad (4.6)$$

where:

$\delta(\tau)$ = Dirac delta function

ϕ_0 = constant power spectral density of the white noise process

A shot noise process with homogeneous Poisson arrival times tends to a Gaussian white noise as the mean occurrence rate λ tends to infinity and σ^2 tends to zero in such a way that $\lambda\sigma^2$ remains a constant (Housner & Jennings, 1964).

A general ARMA model is represented by the following linear equation:

$$\mathbf{a}_k - \phi_1 \mathbf{a}_{k-1} - \dots - \phi_p \mathbf{a}_{k-p} = \mathbf{e}_k - \theta_1 \mathbf{e}_{k-1} - \dots - \theta_q \mathbf{e}_{k-q} \quad (4.7)$$

where:

$\mathbf{a}_k = \mathbf{a}(\mathbf{k}\Delta t)$, $k = 0, 1, 2, \dots =$ a discrete stationary correlated process

$\mathbf{e}_k = \mathbf{e}(\mathbf{k}\Delta t) =$ a stationary discrete white-noise process

$\phi_s =$ autoregressive parameters

$\theta_s =$ moving average parameters

A special case of ARMA models is the stationary ARMA(2,1) model defined by the following difference equation:

$$\mathbf{a}_k - \phi_1 \mathbf{a}_{k-1} - \phi_2 \mathbf{a}_{k-2} = \mathbf{e}_k - \theta_1 \mathbf{e}_{k-1} \quad (4.8)$$

The ARMA(2,1) model, with modulating functions to introduce the non-stationarity, is used in this study.

The process \mathbf{a} should be stationary and invertible in order to be physically realizable. The stationarity conditions ensure that the process \mathbf{a} has a finite variance. The stationarity is controlled by the autoregressive part only and is achieved when the following conditions are satisfied:

$$\begin{aligned} \phi_1 + \phi_2 &< 1 \\ \phi_1 - \phi_2 &< 1 \\ |\phi_2| &< 1 \end{aligned} \quad (4.9)$$

The idea of invertibility is illustrated by means of a first order moving average process represented by the following equation .

$$\mathbf{a}_k = \mathbf{e}_k - \theta_1 \mathbf{e}_{k-1} \quad (4.10)$$

Equation 4.10 can be written in terms of the previous values of \mathbf{e}_k as shown in the following equation:

$$\mathbf{a}_k = \mathbf{e}_k - \theta_1 \mathbf{a}_{k-1} - \theta_1^2 \mathbf{a}_{k-2} - \dots - \theta_1^n \mathbf{a}_{k-n} - \theta_1^{n+1} \mathbf{e}_{k-n-1} \quad (4.11)$$

If \mathbf{a}_k is not to depend on some point in the remote past, θ_1 must be less than one in absolute value. If n is allowed to go to infinity, the last term in equation 3.23 vanishes and \mathbf{a}_k can be written as an infinite autoregressive process with declining weights as shown in the following equation:

$$\mathbf{a}_k = \sum_{n=1}^{\infty} -\theta_1^n \mathbf{a}_{k-n} + \mathbf{e}_k \quad (4.12)$$

The reason for excluding the non-invertible processes is that they are not physically realizable. In a non-invertible process a small perturbation in the distant past can have a tremendous effect on the present process \mathbf{a}_k .

The parameters of the ARMA(2,1) model corresponding to the Kanai-Tajimi (Tajimi, 1960) stochastic earthquake model (equation 3.1) can be computed from the following equations when the system is assumed to be underdamped:

$$\phi_1 = 2 e^{-\xi_g \omega_g \Delta t} \cos(\omega_g \sqrt{1 - \xi_g^2} \Delta t) \quad (4.13)$$

$$\phi_2 = - e^{-2\xi_g \omega_g \Delta t} \quad (4.14)$$

θ_1 is the solution of:

$$\theta_1^2 + \frac{2\rho_1\phi_1 - \phi_1^2 + \phi_2^2 - 1}{\phi_1 - \rho_1(1-\phi_2)} \theta_1 + 1 = 0, \quad |\theta_1| < 1 \quad (4.15)$$

where:

$$\rho_1 = \rho(\Delta t) = \frac{1}{2} \frac{\left(\frac{C_s}{C_d}\right)^2 - 4\xi_g^2}{\left(\frac{C_s}{C_d}\right)^2 + 4\xi_g^2} \frac{\xi_g}{\sqrt{1 - \xi_g^2}} \sqrt{-(\phi_1^2 + 4\phi_2)} + \frac{1}{2} \phi_1 \quad (4.16)$$

where $C_s = C_d = 1.0$.

The ARMA(2,1) spectrum is defined for all frequencies smaller or equal to the Nyquist frequency. Therefore the following condition should be satisfied:

$$0 < \omega_g \sqrt{1 - \xi_g^2} \leq \frac{\pi}{\Delta t} \quad (4.17)$$

The parameters ω_g and ξ_g are the parameters used to define the Kanai-Tajimi power spectral density.

Thus, the following steps are involved in the generation of artificial time histories using ARMA models:

1. Generation of a stationary discrete white-noise $\{e_k, k = 1, \dots, N\}$ where e_k is the shot noise impulse at time t_k .
2. Time modulation of the stationary white-noise by means of the following equation:

$$\mathbf{w}_k = \psi(t_k) \mathbf{e}_k \quad \mathbf{k} = 1, \dots, \mathbf{N} \quad (4.18)$$

where:

$\psi(t_k)$ = envelope function

The Shinozuka-Sato (1967) envelope function is used in this study and is defined by equation 4.19.

3. ARMA filtering of the non-stationary white-noise. ARMA (2,1) model given by equation 3.19 is used in the simulation process.

4.1.3.1 Simulation of Time Histories with Specified RMS and Duration

A time history with a specified root mean square acceleration and strong motion duration is required for each sample. The procedure for satisfying the desired root mean square acceleration and strong motion duration is presented in this section. Artificial time histories corresponding to a specified RMS are generated using the ARMA model. The ARMA parameters are computed for the Kanai-Tajimi (Tajimi, 1960) power spectral density function. Stationary shot noise is first generated which is then made non-stationary by modulating it with a time envelope. The time

enveloping function suggested by Shinozuka and Sato (1967) is used in this study. This envelope function is given by:

$$\psi(t) = e^{-\alpha t} - e^{-\beta t} \quad \beta > \alpha > 0 \quad (4.19)$$

The parameters α and β in the above function need to be determined to correspond to the known strong motion duration.

Duration Calibration

The parameters α and β of the envelope function can be determined by means of the following two equations based on the Trifunac and Brady definition of strong motion duration:

$$0.05 \int_0^{T_d} |\psi(t)|^2 dt = \int_0^{T_1} |\psi(t)|^2 dt \quad (4.20)$$

and

$$0.95 \int_0^{T_d} |\psi(t)|^2 dt = \int_0^{T_2} |\psi(t)|^2 dt \quad (4.21)$$

where:

T_1 = start of the strong motion duration

T_2 = end of the strong motion duration

T_s = strong motion duration

T_d = total duration of the motion

Using equation 4.19, equations 4.20 and 4.21 can be expressed as follows:

$$\frac{\alpha^2 - 2\alpha\beta + \beta^2 + 4\alpha\beta e^{-(\alpha+\beta)T_d} - \alpha\beta e^{-2\alpha T_d} - \alpha\beta e^{-2\beta T_d} - \alpha^2 e^{-2\beta T_d} - \beta^2 e^{-2\alpha T_d}}{40 \alpha\beta(\alpha + \beta)} = \frac{\alpha^2 - 2\alpha\beta + \beta^2 + 4\alpha\beta e^{-(\alpha+\beta)T_2} - \alpha\beta e^{-2\alpha T_2} - \alpha\beta e^{-2\beta T_2} - \alpha^2 e^{-2\beta T_2} - \beta^2 e^{-2\alpha T_2}}{2\alpha\beta(\alpha + \beta)} \quad (4.22)$$

and

$$\frac{\alpha^2 - 2\alpha\beta + \beta^2 + 4\alpha\beta e^{-(\alpha+\beta)T_d} - \alpha\beta e^{-2\alpha T_d} - \alpha\beta e^{-2\beta T_d} - \alpha^2 e^{-2\beta T_d} - \beta^2 e^{-2\alpha T_d}}{40 \alpha\beta(\alpha + \beta)} = \frac{\alpha^2 - 2\alpha\beta + \beta^2 + 4\alpha\beta e^{-(\alpha+\beta)T_2} - \alpha\beta e^{-2\alpha T_2} - \alpha\beta e^{-2\beta T_2} - \alpha^2 e^{-2\beta T_2} - \beta^2 e^{-2\alpha T_2}}{2\alpha\beta(\alpha + \beta)} \quad (4.23)$$

Applying the conditions that $T_2 - T_1$ is a known strong motion duration and $\alpha > \beta > 0$, equations 4.22 and 4.23 are solved by a predictor-corrector method for the parameters α and β .

The values of α and β obtained by solving equations 4.22 and 4.23 would satisfy the given strong motion duration if the time history is ergodic. However, in reality, the time history is not ergodic. Therefore, iterations are performed in the neighborhood of the values of α and β until the duration of the generated ground motion is within 0.01 sec of the desired duration.

RMS Calibration

The ARMA parameters are computed for the Kanai-Tajimi (Tajimi, 1960) power spectral density function using equations 4.13 through 4.15. The procedure to determine the variance of the shot noise process, e_k in equation 4.8, is presented in this section.

Let $X(t)$ represent the stationary filtered process obtained after ARMA filtering and $Y(t)$ be the process obtained after $X(t)$ is modulated by the enveloping function. Thus

$$Y(t) = \psi(t) X(t) \quad (4.24)$$

The Arias intensity, I of the final process $Y(t)$ is given by

$$I = \int_0^{T_d} Y^2(t) dt \quad (4.25)$$

where:

T_d = total duration of the simulated process

The expected value of the Arias intensity can be written as follows:

$$E[I] = \int_0^{T_d} E[Y^2(t)]dt = \int_0^{T_d} \sigma_Y^2 dt \quad (4.26)$$

Since $Y(t)$ is a process with zero mean, $E[Y^2] = \sigma_Y^2$.

It can be shown (Nigam, 1983) that

$$\sigma_Y^2 = \sigma_X^2 |\psi(t)|^2 \quad (4.27)$$

where:

$$\sigma_X^2 = E[X^2(t)]$$

Equations 4.26 and 4.27 can be combined to yield:

$$E[I] = \int_0^{T_d} E[\psi(t)X(t)]^2 dt = \sigma_X^2 \int_0^{T_d} |\psi(t)|^2 dt \quad (4.28)$$

The variance σ_X can be related to the expected value of RMS based on equations 1.7 and 4.28. To a first order approximation for the expected values, the relationship between the two parameters is expressed as follows:

$$E[\text{RMS}] = \sqrt{\frac{0.9 E[I]}{T_s}} = \frac{\sigma_X}{\sqrt{T_s}} \sqrt{0.9 \int_0^{T_d} |\psi(t)|^2 dt} \quad (4.29)$$

or

$$\sigma_X = E[\text{RMS}] \sqrt{\frac{T_s}{0.9 \int_0^{T_d} |\psi(t)|^2 dt}} \quad (4.30)$$

where:

T_d = total duration of the simulated process

T_s = Trifunac-Brady strong motion duration

A factor of 0.9 is used in equation 4.29 as the Trifunac-Brady definition of strong motion is the time interval to accumulate 90 percent of the total energy.

The variance of the stationary, filtered process $X(t)$ can be related to the variance of the input shot noise process by means of the following equation:

$$\sigma_X^2 = \frac{(1 - \phi_2)(1 + \theta_1^2) - 2\phi_1\theta_1}{(1 + \phi_2) ((1 - \phi_2)^2 - \phi_1^2)} \sigma_e^2 \quad (4.31)$$

where:

σ_e^2 = variance of the shot noise process

ϕ_1, ϕ_2, θ_1 = ARMA parameters

σ_X^2 = variance of the stationary filtered process $X(t)$

The value of the variance of the shot noise process, σ_e^2 , has to match the expected value of RMS. This value is determined by solving equations 4.30 and 4.31 simultaneously. It is obvious that using this value of variance of the shot noise process will lead to the RMS being satisfied only in the ensemble mean.

In order to match the desired root mean square acceleration, the process generated by using the calculated value of σ_e^2 needs to be modified. Let the generated process be denoted by $Y_1(t)$ and its root mean square acceleration by RMS_1 . The ratio of the desired RMS to RMS_1 is then used to scale the amplitudes of the time history $Y_1(t)$ to yield $Y(t)$. The resulting time history $Y(t)$ has the desired strong motion duration and root mean square acceleration.

4.2 Damage Simulation

The computer program IDARC2D, *Inelastic Damage Analysis of Reinforced Concrete Frame - Shear Wall Structures*, (Park et al., 1987, Kunnath and Reinhorn, 1994) is used for nonlinear structural dynamic analysis. IDARC2D (Park et al., 1987) and IDARC2D (Kunnath and Reinhorn, 1994) evaluate the original Park-Ang (1984) and modified damage index (Kunnath et al., 1992) respectively, for each member as well as the overall structure. Nonlinear dynamic analysis is carried out for each generated time history. Thus, for an ensemble of artificial time histories, the statistics of the Park-Ang index are computed.

At each ground motion level, a lognormal distribution of the Park-Ang damage index is assumed. The parameters of the distribution are obtained from the ensemble mean and variance of the Park-Ang index. The probabilities of the different damage states at a specified ground motion level are then evaluated by computing the probabilities of the Park-Ang damage index lying within the ranges for the different damage states specified in table 2-III.

SECTION 5

IMPLEMENTATION OF THE METHODOLOGY

This section presents the results of damage analysis of three example buildings: two, six, and thirteen story buildings. The buildings are considered for the illustration of the methodology for the development of fragility curves and damage probability matrices. The two, six and thirteen story buildings correspond respectively to low-rise, mid-rise and high-rise reinforced concrete moment resisting frames in ATC-13 (1985). These buildings were selected for their plan and elevation regularity and thus can be considered to represent the "average" behavior of buildings in the respective structural classes.

The results of damage analysis at given ground motion levels are presented as conditional probabilities of being in different damage states. The ground motion is characterized by root mean square acceleration, average spectral ordinate and modified Mercalli intensity (MMI). The original Park and Ang (1984) and the modified version of the Park-Ang (Kunnath et al., 1992) damage indices are used to identify the different damage states as discussed in Section 2. The results of the damage analysis are presented as damage probability matrices and fragility curves. The relationships between spectral acceleration and MMI, obtained in Section 3, are used to obtain the damage probability matrices from the fragility curves for the three example buildings. The formulation for obtaining the damage probability matrices from fragility curves was presented in Section 3.4. The damage probability matrices for the three example buildings, so obtained, are compared to those in ATC-13 (1985).

5.1 Description of the Two-Story Building

The building is rectangular in plan with sides measuring 109'-9" and 91'-5 1/2". The plan of the building is shown in figure 5-1. The building has six equal bays along the long direction and five equal bays along the short direction. The lateral load resisting system of the building consists of perimeter moment frames.

The structure is analyzed for earthquake forces to be resisted by the frames along the short direction(frames A and B in figure 5-1). The elevation of the frames is shown in figure 5-2. As the properties of the beams and columns of the frames in the two directions are similar, earthquake forces along the short direction are considered to be critical to the damage of the building. The properties of the beams and columns in frames A and B are shown in table 5-I.

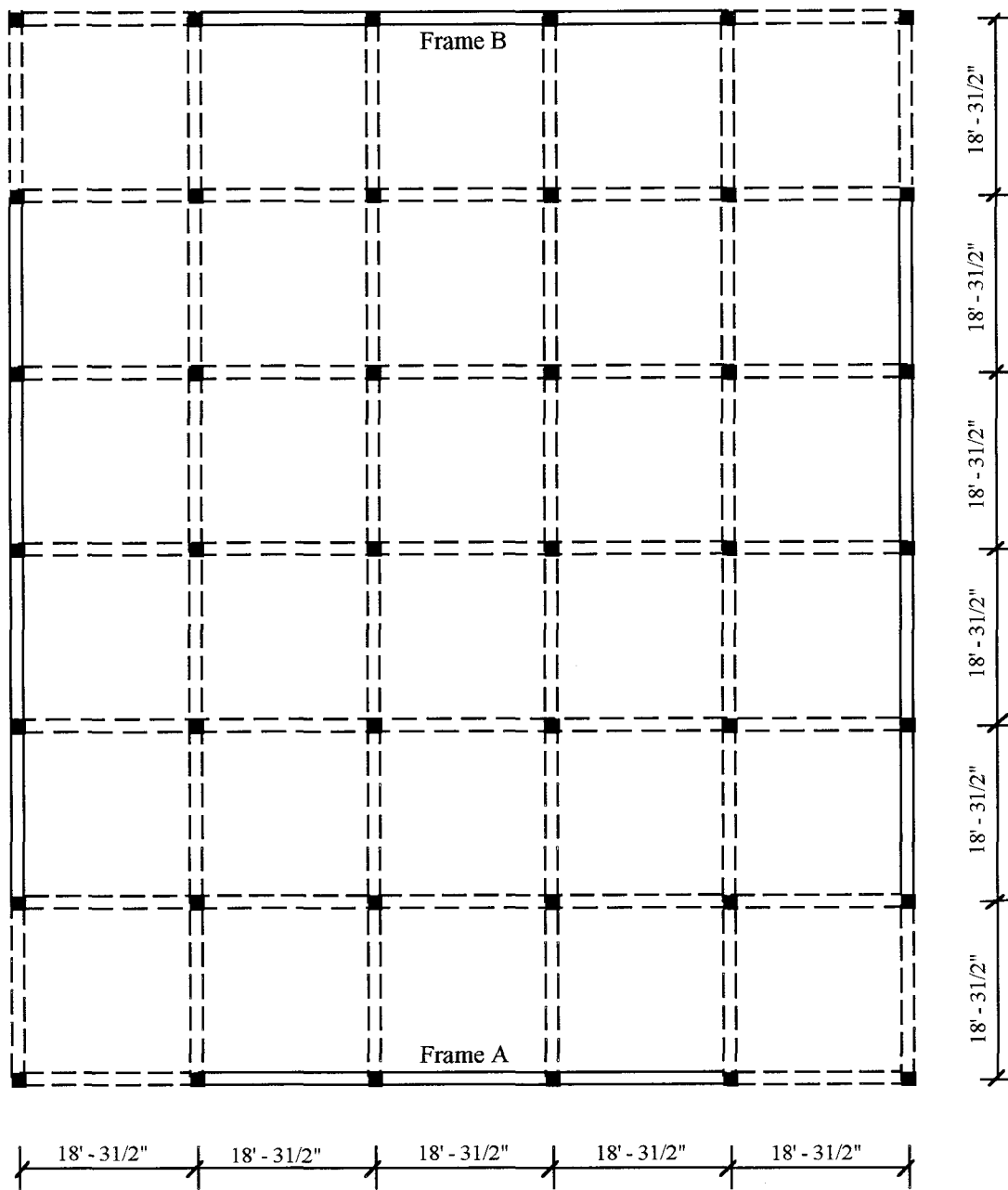


FIGURE 5-1 Typical floor plan of the two story building

TABLE 5-I Properties of beams and columns in frames A and B in figure 5-1

Properties	Beams	Columns
Dimensions	16" x 30"	25" x 25"
Main Reinforcement	3 in ² (B); 6 in ² (T)	7.8 in ² (S); 11.4 in ² (F)
Concrete strength	4 ksi	4 ksi
Steel strength	60 ksi	60 ksi

T-top; B-bottom; F-1st story; S-2nd story

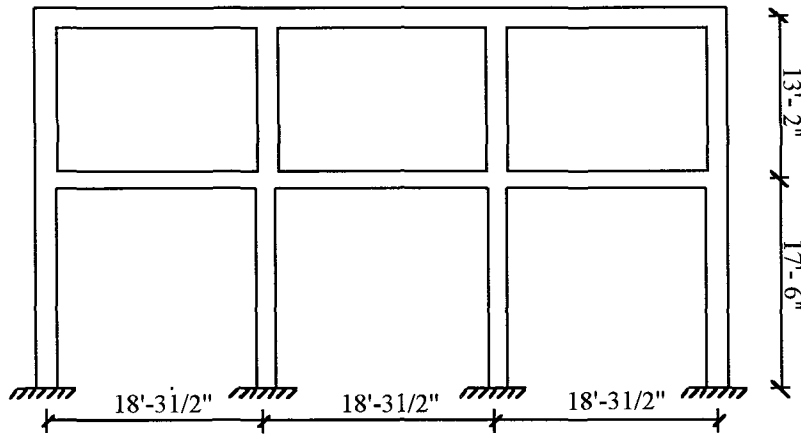


FIGURE 5-2 Elevation of frames A and B in figure 5-1

5.1.1 Fragility Curves

Results are obtained for the ensemble mean and variance of the Park and Ang damage index at different ground motion levels. The program IDARC2D (Park et al., 1987, Kunnath and Reinhorn, 1994) is used to obtain the damage index for each time history. Two ground motion parameters are used to characterize the ground motion for the two story building. These are root mean square acceleration (RMS) and average spectral acceleration in the period range 0.1-0.45 sec. An interval of 0.1g between the average spectral acceleration values and 25 cm/sec² between RMS values is used for the generation of artificial time histories. One hundred artificial ground motions are generated at each value of RMS and spectral acceleration. A time step of 0.002 sec was used during the nonlinear time history analysis. The mean and the variance of the strong motion duration are estimated at the mean RMS (equations 3.4 and 3.5). IDARC2D (Park et al., 1987) and IDARC2D (Kunnath and Reinhorn, 1994) are used when the ground motion is characterized by RMS and spectral acceleration respectively.

The statistics of the original Park and Ang (1984) and modified (Kunnath et al., 1992) damage index obtained by simulation are presented in tables 5-II and 5-III respectively. Table 5-II shows the statistics when the ground motion characterized by root mean square acceleration. Table 5-III presents the statistics for the damage index when the ground motion is characterized by average spectral acceleration.

Lognormal distribution with parameters given in tables 5-II and 5-III are used to compute the conditional probabilities of being in different damage states at each value of the ground motion parameter. Figures 5-3 through 5-5 present the fragility curves obtained by plotting these

conditional probabilities against the corresponding values of the ground motion parameter. These figures show the simulated results as well as the fitted fragility curves. These fitted fragility curves are obtained by arbitrarily fitting lognormal distribution functions to the simulation results. Figures 5-3 and 5-4 are the fragility curves associated with root mean square acceleration, figure 5-3 for sites with distances to rupture zone less than 50 km and figure 5-4 for sites with distance greater than 50 km. The parameters of the lognormal distribution functions shown in figures 5-3 and 5-4 are shown in table 5-IV. Figure 5-5 presents the fragility curves associated with the average spectral acceleration in the period range 0.1-0.45 sec. The parameters of the lognormal distribution functions shown in figure 5-5 are shown in table 5-V.

TABLE 5-II Mean and standard deviation of the damage index at the mean value of RMS (in cm/sec²) for the two story building

Mean RMS	Damage Index for distance < 50 Km.		Damage Index for distance > 50 Km.	
	Mean	Standard Deviation	Mean	Standard Deviation
25	0.0421	0.0236	0.0405	0.0231
50	0.0743	0.0311	0.0728	0.0338
75	0.1142	0.0606	0.0991	0.0508
100	0.1506	0.0755	0.1354	0.0665
125	0.1927	0.1099	0.1697	0.1022
150	0.2408	0.1141	0.1934	0.0937
175	0.2837	0.1721	0.2361	0.1246
200	0.3370	0.1986	0.2867	0.1716
225	0.3938	0.2382	0.3479	0.2529
250	0.4269	0.2302	0.3636	0.2291
275	0.4941	0.2964	0.4108	0.2796
300	0.5153	0.2949	0.4299	0.2677
325	0.6154	0.3937	0.4834	0.2718
350	0.6522	0.4103	0.5283	0.3409
375	0.7733	0.4980	0.6206	0.4010
400	0.8401	0.5101	0.6574	0.4121
425	0.8836	0.5414	0.6843	0.4987
450	0.9654	0.5867	0.7241	0.4955
475	0.9737	0.6390	0.8422	0.6739
500	1.1422	0.7303	0.8901	0.5681

TABLE 5-III Mean and standard deviation of the maximum story damage index for spectral acceleration in the period range 0.1-0.45 sec for the two story building

Average spectral acceleration (g)	Mean Park-Ang damage index	Standard Deviation of Park-Ang damage index
0.1	0.010	0.005
0.2	0.022	0.007
0.3	0.039	0.015
0.4	0.066	0.023
0.5	0.103	0.036
0.6	0.124	0.037
0.7	0.160	0.049
0.8	0.190	0.065
0.9	0.227	0.091
1.0	0.250	0.086
1.1	0.300	0.117
1.2	0.320	0.120
1.3	0.372	0.150
1.4	0.439	0.200
1.5	0.481	0.225
1.6	0.484	0.236
1.7	0.506	0.210
1.8	0.565	0.240
1.9	0.585	0.183
2.0	0.655	0.228
2.1	0.670	0.250
2.2	0.684	0.266
2.3	0.700	0.278
2.4	0.750	0.302
2.5	0.843	0.320

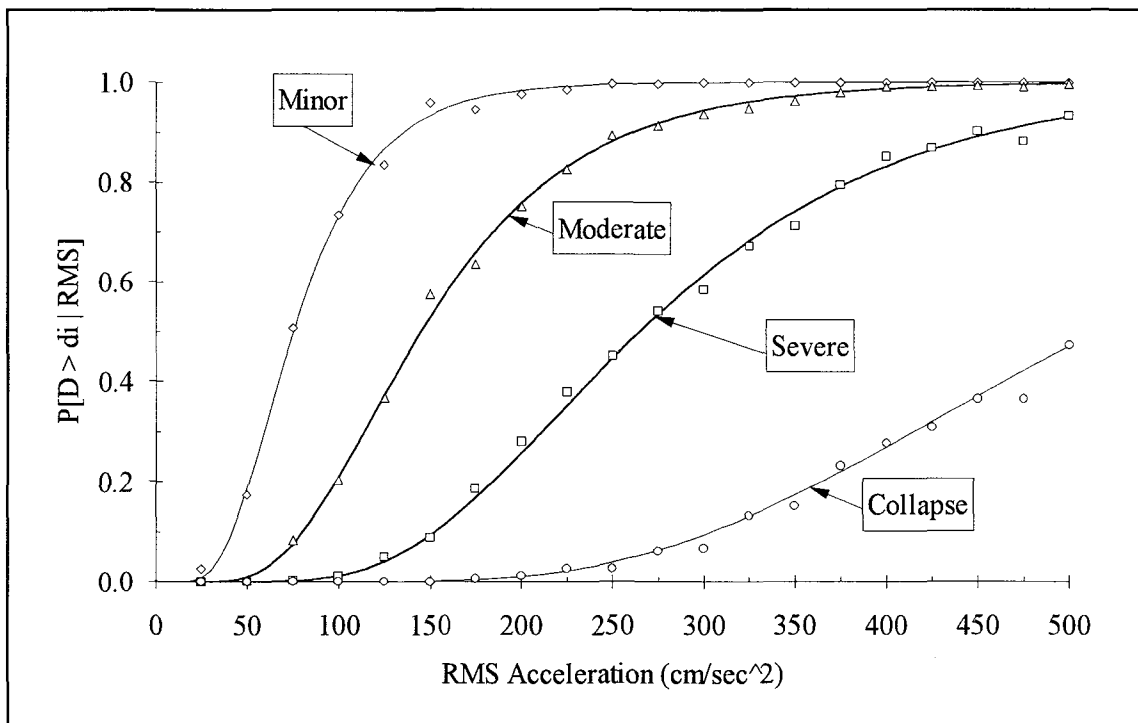


FIGURE 5-3 Simulated and fitted fragility curves for the two story building for sites with distances to rupture zones less than 50 km.

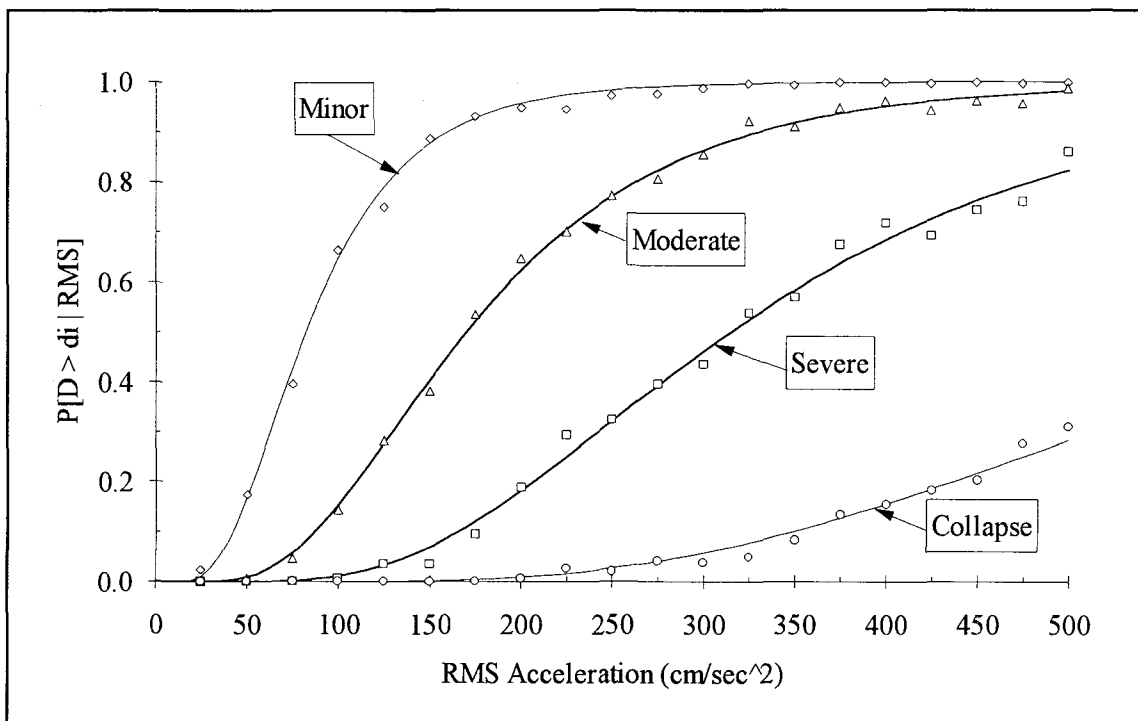


FIGURE 5-4 Simulated and fitted fragility curves for the two story building for sites with distances to rupture zones greater than 50 km.

TABLE 5-IV Parameters of the lognormal distribution functions in figures 5-3 and 5-4

Damage State	Parameters for distance < 50 Km.		Parameters for distance > 50 Km.	
	Median RMS	$\sigma_{\ln(\text{RMS})}$	Median RMS	$\sigma_{\ln(\text{RMS})}$
Minor	75.0	0.46	82.0	0.52
Moderate	140.0	0.46	170.0	0.55
Severe	265.0	0.45	325.0	0.55
Collapse	510.0	0.41	650.0	0.53

TABLE 5-V Parameters of the lognormal distribution functions in figure 5-5

Damage State	Median S_a (g)	$\sigma_{\ln(S_a)}$
Minor	0.52	0.25
Moderate	0.90	0.25
Severe	1.45	0.30
Collapse	3.10	0.30

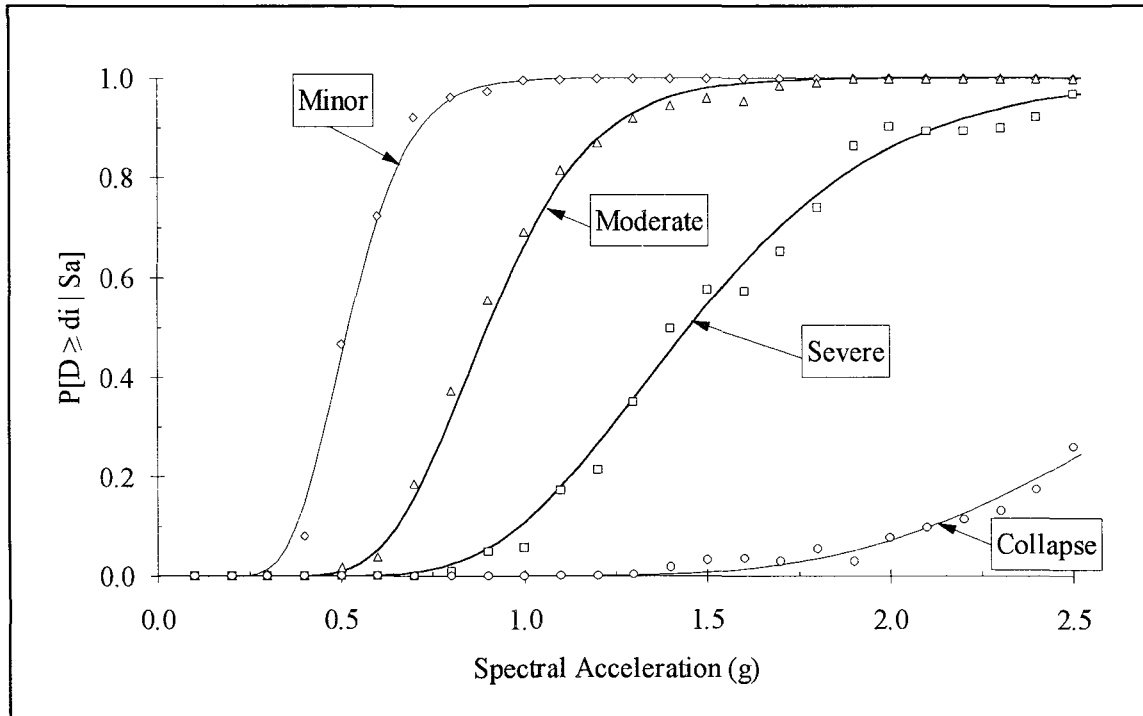


FIGURE 5-5 Simulated and fitted fragility curves for the two story building with ground motion characterized by spectral acceleration in the period range 0.1-0.45 sec.

5.1.2 Damage Probability Matrix

The fragility curves developed in Section 5.1.1, and the relationship between spectral acceleration in the period range $0.1 \leq T \leq 0.45$ sec and modified Mercalli intensity are used to obtain the damage probability matrices. The formulation for obtaining the damage probability matrices was discussed in Section 3.4. The probabilities of being in a particular damage state, at a specified MMI, are presented as a damage probability matrix in table 5-VI.

The damage probability matrices of ATC-13 (1985) were transformed to correspond to the damage states used in this study. The transformed damage probability matrices for ductile and non-ductile reinforced concrete frames are presented in tables 5-VII and 5-VIII respectively. It is observed that the damage probability matrices of ATC-13 are confined to a narrow band whereas the damage probability matrix from this study has a larger band width. Also, the damage probability matrices of ATC-13 show much less damage even at higher levels of MMI.

TABLE 5-VI Damage probability matrix for the two story building

MMI	V	VI	VII	VIII	IX	X	XI	XII
No Damage	97.1	88.9	63.2	20.9	1.2			
Minor	2.4	8.9	26.3	38.7	13.2	0.4		
Moderate	0.5	1.8	8.1	26.9	34.8	7.8	0.1	
Severe		0.4	2.3	12.9	44.6	54.9	13.0	0.3
Collapse			0.1	0.6	6.2	36.9	86.9	99.7

TABLE 5-VII Damage probability matrix for low-rise, ductile moment resisting frames (ATC-13,1985)

MMI	VI	VII	VIII	IX	X	XI	XII
No Damage	2.5						
Minor	97.5	100.0	99.6	63.2	7.3	0.1	
Moderate			0.4	36.8	92.7	99.9	99.5
Severe							0.5
Collapse							

TABLE 5-VIII Damage probability matrix for low-rise, non-ductile moment resisting frames (ATC-13,1985)

MMI	VI	VII	VIII	IX	X	XI	XII
No Damage	2.9						
Minor	97.1	99.0	37.5	2.5	0.4		
Moderate		1.0	62.5	97.5	99.2	85.4	42.1
Severe					0.4	14.6	57.9
Collapse							

5.2 Description of the Six-Story Building

The second example structure is a six story building with reinforced concrete moment resisting frames. The building is again rectangular in plan with sides measuring 192' and 80'. The plan of the building is shown in figure 5-6. The building has five equal bays along the short direction and twelve equal bays along the long direction. Again, as the properties of the beams and columns of the frames in the two directions are similar, earthquake forces along the short direction are considered to be critical to the damage of the building. The elevation of the frames, A and B in figure 5-6, used for analysis is shown in figure 5-7. The typical properties of the beams and columns in frames A and B are shown in table 5-IX.

TABLE 5-IX Properties of beams and columns in frames A and B in figure 5-6

Properties	Beams	Columns
Dimensions	18" x 34"	30" x 30"
Concrete strength	5 ksi	5 ksi
Steel strength	60 ksi	60 ksi

5.2.1 Fragility Curves

Results are obtained for the ensemble mean and variance of the modified Park and Ang (Kunnath et al., 1992) damage index at different ground motion levels. The program IDARC2D (Kunnath and Reinhorn, 1994) is used to obtain the damage index for each time history. The ground motion parameter used for obtaining the fragility curves is the average spectral acceleration in the period range 0.45-0.85 sec. Root mean square acceleration is not used for characterizing the ground motion as it does not embody any ground motion characteristics critical to a specific class of structures. One hundred artificial ground motions are generated at each value of average spectral acceleration. A time step of 0.002 sec was used during the nonlinear time history analysis.

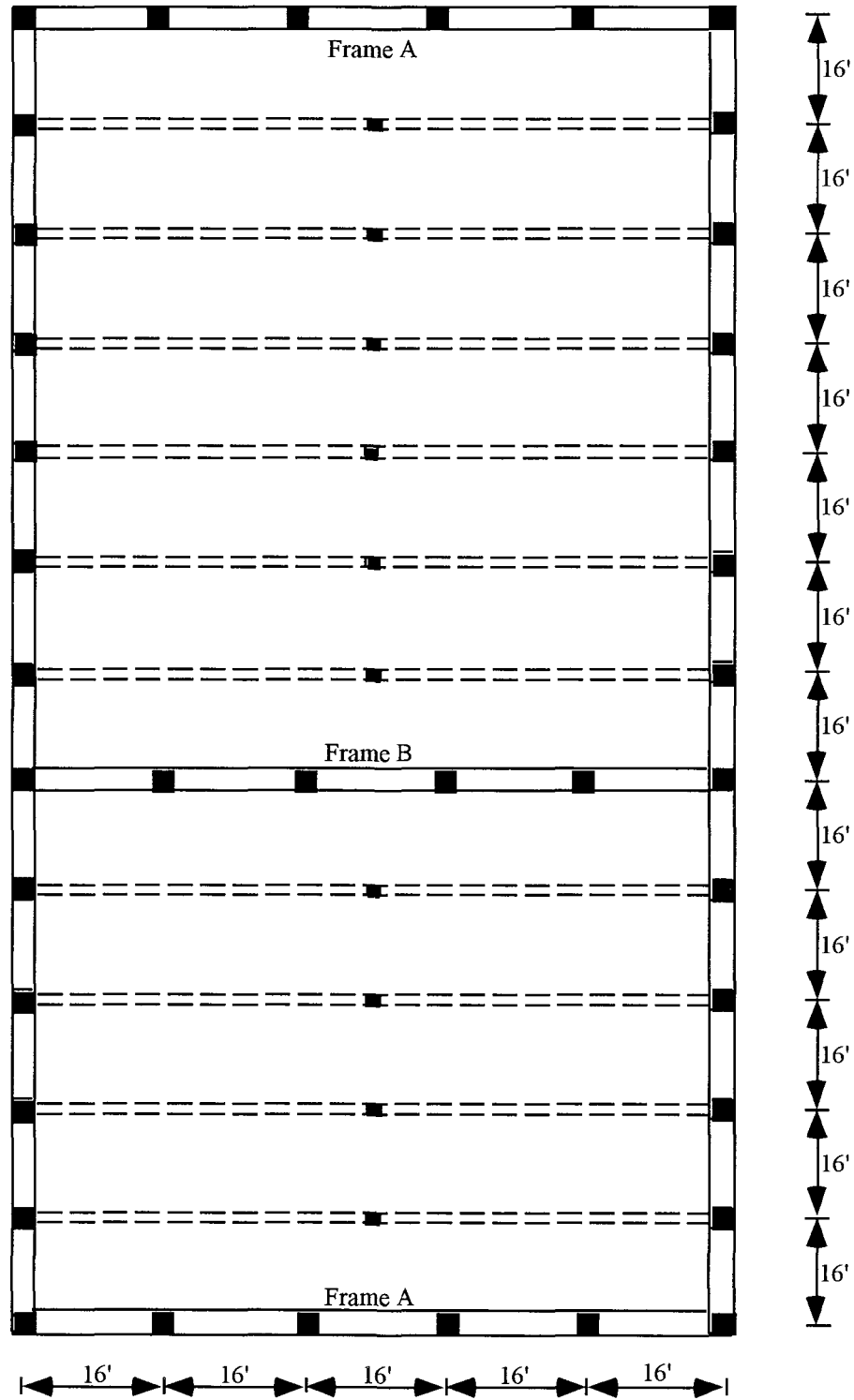


FIGURE 5-6 Typical floor plan of the six story building

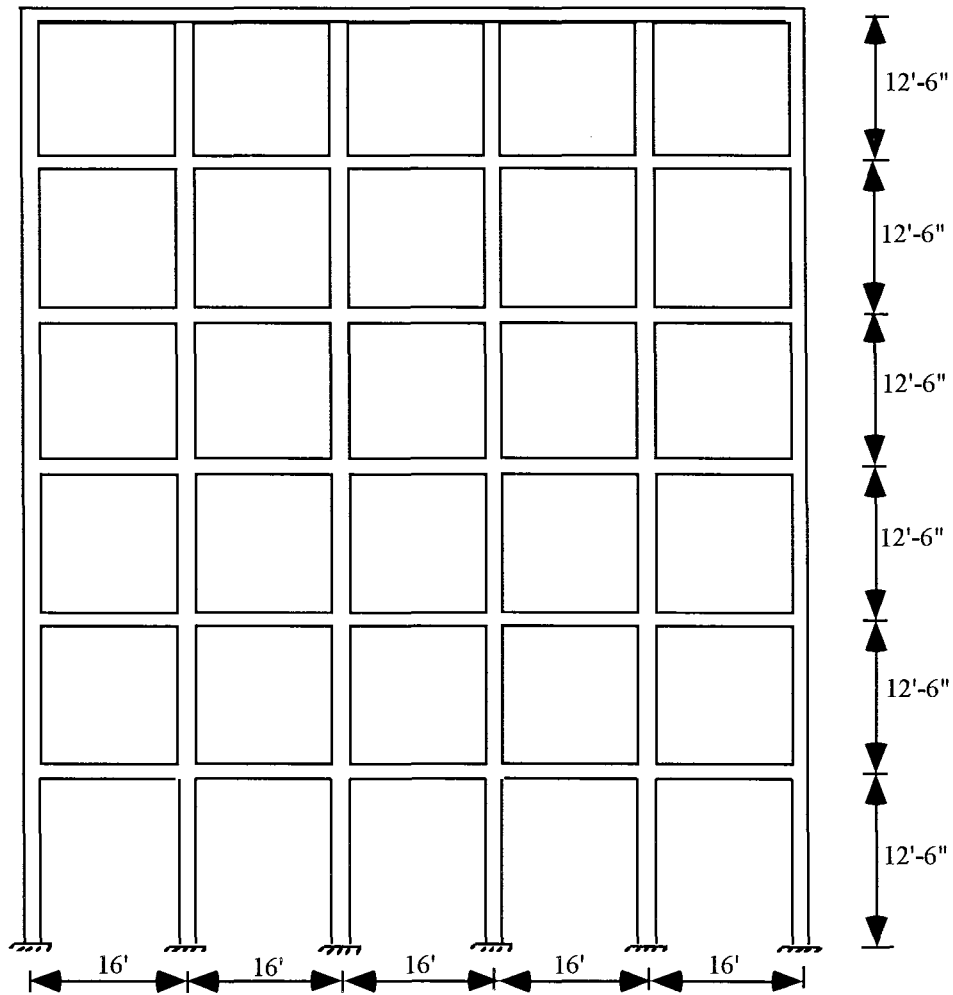


FIGURE 5-7 Elevation of frames A and B in figure 5-6

The statistics of the modified Park and Ang damage index obtained by simulation are presented in table 5-X. Lognormal distribution with parameters given in table 5-X are used to compute the conditional probabilities of being in different damage states at each value of the ground motion parameter. Figure 5-8 presents the fragility curves obtained by plotting these conditional probabilities against the corresponding values of the ground motion parameter. The simulated as well as the fitted fragility curves are shown in figure 5-8. The fitted fragility curves are obtained by arbitrarily fitting lognormal distribution functions to the simulation results. The parameters of these functions are shown in table 5-XI.

TABLE 5-X Mean and standard deviation of the maximum story damage index for the six story building

Average spectral acceleration (g)	Mean Park-Ang damage index	Standard deviation of Park-Ang damage index
0.1	0.020	0.005
0.2	0.043	0.016
0.3	0.065	0.028
0.4	0.095	0.046
0.5	0.121	0.055
0.6	0.153	0.098
0.7	0.179	0.116
0.8	0.210	0.146
0.9	0.235	0.168
1.0	0.275	0.198
1.1	0.303	0.205
1.2	0.337	0.245
1.3	0.376	0.240
1.4	0.421	0.228
1.5	0.451	0.285
1.6	0.463	0.283
1.7	0.533	0.338
1.8	0.576	0.390
1.9	0.629	0.397
2.0	0.685	0.461

TABLE 5-XI Parameters of the lognormal distribution functions in figure 5-8

Damage State	Median S_a (g)	$\sigma_{\ln(S_a)}$
Minor	0.50	0.50
Moderate	0.90	0.45
Severe	1.55	0.48
Collapse	3.30	0.50

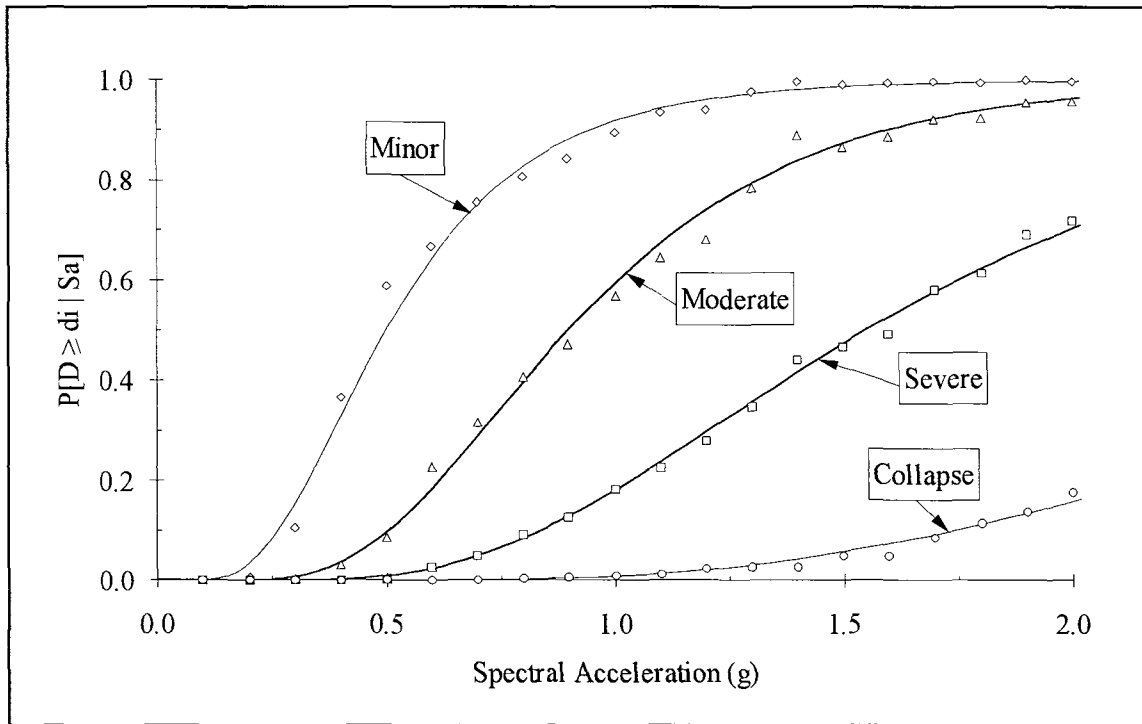


FIGURE 5-8 Simulated and fitted fragility curves for the six story building with ground motion characterized by spectral acceleration in the period range 0.45-0.85 sec.

5.2.2 Damage Probability Matrix

The fragility curves developed in Section 5.2.1, and the relationship between spectral acceleration in the period range $0.45 \leq T \leq 0.85$ sec and modified Mercalli intensity are used to obtain the damage probability matrices. The formulation for obtaining the damage probability matrices was discussed in Section 3.4. The probabilities of being in a particular damage state, at a specified MMI, are presented as a damage probability matrix in table 5-XII.

The damage probability matrices of ATC-13 (1985) were transformed to correspond to the damage states used in this study. The transformed damage probability matrices for ductile and non-ductile reinforced concrete frames are presented in tables 5-XIII and 5-XIV, respectively. It is observed that the damage probability matrices of ATC-13 are confined to a narrow band whereas the damage probability matrix from this study has a larger band width. Also, the damage probability matrices of ATC-13 show much less damage even at higher levels of MMI.

TABLE 5-XII Damage probability matrix for the six story building

MMI	V	VI	VII	VIII	IX	X	XI	XII
No Damage	98.6	93.7	77.5	44.3	12.3	1.1		
Minor	1.2	5.2	16.4	30.8	24.8	5.8	0.3	
Moderate	0.2	0.9	4.7	16.9	31.4	21.3	3.7	0.1
Severe		0.2	1.3	7.2	25.6	44.2	27.5	4.7
Collapse			0.1	0.8	5.9	27.6	68.5	95.2

TABLE 5-XIII Damage probability matrix for mid-rise, ductile moment resisting frames (ATC-13, 1985)

MMI	VI	VII	VIII	IX	X	XI	XII
No Damage	0.3						
Minor	99.7	99.8	91.8	46.7	9.0		
Moderate		0.2	8.2	53.3	91.0	100.0	99.6
Severe							0.4
Collapse							

TABLE 5-XIV Damage probability matrix for mid-rise, non-ductile moment resisting frames (ATC-13, 1985)

MMI	VI	VII	VIII	IX	X	XI	XII
No Damage	0.3						
Minor	99.7	97.2	33.6	1.9	0.2		
Moderate		2.8	66.4	98.1	98.5	73.6	28.4
Severe					1.3	26.4	71.2
Collapse							0.4

5.3 Description of the Thirteen-Story Building

The third example structure is a thirteen story building with reinforced concrete moment resisting frames. The building is rectangular in plan with sides measuring 189' and 72'. The plan of the building is shown in figure 5-9. The building has two equal bays along the short direction and

seven equal bays along the long direction. Again, as the properties of the beams and columns of the frames in the two directions are similar, earthquake forces along the short direction are considered to be critical to the damage of the building. The elevation of the frames (A and B in figure 5-9) used for analysis is shown in figure 5-10. The typical properties of the beams and columns in frames A and B are shown in table 5-XV.

TABLE 5-XV Properties of beams and columns in frames A and B in figure 5-9

Properties	Beams	Columns
Dimensions	18" x 39" (Frame A) 24" x 33" (Frame B)	36" x 24" (Exterior) 36" x 36" (Interior)
Concrete strength	3.75 ksi	3.75 ksi
Steel strength	60 ksi	60 ksi

5.3.1 Fragility Curves

Results are obtained for the ensemble mean and variance of the modified Park and Ang (Kunnath et al., 1992) damage index at different ground motion levels. The program IDARC2D (Kunnath and Reinhorn, 1994) is used to obtain the damage index for each time history. The ground motion parameter, used for obtaining the fragility curves, is the average spectral acceleration in the period range 0.85-2.5 sec. Root mean square acceleration is again not used for characterizing the ground motion as it does not include any ground motion characteristics important for a specific class of structures. One hundred artificial ground motions are generated at each value of average spectral acceleration. A time step of 0.002 sec was used during the nonlinear time history analysis.

The statistics of the modified Park and Ang damage index obtained by simulation are presented in table 5-XVI. Lognormal distribution with parameters given in table 5-XVI are used to compute the conditional probabilities of being in different damage states at each value of the ground motion parameter. Figure 5-11 presents the fragility curves obtained by plotting these conditional probabilities against the corresponding values of the ground motion parameter. The simulated as well as the fitted fragility curves are shown in figure 5-11. The fitted fragility curves are obtained by arbitrarily fitting lognormal distribution functions to the simulation results. The parameters of these lognormal distribution functions are shown in table 5-XVII.

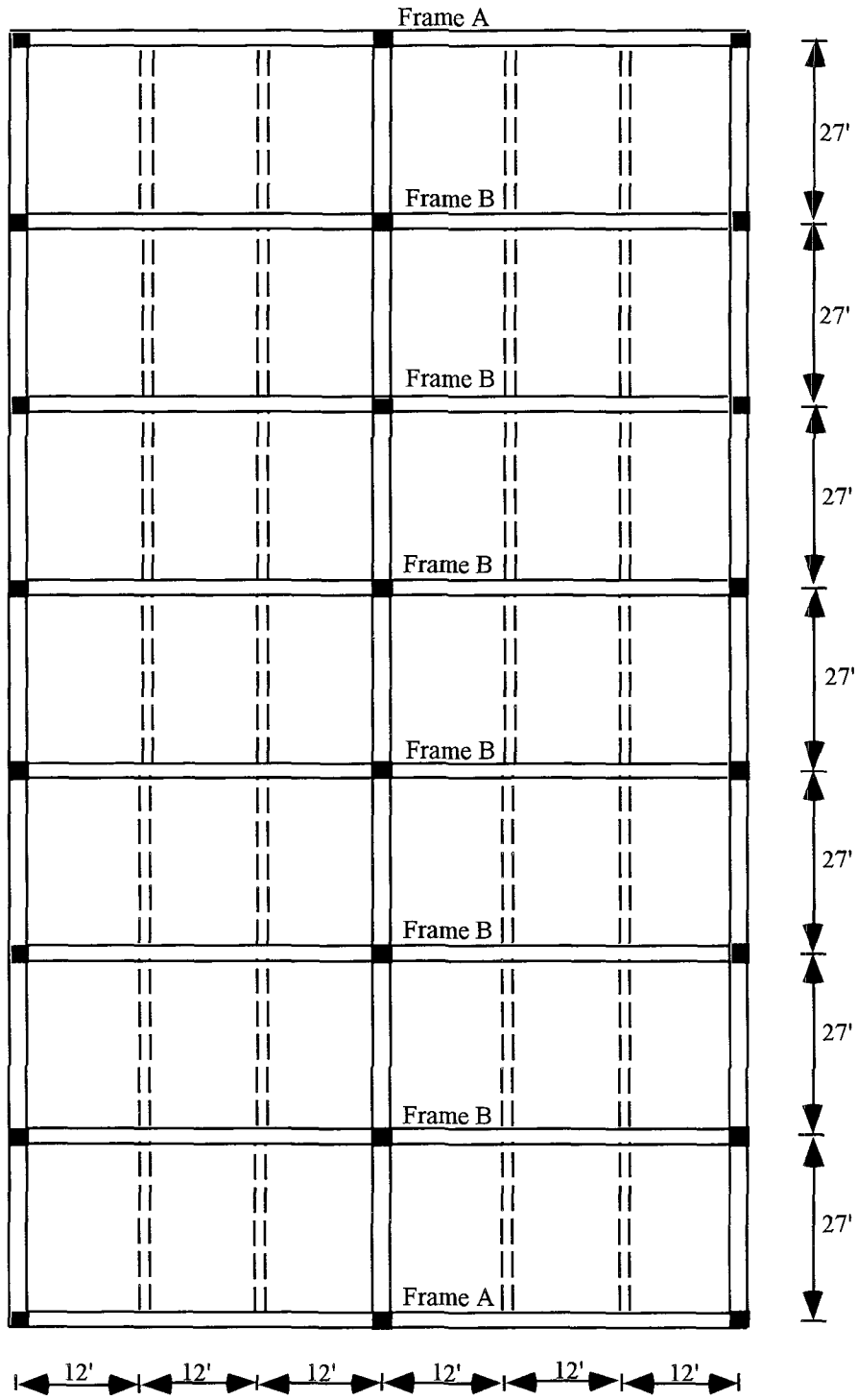


FIGURE 5-9 Typical floor plan of the thirteen story building

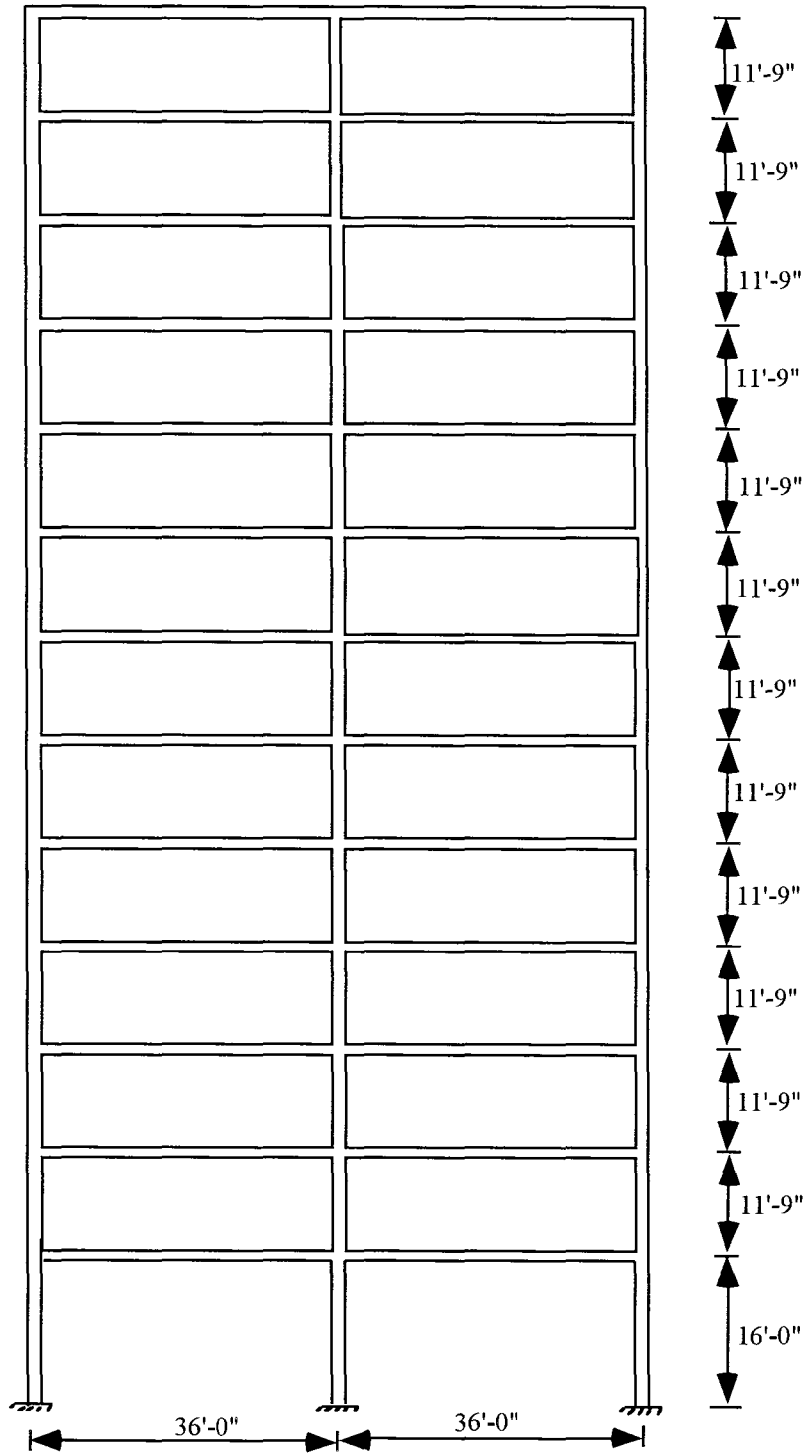


FIGURE 5-10 Elevation of frames A and B in figure 5-9

TABLE 5-XVI Mean and standard deviation of the maximum story damage index for the thirteen story building

Average spectral acceleration (g)	Mean Park-Ang damage index	Standard deviation of Park-Ang damage index
0.1	0.013	0.005
0.2	0.033	0.017
0.3	0.056	0.022
0.4	0.089	0.045
0.5	0.117	0.058
0.6	0.134	0.060
0.7	0.180	0.101
0.8	0.199	0.089
0.9	0.224	0.094
1.0	0.271	0.161
1.1	0.302	0.164
1.2	0.326	0.165
1.3	0.345	0.164
1.4	0.385	0.231
1.5	0.429	0.239
1.6	0.463	0.269
1.7	0.505	0.285
1.8	0.525	0.320
1.9	0.564	0.309
2.0	0.617	0.318

TABLE 5-XVII Parameters of the lognormal distribution functions in figure 5-11

Damage State	Median S_a (g)	$\sigma_{\ln(S_a)}$
Minor	0.49	0.37
Moderate	0.89	0.43
Severe	1.58	0.41
Collapse	2.80	0.30

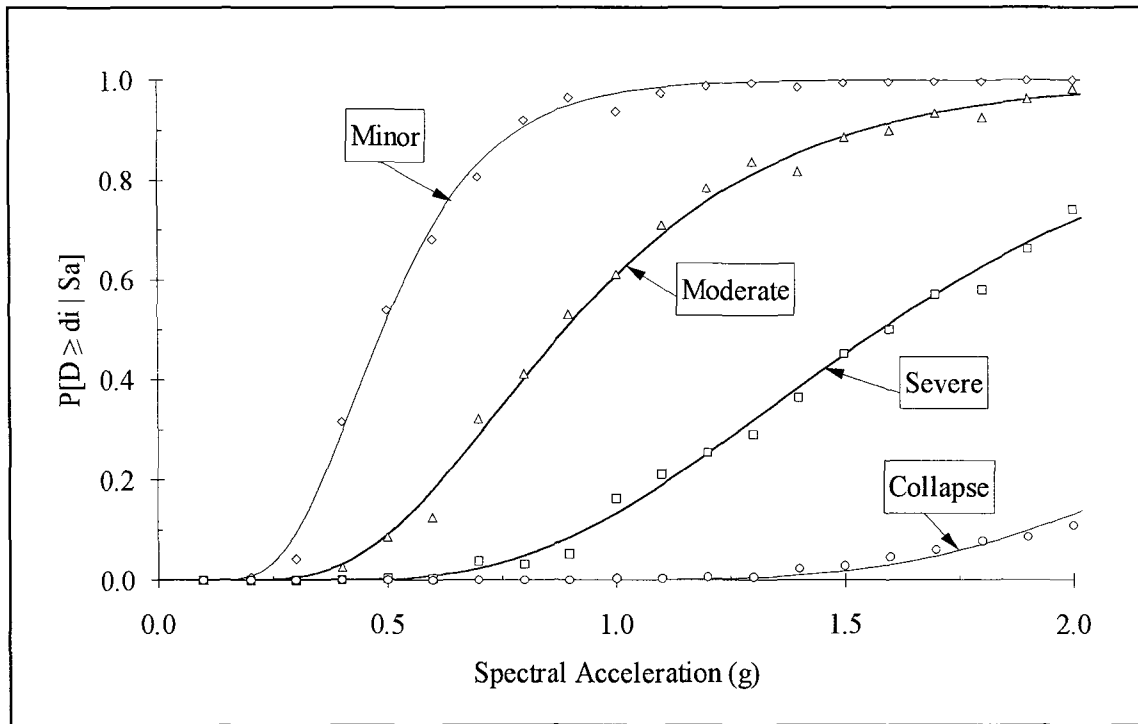


FIGURE 5-11 Simulated and fitted fragility curves for the thirteen story building with ground motion characterized by spectral acceleration in the period range 0.85-2.5 sec.

5.3.2 Damage Probability Matrix

The fragility curves developed in Section 5.3.1 and the relationship between spectral acceleration, in the period range $0.85 \leq T \leq 2.5$ sec, and modified Mercalli intensity are used to obtain the damage probability matrices. The formulation for obtaining the damage probability matrices was discussed in Section 3.4. The probabilities of being in a particular damage state, at a specified MMI, are presented as a damage probability matrix in table 5-XVIII.

The damage probability matrices of ATC-13 (1985) were transformed to correspond to the damage states used in this study. The transformed damage probability matrices for ductile and non-ductile reinforced concrete frames are presented in tables 5-XIX and 5-XX respectively. It is observed that the damage probability matrices of ATC-13 are confined to a narrow band whereas the damage probability matrix from this study has a larger band width. Also, the damage probability matrices of ATC-13 show much less damage at higher levels of MMI.

TABLE 5-XVIII Damage probability matrix for the thirteen story building

MMI	V	VI	VII	VIII	IX	X	XI	XII
No Damage	100.0	99.1	99.0	86.9	30.3	0.6		
Minor		0.1	0.9	11.0	44.2	14.3	0.2	
Moderate			0.1	2.0	21.9	40.6	3.7	
Severe				0.1	3.6	39.9	23.3	0.1
Collapse						4.6	72.8	99.9

TABLE 5-XIX Damage probability matrix for high-rise, ductile moment resisting frames (ATC-13, 1985)

MMI	VI	VII	VIII	IX	X	XI	XII
No Damage							
Minor	100.0	100.0	83.6	27.6	3.1	0.4	0.1
Moderate			16.4	72.4	96.9	99.2	96.4
Severe						0.4	3.5
Collapse							

TABLE 5-XX Damage probability matrix for high-rise, non-ductile moment resisting frames (ATC-13, 1985)

MMI	VI	VII	VIII	IX	X	XI	XII
No Damage	0.1						
Minor	99.9	91.5	32.2	3.0			
Moderate		8.5	67.8	97.0	94.1	61.7	12.5
Severe					5.9	38.3	84.3
Collapse							3.2

5.4 Comparison of Results

The fragility curves for the three example buildings, developed in Sections 5.1.1, 5.2.1 and 5.3.1, are associated with the average spectral acceleration in three different period bands. Thus, it is difficult to directly compare the relative vulnerabilities of the three buildings using the fragility curves. The comparison of the damage probability matrices for the three buildings reveals that the vulnerabilities of the buildings decrease with height. The damage probability matrices for concrete moment resisting frames in ATC-13 (1985) suggest an increase in vulnerability of

moment resisting frames with height. The P-delta effect, not considered in this study while performing the nonlinear dynamic analysis, could partially explain the trend observed in this study. It is anticipated that consideration of the P-delta effect will produce results that have the same trend as those in ATC-13, as this effect will increase the damageability of the structures with height.

The fragility curves and damage probability matrices, for the three classes of reinforced concrete frames, developed in this study are obtained using a representative building in each class. In order to obtain more general results, additional example buildings in each class need to be analyzed.

The average value of the spectral acceleration, obtained over a period band, is used to characterize the ground motion for the three classes of reinforced concrete frames. However, the spectrum is likely to vary considerably over the period band. Thus, buildings with natural periods close to the edges of the period bands will show different behavior compared to those buildings whose natural periods are away from the edges. This effect will be more pronounced for the high-rise structures as the period band is large and the dynamic amplification factors, shown in figure 3-1, vary considerably at the two bounds of the band.

5.5 Comments on Damage Measures

In this study, the measures of damage that have been used are the original Park-Ang (1984) and the modified (Kunnath et al., 1992) damage indices. Another possible measure of structural damage is the interstory drift ratio. In this section, the simulation results obtained in this study are used to compare these two measures of damage for the three example buildings.

Figures 5-12 through 5-14 present the relationships between the mean maximum Park-Ang story damage indices and the mean maximum interstory drift ratios for the three example buildings. Linear relationships are observed between these two parameters for all three buildings. The Park-Ang damage index as expressed by equations 1.12 and 2.5 represent a linear combination of damage due to maximum deformation and dissipated hysteretic energy. However, figures 5-12 through 5-14 suggest that the contribution of the hysteretic energy dissipation part of that index is captured by the interstory drift.

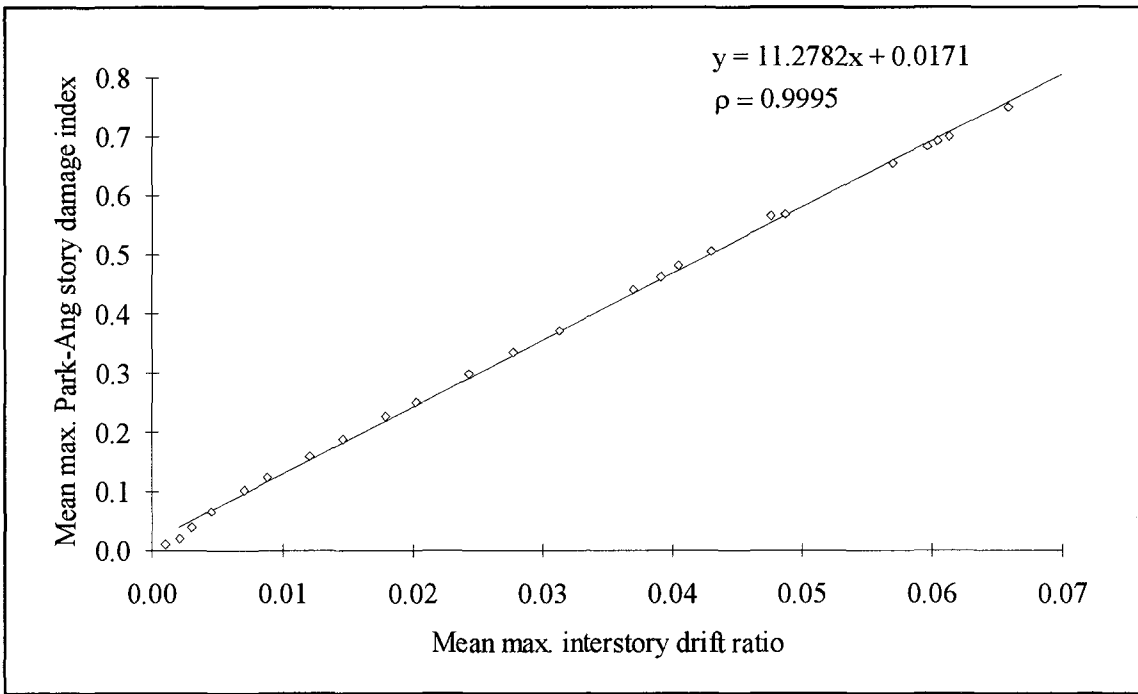


FIGURE 5-12 Relationship between Park-Ang damage index and interstory drift ratio for the two story building

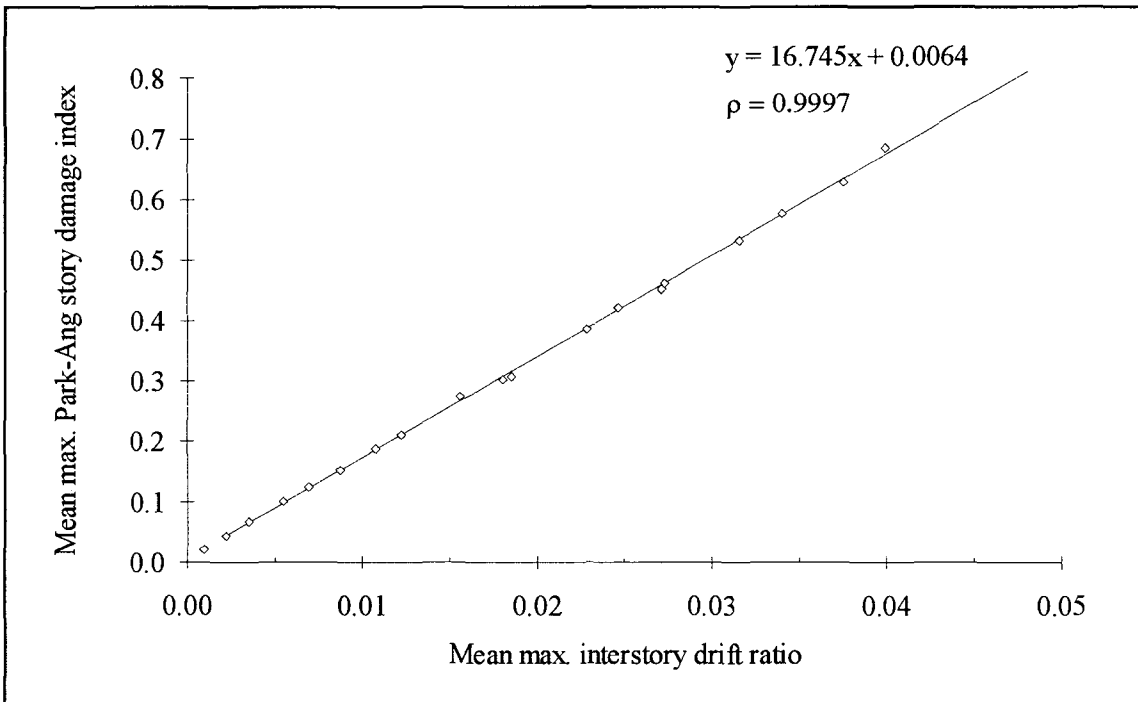


FIGURE 5-13 Relationship between Park-Ang damage index and interstory drift ratio for the six story building

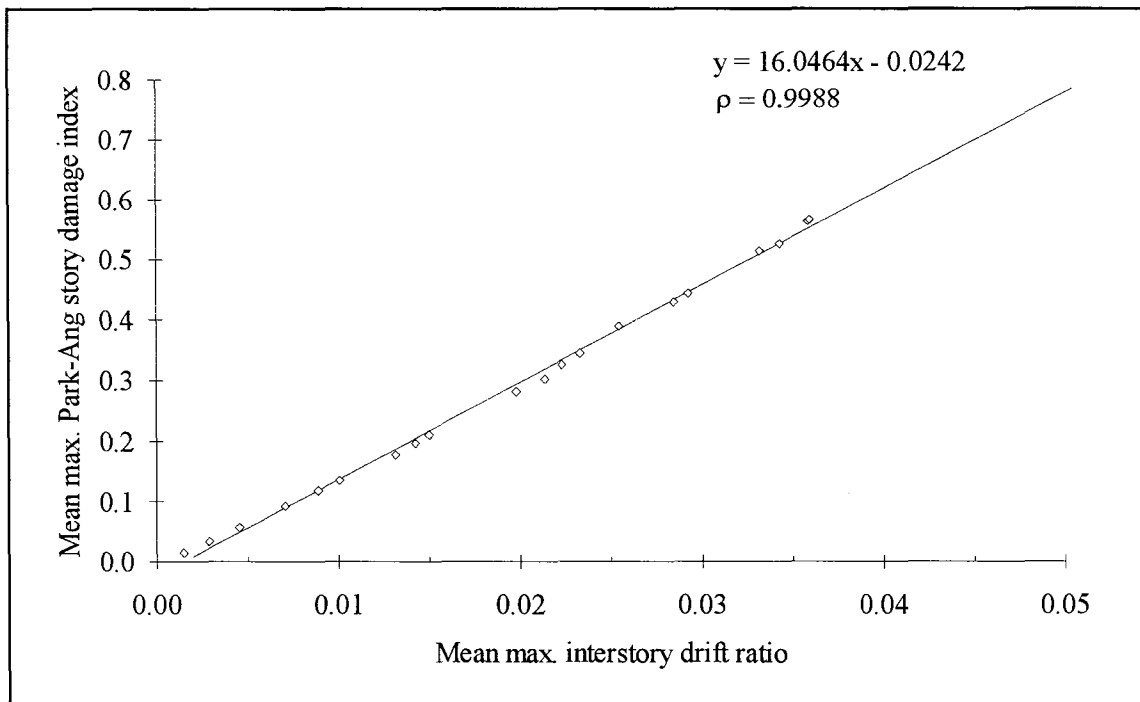


FIGURE 5-14 Relationship between Park-Ang damage index and interstory drift ratio for the thirteen story building



SECTION 6

SUMMARY AND FUTURE WORK

6.1 Summary

This study demonstrates that generic fragility curves and damage probability matrices can be generated using simulation methods. Various ground motion characterizations along with the different structural damage indices are reviewed. Root mean square (RMS) acceleration, average spectral acceleration in three different period bands corresponding to low, mid and high rise concrete frames, and modified Mercalli intensity are used as the ground motion characterizations. The original (1984) and the modified (Kunnath et al., 1992) Park-Ang damage indices are used to characterize the structural damage.

The program IDARC2D (Park et al., 1987, Kunnath and Reinhorn, 1994) is used for the inelastic dynamic analysis and the computation of the Park and Ang damage index. The computation of the fragility curves and the damage probability matrices requires an ensemble of time histories for specified ground motion parameters. The Latin Hypercube sampling technique is used to reduce the number of samples required in the ensemble.

Various techniques for the simulation of ground motion are briefly reviewed. In this study, time histories are generated using Gaussian stationary models with modulating functions, and ARMA models. Gaussian models are used for the generation of time histories corresponding to a specified spectral acceleration. Trapezoidal modulating functions are used to introduce the nonstationarity. ARMA models are used for the generation of time histories associated with a Kanai-Tajimi (Tajimi, 1960) power spectral density. The nonstationarity in the time domain is incorporated using the Shinozuka-Sato (1967) envelope function. The parameters of the envelope are chosen so as to produce a time history with the required RMS.

As examples of the approach considered in this study, fragility curves and damage probability matrices are developed for buildings corresponding to low, mid and high rise structures. The buildings selected include two, six and thirteen story structures which were selected for their plan and elevation regularity so as to represent "average" behavior of buildings in their respective structural classes. However, it is difficult to generalize the fragility curves and the damage probability matrices, obtained in this study, as those corresponding to "average" low, mid and high rise frames. More example buildings in each category are required to generalize the results.

The Park and Ang damage index is used to identify the different damage states. Another possible measure of structural damage is the interstory drift ratio. The relationships between the mean maximum Park-Ang story damage indices and the mean maximum interstory drift ratios, for the three example buildings, are investigated. Linear relationships are observed between these two parameters for all three buildings. The original (1984) and the modified (Kunnath et al., 1992) Park-Ang damage indices, as expressed by equations 1.12 and 2.5 respectively, represent a linear combination of damage due to maximum deformation and dissipated hysteretic energy. However, linear relationships between the Park-Ang index and the interstory drift ratio suggest that the contribution of the dissipated hysteretic energy to the global damage index based on Park and Ang is captured by the inter-story drift component of the equation.

The P-delta effect is not considered, in this study, while performing the nonlinear dynamic analysis. This effect will increase the damageability of the structures with height. Thus, it is expected that consideration of the P-delta effect will produce results that have the same trend as that in ATC-13 (1985).

The average value of the spectral acceleration, obtained over a period band, is used to characterize the ground motion for the three classes of reinforced concrete frames. However, this may not be a very good parameter when individual buildings are considered.

6.2 Future Work

The validity of the fragility curves and damage probability matrices, developed in this study, still remains to be assessed. Ideally, such curves and matrices should be developed from observed damage data. However, such data are very limited and usually not in the proper format to generate these curves and matrices.

The variations in the fragility curves due to plan and elevation irregularities need to be determined. The program IDARC2D (Park et al., 1987, Kunnath and Reinhorn, 1994) is incapable of performing a three dimensional analysis. Thus, a procedure for incorporating plan irregularity needs to be investigated. Also, the P-delta effect will be included while performing the nonlinear dynamic analysis.

An enormous computational effort is required in evaluating the fragility curves through simulation. Procedures for obtaining the fragility curves with reduced computational effort need to be investigated. Techniques for combining expert judgment with simulation results also need

to be investigated. The Bayesian technique is an approach to update the parameters of the distributions of the damage measure with the simulation results. A brief overview of the Bayesian technique is provided in Appendix A. The damage states given in ATC-13 (1985) will be correlated to the Park and Ang damage index. This correlation will be used to obtain "prior" estimates of the parameters of the probability distributions of the Park and Ang damage index at various levels of ground motion for the different classes of moment resisting reinforced frames defined in ATC-13. The parameters of the probability distributions of the Park and Ang damage index at various levels of ground motion, developed using the methodology presented in this study, will be used to evaluate the likelihood functions in the Bayesian updating technique. Gunturi (1992) provides some preliminary information on the correlation between the monetary loss used to define the damage states in ATC-13 and the structural damage indices. The posterior distributions of the parameters will be determined and used to update fragility curves and damage probability matrices.

SECTION 7

REFERENCES

1. Arias, A., (1970), "A measure of earthquake intensity", *Seismic Design of Nuclear Power Plants*, R. Hansen, Editor, M.I.T. Press, pp. 438-483.
2. ATC 3-06, (Tentative 1978), "Tentative provisions for the development of seismic regulations for buildings", *Applied Technology Council*, NBS Special Publication 510, NSF Publication 78-08.
3. ATC-13, (1985), "Earthquake damage evaluation data for California", *Applied Technology Council*.
4. Ayyub, B.M., and Lai, K-L., (1989), "Structural reliability assessment using Latin Hypercube sampling", *Proceedings of the 5th International conference on Structural Safety and Reliability*, pp. 1177-1184.
5. Bazant, Z.P., and Oh, B.H., (1983a), "Spacing of cracks in reinforced concrete", *Journal of Structural Engineering*, ASCE, Vol. 109, No. 9, pp. 2066-2085.
6. Bazant, Z.P., and Oh, B.H., (1983b), "Crack spacing in reinforced concrete: approximate solution", *Journal of Structural Engineering*, ASCE, Vol. 109, No. 1, pp. 93-108.
7. Beshara, F.B.A., (1993), "Smearred crack analysis for reinforced concrete structures under blast-type loading", *Engineering Fracture Mechanics*, Vol. 45, No. 1, pp. 119-140.
8. Bolt, B.A., (1973), "Duration of strong ground motions", *Proceedings 5th World Conference on Earthquake Engineering*, Vol. 1, pp. 1304-1313, Rome, Italy.
9. Chung, Y.S., Meyer, C., and Shinozuka, M., (1987), "Seismic assessment of reinforced concrete members", *NCEER-87-0022 National Center for Earthquake Engineering Research*, State University of New York at Buffalo.
10. Chung, Y.S., Meyer, C., and Shinozuka, M., (1989), "Modeling of concrete damage", *ACI Structural Journal*, Vol. 86, No. 3, pp. 259-271.
11. Chung, Y.S., Meyer, C., and Shinozuka, M., (1990), "Automatic seismic design of reinforced concrete building frames", *ACI Structural Journal*, Vol. 87, No. 3, pp. 326-340.
12. Conte, J.P., Pister, K.S., and Mahin, S.A., (1992), "Nonstationary ARMA modeling of seismic motions", *Soil Dynamics and Earthquake Engineering*, November, pp. 411-426.
13. DiPasquale, E., and Cakmak, A.S., (1990), "Seismic damage assessment using linear models", *Soil Dynamics and Earthquake Engineering*, Vol. 9, No. 4, pp. 194-215.

14. Galambos, T.V., Ellingwood, B., MacGregor, J.G., and Cornell, C.A., (1982), "Probability based load criteria : Assessment of current design practice", *Journal of the Structural Division*, ASCE, Vol. 108, No. ST5, pp. 959-977.
15. Gere, J., and Shah, H.C., (1984), "Terra Non Ferma - understanding and preparing for earthquakes", W.H. Freeman and Co., San Francisco, California, 1984.
16. Gergely, P., and Lutz, L.A., (1968) "Maximum crack width in reinforced concrete flexural members", *Causes, Mechanism, and Control of Cracking in Concrete*, SP-20, American Concrete Institute, Detroit, pp. 87-117.
17. Gunturi, S.K., (1992), "Building specific earthquake damage estimation", *Ph.D. Thesis* submitted to Stanford University.
18. Hatamoto, H., Chung, Y.S., and Shinozuka, M., (1990), "Seismic capacity enhancement of R/C frames by means of damage control design", *Proceedings of Fourth U.S. National Conference on Earthquake Engineering*, Vol. 2, Palm Springs, California, May 20-24, pp. 279-288.
19. Housner, G.W., (1952), "Intensity of ground motion during strong earthquake", *Earthquake Research Laboratory*, California Institute of Technology, Pasadena, California, August.
20. Housner, G.W., and Jennings, P.C., (1964), "Generation of artificial earthquakes", *Journal of the Engineering Mechanics Division*, ASCE, Vol. 90, No. EM1, pp. 113-150.
21. Housner, G.W., (1990), "Competing against time", *Report to Governor George Deukmejian* from the Governor's Board of Inquiry on the 1989 Loma Prieta Earthquake, May.
22. Huang, H.H.M., and Jaw, J-W., (1989), "Seismic fragility analysis of shear wall structures", *Proceedings of the 5th International Conference on Structural Safety and Reliability*, pp. 399-406.
23. Jennings, P.C., (1971), "Engineering features of the San Fernando earthquake of February 9, 1971", *EERL 71-02*, Earthquake Engineering Research Laboratory, Pasadena, California.
24. Kiremidjian, A.S., and Shah, H.C., (1980), "Probabilistic site-dependent response spectra", *Journal of Structural Engineering*, ASCE, Vol. 106, No. ST1, pp. 69-86.
25. Kiremidjian, A.S., (1985), "Subjective probabilities for earthquake damage and loss", *Structural Safety*, Vol. 2, pp. 309-317.
26. Kunnath, S.K., Reinhorn, A.M., and Lobo, R.F., (1992), "IDARC Version 3.0: A program for the inelastic damage analysis of reinforced concrete structures", *NCEER-92-0022*, National Center for Earthquake Engineering Research, State University of New York at Buffalo.

27. Kunnath, S.K., and Reinhorn, A.M.,(1994), "IDARC2D Version 3.1: Inelastic damage analysis of RC building structures, Users Manual", Department of Civil Engineering, State University of New York at Buffalo, September.
28. Lai, S-S.P., (1982), "Statistical characterization of strong ground motions using power spectral density function", *Bulletin of the Seismological Society of America*, Vol. 72, No. 1, pp. 259-274.
29. Liu, S.C., and Jhaveri, D.P., (1969), "Spectral simulation and earthquake site properties", *Journal of the Engineering Mechanics Division*, ASCE, Vol. 95, No. EM5, pp. 1145-1168.
30. Liu, S.C., (1970), "Evolutionary power spectral density of strong motion earthquake", *Bulletin of the Seismological Society of America*, Vol. 60, No. 3, pp. 891-900.
31. Manual for Repair Methods of Civil Engineering Structures Damaged by Earthquakes, (1987), Published by the Public Works Research Institute, Ministry of Construction, December.
32. McCann, M.W., (1980), "RMS acceleration and duration of strong ground motion", *John A. Blume Earthquake Engineering Center Report No. 46*, Department of Civil Engineering, Stanford University, October.
33. Murphy, L.M., (1973), "San Fernando California earthquake of February 9, 1971", U.S. Department of Commerce, National Oceanic and Atmospheric Administration, Washington, D.C.
34. Nau, R.F., Oliver, R.M., and Pister, K.S., (1982), "Simulating and analyzing artificial nonstationary ground motions", *Bulletin of the Seismological Society of America*, Vol. 72, No. 2, pp. 615-636.
35. Nielsen, S.R.K., Koyluoglu, H.U., and Cakmak, A.S., (1992), "One and two-dimensional maximum softening damage indicators for reinforced concrete structures under seismic excitation", *Soil Dynamics and Earthquake Engineering*, Vol. 11, No. 4, pp. 435-443.
36. Nigam, N.C., (1983), "Introduction to random vibrations", MIT Press, Cambridge, Massachusetts.
37. Ogawa, S., Elms, D.G., and Paulay, T., (1988), "A simplified procedure for assessing failure probabilities of reinforced concrete frame buildings under earthquake loading", 88-11, Department of Civil Engineering, University of Canterbury, Christchurch, New Zealand.
38. Oh, B.H., and Kang, Y-J, (1987), "New formulas for maximum crack width and crack spacing in reinforced concrete flexural members", *ACI Structural Journal*, March-April, pp. 103-112.

39. Park, Y-J., Ang, A.H-S., and Wen, Y.K., (1984), "Seismic damage analysis and damage-limiting design of RC buildings", *Structural Research Series, Report No. UILU-ENG-84-2007*, University of Illinois at Urbana-Champaign, Urbana, Illinois, Oct.
40. Park, Y-J., and Ang, A.H-S., (1985a), "Mechanistic seismic damage model for reinforced concrete", *Journal of Structural Engineering*, ASCE, Vol. 111, No. 4, pp. 722-739.
41. Park, Y-J., and Ang, A.H-S., (1985b), "Seismic damage analysis of reinforced concrete buildings", *Journal of Structural Engineering*, ASCE, Vol. 111, No. 4, pp. 740-757.
42. Park, Y.J., Ang, A.H-S., and Wen, Y.K., (1987), "Damage-limiting aseismic design of buildings", *Earthquake Spectra*, Vol. 3, No. 1, pp. 1-26.
43. Park, Y.J., Reinhorn, A.M., and Kunnath, S.K., (1987), "IDARC : Inelastic damage analysis of reinforced concrete Frame - Shear-Wall structures", *NCEER-87-0008*, National Center for Earthquake Engineering Research, State University of New York at Buffalo.
44. Polhemus, N.W., and Cakmak, A.S., (1981), "Simulation of earthquake ground motions using autoregressive moving average (ARMA) models", *Earthquake Engineering and Structural Dynamics*, Vol. 9, pp. 343-354.
45. Powell, G.H., and Allahabadi, R., (1988), "Seismic damage prediction by deterministic methods : concepts and procedures", *Earthquake Engineering and Structural Dynamics*, Vol. 16, pp. 719-734.
46. Shakal, A.F., Huang, M.J., Reichle, M., Ventura, C.E., Cao, T.Q., Sherburne, R.W., Savage, M., Darragh, R., and Petersen, C., (1989), "CSMIP strong-motion records from the Santa Cruz Mountains (Loma Prieta), California earthquake of 17 October 1989", *Report No. OSMS 89-06*, California Strong Motion Instrumentation Program, Division of Mines and Geology, California Department of Conservation, November 17.
47. Shakal, A.F., Huang, M.J., Ventura, C.E., Parke, D.L., Cao, T.Q., Sherburne, R.W., and Blazquez, R., (1987), "CSMIP strong-motion records from the Whittier, California earthquake of 1 October 1987", *Report No. OSMS 87-05*, California Strong Motion Instrumentation Program, Division of Mines and Geology, California Department of Conservation, October 31.
48. Shakal, A.F., Huang, M.J., Parke, D.L., and Sherburne, R.W., (1985), "Processed data from the strong-motion records of the Morgan Hill earthquake of 24 April 1984", *Report No. OSMS 85-04*, California Strong Motion Instrumentation Program, Division of Mines and Geology, California Department of Conservation, May.

49. Shahrooz, B.M., and Moehle, J.P., (1990), "Evaluation of seismic performance of reinforced concrete frames", *Journal of Structural Engineering*, ASCE, Vol. 116, No. 5, pp. 1403-1422.
50. Shinozuka, M., and Sato, Y., (1967), "Simulation of nonstationary random process", *Journal of the Engineering Mechanics Division*, ASCE, Vol. 93, No. EM1, pp. 11-40.
51. Shinozuka, M. and Deodatis G., (1991), "Simulation of stochastic processes by spectral representation", *Applied Mechanics Reviews*, ASME, Vol. 44, No. 4, pp. 191-204.
52. SIMQKE, (1976), User's Manual and Documentation, Department of Civil Engineering, Massachusetts Institute of Technology, November.
53. Suzuki, S., and Kiremidjian, A.S., (1989), "Risk-consistent ground motions from a geophysical source and source to site model", *Proceedings of the 7th Japan Society of Civil Engineers Conference*, Tokyo, Japan.
54. The Morgan Hill Earthquake of April 24, 1984, (1985), *Earthquake Spectra*, EERI, Vol. 1, Number 3, May.
55. The Whittier Narrows Earthquake of October 1, 1987, (1988), *Earthquake Spectra*, EERI, Vol. 4, Number 1.
56. Tajimi, H., (1960), "A standard method of determining the maximum response of a building structure during an earthquake", *Proceedings 2nd World Conference on Earthquake Engineering*, Vol. 2, pp. 781-798.
57. Trifunac, M.D., and Brady, A.G., (1975), "A study on the duration of strong earthquake ground motion", *Bulletin of the Seismological Society of America*, Vol. 65, No. 3, pp. 581-626.
58. Vanmarcke, E.H., and Lai, S-S.P., (1980), "Strong-motion duration and RMS amplitude of earthquake records", *Bulletin of the Seismological Society of America*, Vol. 70, No. 4, pp. 1293-1307.

APPENDIX A
BAYESIAN TECHNIQUE

Bayes' theorem provides an approach for updating subjective knowledge with experimental results. If the experimental outcome is a set of observed values x_1, x_2, \dots, x_n from a population X with underlying probability density function $f_X(x)$, the parameters of the distribution, represented by the vector Θ , are revised in light of the experimental results by the following expression:

$$f''(\Theta) = \frac{\left[\prod_{i=1}^n f_X(x_i | \Theta) \right] f'(\Theta)}{\int_{\Theta} \left[\prod_{i=1}^n f_X(x_i | \Theta) \right] f'(\Theta) d\Theta} \quad (\text{A.1})$$

where

$f'(\Theta)$ = prior density function of Θ

$f''(\Theta)$ = posterior density function of Θ

$\Theta = \{\theta_1, \theta_2, \dots, \theta_m\}$

The prior density incorporates all prior knowledge about the unknown parameters. The prior knowledge can be in the form of subjective information. Equation 8.1 can be written as:

$$f''(\Theta) = kL(X|\Theta)f'(\Theta) \quad (\text{A.2})$$

where

$$k = \text{normalizing constant} = \left[\int_{\Theta} \left(\prod_{i=1}^n f_X(x_i | \Theta) \right) f'(\Theta) d\Theta \right]^{-1}$$

$$L(X | \Theta) = \text{likelihood function} = \prod_{i=1}^n f_X(x_i | \Theta)$$

The likelihood function is proportional to the probability of making specific observations, $X = x_i$, given the values Θ of the parameters. The initial belief about the stochastic behavior of the parameters of the distributions is thus updated using the observations.

Considerable mathematical simplification can be achieved if the distributions of the parameters are appropriately chosen with respect to the underlying random variable X . Such pairs of distributions are known as conjugate distributions. By choosing prior distributions that are conjugate of the distribution of the underlying random variable, one thereby obtains convenient posterior distributions, which are usually of the same mathematical form as the prior.

The uncertainty associated with parameters Θ is combined with the inherent variability of the underlying random variable, X , to obtain the total uncertainty associated with X . Using the total probability theorem, the posterior probability density function of X is expressed as follows:

$$\hat{f}_X(x) = \int_{\Theta} K L(X|\Theta) f_X(x | \Theta) f'(\Theta) d\Theta \quad (\text{A.3})$$

This approach will be used in the next phase of the study.

**NATIONAL CENTER FOR EARTHQUAKE ENGINEERING RESEARCH
LIST OF TECHNICAL REPORTS**

The National Center for Earthquake Engineering Research (NCEER) publishes technical reports on a variety of subjects related to earthquake engineering written by authors funded through NCEER. These reports are available from both NCEER's Publications Department and the National Technical Information Service (NTIS). Requests for reports should be directed to the Publications Department, National Center for Earthquake Engineering Research, State University of New York at Buffalo, Red Jacket Quadrangle, Buffalo, New York 14261. Reports can also be requested through NTIS, 5285 Port Royal Road, Springfield, Virginia 22161. NTIS accession numbers are shown in parenthesis, if available.

- NCEER-87-0001 "First-Year Program in Research, Education and Technology Transfer," 3/5/87, (PB88-134275).
- NCEER-87-0002 "Experimental Evaluation of Instantaneous Optimal Algorithms for Structural Control," by R.C. Lin, T.T. Soong and A.M. Reinhorn, 4/20/87, (PB88-134341).
- NCEER-87-0003 "Experimentation Using the Earthquake Simulation Facilities at University at Buffalo," by A.M. Reinhorn and R.L. Ketter, to be published.
- NCEER-87-0004 "The System Characteristics and Performance of a Shaking Table," by J.S. Hwang, K.C. Chang and G.C. Lee, 6/1/87, (PB88-134259). This report is available only through NTIS (see address given above).
- NCEER-87-0005 "A Finite Element Formulation for Nonlinear Viscoplastic Material Using a Q Model," by O. Gyebe and G. Dasgupta, 11/2/87, (PB88-213764).
- NCEER-87-0006 "Symbolic Manipulation Program (SMP) - Algebraic Codes for Two and Three Dimensional Finite Element Formulations," by X. Lee and G. Dasgupta, 11/9/87, (PB88-218522).
- NCEER-87-0007 "Instantaneous Optimal Control Laws for Tall Buildings Under Seismic Excitations," by J.N. Yang, A. Akbarpour and P. Ghaemmaghami, 6/10/87, (PB88-134333). This report is only available through NTIS (see address given above).
- NCEER-87-0008 "IDARC: Inelastic Damage Analysis of Reinforced Concrete Frame - Shear-Wall Structures," by Y.J. Park, A.M. Reinhorn and S.K. Kunnath, 7/20/87, (PB88-134325).
- NCEER-87-0009 "Liquefaction Potential for New York State: A Preliminary Report on Sites in Manhattan and Buffalo," by M. Budhu, V. Vijayakumar, R.F. Giese and L. Baumgras, 8/31/87, (PB88-163704). This report is available only through NTIS (see address given above).
- NCEER-87-0010 "Vertical and Torsional Vibration of Foundations in Inhomogeneous Media," by A.S. Veletsos and K.W. Dotson, 6/1/87, (PB88-134291).
- NCEER-87-0011 "Seismic Probabilistic Risk Assessment and Seismic Margins Studies for Nuclear Power Plants," by Howard H.M. Hwang, 6/15/87, (PB88-134267).
- NCEER-87-0012 "Parametric Studies of Frequency Response of Secondary Systems Under Ground-Acceleration Excitations," by Y. Yong and Y.K. Lin, 6/10/87, (PB88-134309).
- NCEER-87-0013 "Frequency Response of Secondary Systems Under Seismic Excitation," by J.A. HoLung, J. Cai and Y.K. Lin, 7/31/87, (PB88-134317).
- NCEER-87-0014 "Modelling Earthquake Ground Motions in Seismically Active Regions Using Parametric Time Series Methods," by G.W. Ellis and A.S. Cakmak, 8/25/87, (PB88-134283).
- NCEER-87-0015 "Detection and Assessment of Seismic Structural Damage," by E. DiPasquale and A.S. Cakmak, 8/25/87, (PB88-163712).

- NCEER-87-0016 "Pipeline Experiment at Parkfield, California," by J. Isenberg and E. Richardson, 9/15/87, (PB88-163720). This report is available only through NTIS (see address given above).
- NCEER-87-0017 "Digital Simulation of Seismic Ground Motion," by M. Shinozuka, G. Deodatis and T. Harada, 8/31/87, (PB88-155197). This report is available only through NTIS (see address given above).
- NCEER-87-0018 "Practical Considerations for Structural Control: System Uncertainty, System Time Delay and Truncation of Small Control Forces," J.N. Yang and A. Akbarpour, 8/10/87, (PB88-163738).
- NCEER-87-0019 "Modal Analysis of Nonclassically Damped Structural Systems Using Canonical Transformation," by J.N. Yang, S. Sarkani and F.X. Long, 9/27/87, (PB88-187851).
- NCEER-87-0020 "A Nonstationary Solution in Random Vibration Theory," by J.R. Red-Horse and P.D. Spanos, 11/3/87, (PB88-163746).
- NCEER-87-0021 "Horizontal Impedances for Radially Inhomogeneous Viscoelastic Soil Layers," by A.S. Veletsos and K.W. Dotson, 10/15/87, (PB88-150859).
- NCEER-87-0022 "Seismic Damage Assessment of Reinforced Concrete Members," by Y.S. Chung, C. Meyer and M. Shinozuka, 10/9/87, (PB88-150867). This report is available only through NTIS (see address given above).
- NCEER-87-0023 "Active Structural Control in Civil Engineering," by T.T. Soong, 11/11/87, (PB88-187778).
- NCEER-87-0024 "Vertical and Torsional Impedances for Radially Inhomogeneous Viscoelastic Soil Layers," by K.W. Dotson and A.S. Veletsos, 12/87, (PB88-187786).
- NCEER-87-0025 "Proceedings from the Symposium on Seismic Hazards, Ground Motions, Soil-Liquefaction and Engineering Practice in Eastern North America," October 20-22, 1987, edited by K.H. Jacob, 12/87, (PB88-188115).
- NCEER-87-0026 "Report on the Whittier-Narrows, California, Earthquake of October 1, 1987," by J. Pantelic and A. Reinhorn, 11/87, (PB88-187752). This report is available only through NTIS (see address given above).
- NCEER-87-0027 "Design of a Modular Program for Transient Nonlinear Analysis of Large 3-D Building Structures," by S. Srivastav and J.F. Abel, 12/30/87, (PB88-187950).
- NCEER-87-0028 "Second-Year Program in Research, Education and Technology Transfer," 3/8/88, (PB88-219480).
- NCEER-88-0001 "Workshop on Seismic Computer Analysis and Design of Buildings With Interactive Graphics," by W. McGuire, J.F. Abel and C.H. Conley, 1/18/88, (PB88-187760).
- NCEER-88-0002 "Optimal Control of Nonlinear Flexible Structures," by J.N. Yang, F.X. Long and D. Wong, 1/22/88, (PB88-213772).
- NCEER-88-0003 "Substructuring Techniques in the Time Domain for Primary-Secondary Structural Systems," by G.D. Manolis and G. Juhn, 2/10/88, (PB88-213780).
- NCEER-88-0004 "Iterative Seismic Analysis of Primary-Secondary Systems," by A. Singhal, L.D. Lutes and P.D. Spanos, 2/23/88, (PB88-213798).
- NCEER-88-0005 "Stochastic Finite Element Expansion for Random Media," by P.D. Spanos and R. Ghanem, 3/14/88, (PB88-213806).
- NCEER-88-0006 "Combining Structural Optimization and Structural Control," by F.Y. Cheng and C.P. Pantelides, 1/10/88, (PB88-213814).

- NCEER-88-0007 "Seismic Performance Assessment of Code-Designed Structures," by H.H-M. Hwang, J-W. Jaw and H-J. Shau, 3/20/88, (PB88-219423).
- NCEER-88-0008 "Reliability Analysis of Code-Designed Structures Under Natural Hazards," by H.H-M. Hwang, H. Ushiba and M. Shinozuka, 2/29/88, (PB88-229471).
- NCEER-88-0009 "Seismic Fragility Analysis of Shear Wall Structures," by J-W Jaw and H.H-M. Hwang, 4/30/88, (PB89-102867).
- NCEER-88-0010 "Base Isolation of a Multi-Story Building Under a Harmonic Ground Motion - A Comparison of Performances of Various Systems," by F-G Fan, G. Ahmadi and I.G. Tadjbakhsh, 5/18/88, (PB89-122238).
- NCEER-88-0011 "Seismic Floor Response Spectra for a Combined System by Green's Functions," by F.M. Lavelle, L.A. Bergman and P.D. Spanos, 5/1/88, (PB89-102875).
- NCEER-88-0012 "A New Solution Technique for Randomly Excited Hysteretic Structures," by G.Q. Cai and Y.K. Lin, 5/16/88, (PB89-102883).
- NCEER-88-0013 "A Study of Radiation Damping and Soil-Structure Interaction Effects in the Centrifuge," by K. Weissman, supervised by J.H. Prevost, 5/24/88, (PB89-144703).
- NCEER-88-0014 "Parameter Identification and Implementation of a Kinematic Plasticity Model for Frictional Soils," by J.H. Prevost and D.V. Griffiths, to be published.
- NCEER-88-0015 "Two- and Three- Dimensional Dynamic Finite Element Analyses of the Long Valley Dam," by D.V. Griffiths and J.H. Prevost, 6/17/88, (PB89-144711).
- NCEER-88-0016 "Damage Assessment of Reinforced Concrete Structures in Eastern United States," by A.M. Reinhorn, M.J. Seidel, S.K. Kunnath and Y.J. Park, 6/15/88, (PB89-122220).
- NCEER-88-0017 "Dynamic Compliance of Vertically Loaded Strip Foundations in Multilayered Viscoelastic Soils," by S. Ahmad and A.S.M. Israil, 6/17/88, (PB89-102891).
- NCEER-88-0018 "An Experimental Study of Seismic Structural Response With Added Viscoelastic Dampers," by R.C. Lin, Z. Liang, T.T. Soong and R.H. Zhang, 6/30/88, (PB89-122212). This report is available only through NTIS (see address given above).
- NCEER-88-0019 "Experimental Investigation of Primary - Secondary System Interaction," by G.D. Manolis, G. Juhn and A.M. Reinhorn, 5/27/88, (PB89-122204).
- NCEER-88-0020 "A Response Spectrum Approach For Analysis of Nonclassically Damped Structures," by J.N. Yang, S. Sarkani and F.X. Long, 4/22/88, (PB89-102909).
- NCEER-88-0021 "Seismic Interaction of Structures and Soils: Stochastic Approach," by A.S. Veletsos and A.M. Prasad, 7/21/88, (PB89-122196).
- NCEER-88-0022 "Identification of the Serviceability Limit State and Detection of Seismic Structural Damage," by E. DiPasquale and A.S. Cakmak, 6/15/88, (PB89-122188). This report is available only through NTIS (see address given above).
- NCEER-88-0023 "Multi-Hazard Risk Analysis: Case of a Simple Offshore Structure," by B.K. Bhartia and E.H. Vanmarcke, 7/21/88, (PB89-145213).
- NCEER-88-0024 "Automated Seismic Design of Reinforced Concrete Buildings," by Y.S. Chung, C. Meyer and M. Shinozuka, 7/5/88, (PB89-122170). This report is available only through NTIS (see address given above).

- NCEER-88-0025 "Experimental Study of Active Control of MDOF Structures Under Seismic Excitations," by L.L. Chung, R.C. Lin, T.T. Soong and A.M. Reinhorn, 7/10/88, (PB89-122600).
- NCEER-88-0026 "Earthquake Simulation Tests of a Low-Rise Metal Structure," by J.S. Hwang, K.C. Chang, G.C. Lee and R.L. Ketter, 8/1/88, (PB89-102917).
- NCEER-88-0027 "Systems Study of Urban Response and Reconstruction Due to Catastrophic Earthquakes," by F. Kozin and H.K. Zhou, 9/22/88, (PB90-162348).
- NCEER-88-0028 "Seismic Fragility Analysis of Plane Frame Structures," by H.H.M. Hwang and Y.K. Low, 7/31/88, (PB89-131445).
- NCEER-88-0029 "Response Analysis of Stochastic Structures," by A. Kardara, C. Bucher and M. Shinozuka, 9/22/88, (PB89-174429).
- NCEER-88-0030 "Nonnormal Accelerations Due to Yielding in a Primary Structure," by D.C.K. Chen and L.D. Lutes, 9/19/88, (PB89-131437).
- NCEER-88-0031 "Design Approaches for Soil-Structure Interaction," by A.S. Veletsos, A.M. Prasad and Y. Tang, 12/30/88, (PB89-174437). This report is available only through NTIS (see address given above).
- NCEER-88-0032 "A Re-evaluation of Design Spectra for Seismic Damage Control," by C.J. Turkstra and A.G. Tallin, 11/7/88, (PB89-145221).
- NCEER-88-0033 "The Behavior and Design of Noncontact Lap Splices Subjected to Repeated Inelastic Tensile Loading," by V.E. Sagan, P. Gergely and R.N. White, 12/8/88, (PB89-163737).
- NCEER-88-0034 "Seismic Response of Pile Foundations," by S.M. Mamoon, P.K. Banerjee and S. Ahmad, 11/1/88, (PB89-145239).
- NCEER-88-0035 "Modeling of R/C Building Structures With Flexible Floor Diaphragms (IDARC2)," by A.M. Reinhorn, S.K. Kunnath and N. Panahshahi, 9/7/88, (PB89-207153).
- NCEER-88-0036 "Solution of the Dam-Reservoir Interaction Problem Using a Combination of FEM, BEM with Particular Integrals, Modal Analysis, and Substructuring," by C-S. Tsai, G.C. Lee and R.L. Ketter, 12/31/88, (PB89-207146).
- NCEER-88-0037 "Optimal Placement of Actuators for Structural Control," by F.Y. Cheng and C.P. Pantelides, 8/15/88, (PB89-162846).
- NCEER-88-0038 "Teflon Bearings in Aseismic Base Isolation: Experimental Studies and Mathematical Modeling," by A. Mokha, M.C. Constantinou and A.M. Reinhorn, 12/5/88, (PB89-218457). This report is available only through NTIS (see address given above).
- NCEER-88-0039 "Seismic Behavior of Flat Slab High-Rise Buildings in the New York City Area," by P. Weidlinger and M. Ettouney, 10/15/88, (PB90-145681).
- NCEER-88-0040 "Evaluation of the Earthquake Resistance of Existing Buildings in New York City," by P. Weidlinger and M. Ettouney, 10/15/88, to be published.
- NCEER-88-0041 "Small-Scale Modeling Techniques for Reinforced Concrete Structures Subjected to Seismic Loads," by W. Kim, A. El-Attar and R.N. White, 11/22/88, (PB89-189625).
- NCEER-88-0042 "Modeling Strong Ground Motion from Multiple Event Earthquakes," by G.W. Ellis and A.S. Cakmak, 10/15/88, (PB89-174445).

- NCEER-88-0043 "Nonstationary Models of Seismic Ground Acceleration," by M. Grigoriu, S.E. Ruiz and E. Rosenblueth, 7/15/88, (PB89-189617).
- NCEER-88-0044 "SARCF User's Guide: Seismic Analysis of Reinforced Concrete Frames," by Y.S. Chung, C. Meyer and M. Shinozuka, 11/9/88, (PB89-174452).
- NCEER-88-0045 "First Expert Panel Meeting on Disaster Research and Planning," edited by J. Pantelic and J. Stoyke, 9/15/88, (PB89-174460).
- NCEER-88-0046 "Preliminary Studies of the Effect of Degrading Infill Walls on the Nonlinear Seismic Response of Steel Frames," by C.Z. Chrysostomou, P. Gergely and J.F. Abel, 12/19/88, (PB89-208383).
- NCEER-88-0047 "Reinforced Concrete Frame Component Testing Facility - Design, Construction, Instrumentation and Operation," by S.P. Pessiki, C. Conley, T. Bond, P. Gergely and R.N. White, 12/16/88, (PB89-174478).
- NCEER-89-0001 "Effects of Protective Cushion and Soil Compliancy on the Response of Equipment Within a Seismically Excited Building," by J.A. HoLung, 2/16/89, (PB89-207179).
- NCEER-89-0002 "Statistical Evaluation of Response Modification Factors for Reinforced Concrete Structures," by H.H-M. Hwang and J-W. Jaw, 2/17/89, (PB89-207187).
- NCEER-89-0003 "Hysteretic Columns Under Random Excitation," by G-Q. Cai and Y.K. Lin, 1/9/89, (PB89-196513).
- NCEER-89-0004 "Experimental Study of 'Elephant Foot Bulge' Instability of Thin-Walled Metal Tanks," by Z-H. Jia and R.L. Ketter, 2/22/89, (PB89-207195).
- NCEER-89-0005 "Experiment on Performance of Buried Pipelines Across San Andreas Fault," by J. Isenberg, E. Richardson and T.D. O'Rourke, 3/10/89, (PB89-218440). This report is available only through NTIS (see address given above).
- NCEER-89-0006 "A Knowledge-Based Approach to Structural Design of Earthquake-Resistant Buildings," by M. Subramani, P. Gergely, C.H. Conley, J.F. Abel and A.H. Zaghaw, 1/15/89, (PB89-218465).
- NCEER-89-0007 "Liquefaction Hazards and Their Effects on Buried Pipelines," by T.D. O'Rourke and P.A. Lane, 2/1/89, (PB89-218481).
- NCEER-89-0008 "Fundamentals of System Identification in Structural Dynamics," by H. Imai, C-B. Yun, O. Maruyama and M. Shinozuka, 1/26/89, (PB89-207211).
- NCEER-89-0009 "Effects of the 1985 Michoacan Earthquake on Water Systems and Other Buried Lifelines in Mexico," by A.G. Ayala and M.J. O'Rourke, 3/8/89, (PB89-207229).
- NCEER-89-R010 "NCEER Bibliography of Earthquake Education Materials," by K.E.K. Ross, Second Revision, 9/1/89, (PB90-125352).
- NCEER-89-0011 "Inelastic Three-Dimensional Response Analysis of Reinforced Concrete Building Structures (IDARC-3D), Part I - Modeling," by S.K. Kunnath and A.M. Reinhorn, 4/17/89, (PB90-114612).
- NCEER-89-0012 "Recommended Modifications to ATC-14," by C.D. Poland and J.O. Malley, 4/12/89, (PB90-108648).
- NCEER-89-0013 "Repair and Strengthening of Beam-to-Column Connections Subjected to Earthquake Loading," by M. Corazao and A.J. Durrani, 2/28/89, (PB90-109885).
- NCEER-89-0014 "Program EXKAL2 for Identification of Structural Dynamic Systems," by O. Maruyama, C-B. Yun, M. Hoshiya and M. Shinozuka, 5/19/89, (PB90-109877).

- NCEER-89-0015 "Response of Frames With Bolted Semi-Rigid Connections, Part I - Experimental Study and Analytical Predictions," by P.J. DiCorso, A.M. Reinhorn, J.R. Dickerson, J.B. Radzinski and W.L. Harper, 6/1/89, to be published.
- NCEER-89-0016 "ARMA Monte Carlo Simulation in Probabilistic Structural Analysis," by P.D. Spanos and M.P. Mignolet, 7/10/89, (PB90-109893).
- NCEER-89-P017 "Preliminary Proceedings from the Conference on Disaster Preparedness - The Place of Earthquake Education in Our Schools," Edited by K.E.K. Ross, 6/23/89, (PB90-108606).
- NCEER-89-0017 "Proceedings from the Conference on Disaster Preparedness - The Place of Earthquake Education in Our Schools," Edited by K.E.K. Ross, 12/31/89, (PB90-207895). This report is available only through NTIS (see address given above).
- NCEER-89-0018 "Multidimensional Models of Hysteretic Material Behavior for Vibration Analysis of Shape Memory Energy Absorbing Devices, by E.J. Graesser and F.A. Cozzarelli, 6/7/89, (PB90-164146).
- NCEER-89-0019 "Nonlinear Dynamic Analysis of Three-Dimensional Base Isolated Structures (3D-BASIS)," by S. Nagarajaiah, A.M. Reinhorn and M.C. Constantinou, 8/3/89, (PB90-161936). This report is available only through NTIS (see address given above).
- NCEER-89-0020 "Structural Control Considering Time-Rate of Control Forces and Control Rate Constraints," by F.Y. Cheng and C.P. Pantelides, 8/3/89, (PB90-120445).
- NCEER-89-0021 "Subsurface Conditions of Memphis and Shelby County," by K.W. Ng, T-S. Chang and H-H.M. Hwang, 7/26/89, (PB90-120437).
- NCEER-89-0022 "Seismic Wave Propagation Effects on Straight Jointed Buried Pipelines," by K. Elhadi and M.J. O'Rourke, 8/24/89, (PB90-162322).
- NCEER-89-0023 "Workshop on Serviceability Analysis of Water Delivery Systems," edited by M. Grigoriu, 3/6/89, (PB90-127424).
- NCEER-89-0024 "Shaking Table Study of a 1/5 Scale Steel Frame Composed of Tapered Members," by K.C. Chang, J.S. Hwang and G.C. Lee, 9/18/89, (PB90-160169).
- NCEER-89-0025 "DYNA1D: A Computer Program for Nonlinear Seismic Site Response Analysis - Technical Documentation," by Jean H. Prevost, 9/14/89, (PB90-161944). This report is available only through NTIS (see address given above).
- NCEER-89-0026 "1:4 Scale Model Studies of Active Tendon Systems and Active Mass Dampers for Aseismic Protection," by A.M. Reinhorn, T.T. Soong, R.C. Lin, Y.P. Yang, Y. Fukao, H. Abe and M. Nakai, 9/15/89, (PB90-173246).
- NCEER-89-0027 "Scattering of Waves by Inclusions in a Nonhomogeneous Elastic Half Space Solved by Boundary Element Methods," by P.K. Hadley, A. Askar and A.S. Cakmak, 6/15/89, (PB90-145699).
- NCEER-89-0028 "Statistical Evaluation of Deflection Amplification Factors for Reinforced Concrete Structures," by H.H.M. Hwang, J-W. Jaw and A.L. Ch'ng, 8/31/89, (PB90-164633).
- NCEER-89-0029 "Bedrock Accelerations in Memphis Area Due to Large New Madrid Earthquakes," by H.H.M. Hwang, C.H.S. Chen and G. Yu, 11/7/89, (PB90-162330).
- NCEER-89-0030 "Seismic Behavior and Response Sensitivity of Secondary Structural Systems," by Y.Q. Chen and T.T. Soong, 10/23/89, (PB90-164658).

- NCEER-89-0031 "Random Vibration and Reliability Analysis of Primary-Secondary Structural Systems," by Y. Ibrahim, M. Grigoriu and T.T. Soong, 11/10/89, (PB90-161951).
- NCEER-89-0032 "Proceedings from the Second U.S. - Japan Workshop on Liquefaction, Large Ground Deformation and Their Effects on Lifelines, September 26-29, 1989," Edited by T.D. O'Rourke and M. Hamada, 12/1/89, (PB90-209388).
- NCEER-89-0033 "Deterministic Model for Seismic Damage Evaluation of Reinforced Concrete Structures," by J.M. Bracci, A.M. Reinhorn, J.B. Mander and S.K. Kunnath, 9/27/89.
- NCEER-89-0034 "On the Relation Between Local and Global Damage Indices," by E. DiPasquale and A.S. Cakmak, 8/15/89, (PB90-173865).
- NCEER-89-0035 "Cyclic Undrained Behavior of Nonplastic and Low Plasticity Silts," by A.J. Walker and H.E. Stewart, 7/26/89, (PB90-183518).
- NCEER-89-0036 "Liquefaction Potential of Surficial Deposits in the City of Buffalo, New York," by M. Budhu, R. Giese and L. Baumgrass, 1/17/89, (PB90-208455).
- NCEER-89-0037 "A Deterministic Assessment of Effects of Ground Motion Incoherence," by A.S. Veletsos and Y. Tang, 7/15/89, (PB90-164294).
- NCEER-89-0038 "Workshop on Ground Motion Parameters for Seismic Hazard Mapping," July 17-18, 1989, edited by R.V. Whitman, 12/1/89, (PB90-173923).
- NCEER-89-0039 "Seismic Effects on Elevated Transit Lines of the New York City Transit Authority," by C.J. Costantino, C.A. Miller and E. Heymsfield, 12/26/89, (PB90-207887).
- NCEER-89-0040 "Centrifugal Modeling of Dynamic Soil-Structure Interaction," by K. Weissman, Supervised by J.H. Prevost, 5/10/89, (PB90-207879).
- NCEER-89-0041 "Linearized Identification of Buildings With Cores for Seismic Vulnerability Assessment," by I-K. Ho and A.E. Aktan, 11/1/89, (PB90-251943).
- NCEER-90-0001 "Geotechnical and Lifeline Aspects of the October 17, 1989 Loma Prieta Earthquake in San Francisco," by T.D. O'Rourke, H.E. Stewart, F.T. Blackburn and T.S. Dickerman, 1/90, (PB90-208596).
- NCEER-90-0002 "Nonnormal Secondary Response Due to Yielding in a Primary Structure," by D.C.K. Chen and L.D. Lutes, 2/28/90, (PB90-251976).
- NCEER-90-0003 "Earthquake Education Materials for Grades K-12," by K.E.K. Ross, 4/16/90, (PB91-251984).
- NCEER-90-0004 "Catalog of Strong Motion Stations in Eastern North America," by R.W. Busby, 4/3/90, (PB90-251984).
- NCEER-90-0005 "NCEER Strong-Motion Data Base: A User Manual for the GeoBase Release (Version 1.0 for the Sun3)," by P. Friberg and K. Jacob, 3/31/90 (PB90-258062).
- NCEER-90-0006 "Seismic Hazard Along a Crude Oil Pipeline in the Event of an 1811-1812 Type New Madrid Earthquake," by H.H.M. Hwang and C-H.S. Chen, 4/16/90(PB90-258054).
- NCEER-90-0007 "Site-Specific Response Spectra for Memphis Sheahan Pumping Station," by H.H.M. Hwang and C.S. Lee, 5/15/90, (PB91-108811).
- NCEER-90-0008 "Pilot Study on Seismic Vulnerability of Crude Oil Transmission Systems," by T. Ariman, R. Dobry, M. Grigoriu, F. Kozin, M. O'Rourke, T. O'Rourke and M. Shinozuka, 5/25/90, (PB91-108837).

- NCEER-90-0009 "A Program to Generate Site Dependent Time Histories: EQGEN," by G.W. Ellis, M. Srinivasan and A.S. Cakmak, 1/30/90, (PB91-108829).
- NCEER-90-0010 "Active Isolation for Seismic Protection of Operating Rooms," by M.E. Talbott, Supervised by M. Shinozuka, 6/8/9, (PB91-110205).
- NCEER-90-0011 "Program LINEARID for Identification of Linear Structural Dynamic Systems," by C-B. Yun and M. Shinozuka, 6/25/90, (PB91-110312).
- NCEER-90-0012 "Two-Dimensional Two-Phase Elasto-Plastic Seismic Response of Earth Dams," by A.N. Yiagos, Supervised by J.H. Prevost, 6/20/90, (PB91-110197).
- NCEER-90-0013 "Secondary Systems in Base-Isolated Structures: Experimental Investigation, Stochastic Response and Stochastic Sensitivity," by G.D. Manolis, G. Juhn, M.C. Constantinou and A.M. Reinhorn, 7/1/90, (PB91-110320).
- NCEER-90-0014 "Seismic Behavior of Lightly-Reinforced Concrete Column and Beam-Column Joint Details," by S.P. Pessiki, C.H. Conley, P. Gergely and R.N. White, 8/22/90, (PB91-108795).
- NCEER-90-0015 "Two Hybrid Control Systems for Building Structures Under Strong Earthquakes," by J.N. Yang and A. Danielians, 6/29/90, (PB91-125393).
- NCEER-90-0016 "Instantaneous Optimal Control with Acceleration and Velocity Feedback," by J.N. Yang and Z. Li, 6/29/90, (PB91-125401).
- NCEER-90-0017 "Reconnaissance Report on the Northern Iran Earthquake of June 21, 1990," by M. Mehraïn, 10/4/90, (PB91-125377).
- NCEER-90-0018 "Evaluation of Liquefaction Potential in Memphis and Shelby County," by T.S. Chang, P.S. Tang, C.S. Lee and H. Hwang, 8/10/90, (PB91-125427).
- NCEER-90-0019 "Experimental and Analytical Study of a Combined Sliding Disc Bearing and Helical Steel Spring Isolation System," by M.C. Constantinou, A.S. Mokha and A.M. Reinhorn, 10/4/90, (PB91-125385).
- NCEER-90-0020 "Experimental Study and Analytical Prediction of Earthquake Response of a Sliding Isolation System with a Spherical Surface," by A.S. Mokha, M.C. Constantinou and A.M. Reinhorn, 10/11/90, (PB91-125419).
- NCEER-90-0021 "Dynamic Interaction Factors for Floating Pile Groups," by G. Gazetas, K. Fan, A. Kaynia and E. Kausel, 9/10/90, (PB91-170381).
- NCEER-90-0022 "Evaluation of Seismic Damage Indices for Reinforced Concrete Structures," by S. Rodriguez-Gomez and A.S. Cakmak, 9/30/90, PB91-171322).
- NCEER-90-0023 "Study of Site Response at a Selected Memphis Site," by H. Desai, S. Ahmad, E.S. Gazetas and M.R. Oh, 10/11/90, (PB91-196857).
- NCEER-90-0024 "A User's Guide to Strongmo: Version 1.0 of NCEER's Strong-Motion Data Access Tool for PCs and Terminals," by P.A. Friberg and C.A.T. Susch, 11/15/90, (PB91-171272).
- NCEER-90-0025 "A Three-Dimensional Analytical Study of Spatial Variability of Seismic Ground Motions," by L-L. Hong and A.H.-S. Ang, 10/30/90, (PB91-170399).
- NCEER-90-0026 "MUMOID User's Guide - A Program for the Identification of Modal Parameters," by S. Rodriguez-Gomez and E. DiPasquale, 9/30/90, (PB91-171298).
- NCEER-90-0027 "SARCF-II User's Guide - Seismic Analysis of Reinforced Concrete Frames," by S. Rodriguez-Gomez, Y.S. Chung and C. Meyer, 9/30/90, (PB91-171280).

- NCEER-90-0028 "Viscous Dampers: Testing, Modeling and Application in Vibration and Seismic Isolation," by N. Makris and M.C. Constantinou, 12/20/90 (PB91-190561).
- NCEER-90-0029 "Soil Effects on Earthquake Ground Motions in the Memphis Area," by H. Hwang, C.S. Lee, K.W. Ng and T.S. Chang, 8/2/90, (PB91-190751).
- NCEER-91-0001 "Proceedings from the Third Japan-U.S. Workshop on Earthquake Resistant Design of Lifeline Facilities and Countermeasures for Soil Liquefaction, December 17-19, 1990," edited by T.D. O'Rourke and M. Hamada, 2/1/91, (PB91-179259).
- NCEER-91-0002 "Physical Space Solutions of Non-Proportionally Damped Systems," by M. Tong, Z. Liang and G.C. Lee, 1/15/91, (PB91-179242).
- NCEER-91-0003 "Seismic Response of Single Piles and Pile Groups," by K. Fan and G. Gazetas, 1/10/91, (PB92-174994).
- NCEER-91-0004 "Damping of Structures: Part 1 - Theory of Complex Damping," by Z. Liang and G. Lee, 10/10/91, (PB92-197235).
- NCEER-91-0005 "3D-BASIS - Nonlinear Dynamic Analysis of Three Dimensional Base Isolated Structures: Part II," by S. Nagarajaiah, A.M. Reinhorn and M.C. Constantinou, 2/28/91, (PB91-190553).
- NCEER-91-0006 "A Multidimensional Hysteretic Model for Plasticity Deforming Metals in Energy Absorbing Devices," by E.J. Graesser and F.A. Cozzarelli, 4/9/91, (PB92-108364).
- NCEER-91-0007 "A Framework for Customizable Knowledge-Based Expert Systems with an Application to a KBES for Evaluating the Seismic Resistance of Existing Buildings," by E.G. Ibarra-Anaya and S.J. Fenves, 4/9/91, (PB91-210930).
- NCEER-91-0008 "Nonlinear Analysis of Steel Frames with Semi-Rigid Connections Using the Capacity Spectrum Method," by G.G. Deierlein, S-H. Hsieh, Y-J. Shen and J.F. Abel, 7/2/91, (PB92-113828).
- NCEER-91-0009 "Earthquake Education Materials for Grades K-12," by K.E.K. Ross, 4/30/91, (PB91-212142).
- NCEER-91-0010 "Phase Wave Velocities and Displacement Phase Differences in a Harmonically Oscillating Pile," by N. Makris and G. Gazetas, 7/8/91, (PB92-108356).
- NCEER-91-0011 "Dynamic Characteristics of a Full-Size Five-Story Steel Structure and a 2/5 Scale Model," by K.C. Chang, G.C. Yao, G.C. Lee, D.S. Hao and Y.C. Yeh, 7/2/91, (PB93-116648).
- NCEER-91-0012 "Seismic Response of a 2/5 Scale Steel Structure with Added Viscoelastic Dampers," by K.C. Chang, T.T. Soong, S-T. Oh and M.L. Lai, 5/17/91, (PB92-110816).
- NCEER-91-0013 "Earthquake Response of Retaining Walls; Full-Scale Testing and Computational Modeling," by S. Alampalli and A-W.M. Elgamal, 6/20/91, to be published.
- NCEER-91-0014 "3D-BASIS-M: Nonlinear Dynamic Analysis of Multiple Building Base Isolated Structures," by P.C. Tsopelas, S. Nagarajaiah, M.C. Constantinou and A.M. Reinhorn, 5/28/91, (PB92-113885).
- NCEER-91-0015 "Evaluation of SEAOC Design Requirements for Sliding Isolated Structures," by D. Theodossiou and M.C. Constantinou, 6/10/91, (PB92-114602).
- NCEER-91-0016 "Closed-Loop Modal Testing of a 27-Story Reinforced Concrete Flat Plate-Core Building," by H.R. Somaprasad, T. Toksoy, H. Yoshiyuki and A.E. Aktan, 7/15/91, (PB92-129980).
- NCEER-91-0017 "Shake Table Test of a 1/6 Scale Two-Story Lightly Reinforced Concrete Building," by A.G. El-Attar, R.N. White and P. Gergely, 2/28/91, (PB92-222447).

- NCEER-92-0028 "Seismic Resistance of Reinforced Concrete Frame Structures Designed Only for Gravity Loads: Part II - Experimental Performance of Subassemblages," by L.E. Aycardi, J.B. Mander and A.M. Reinhorn, 12/1/92, (PB94-104510, A08, MF-A02).
- NCEER-92-0029 "Seismic Resistance of Reinforced Concrete Frame Structures Designed Only for Gravity Loads: Part III - Experimental Performance and Analytical Study of a Structural Model," by J.M. Bracci, A.M. Reinhorn and J.B. Mander, 12/1/92, (PB93-227528, A09, MF-A01).
- NCEER-92-0030 "Evaluation of Seismic Retrofit of Reinforced Concrete Frame Structures: Part I - Experimental Performance of Retrofitted Subassemblages," by D. Choudhuri, J.B. Mander and A.M. Reinhorn, 12/8/92, (PB93-198307, A07, MF-A02).
- NCEER-92-0031 "Evaluation of Seismic Retrofit of Reinforced Concrete Frame Structures: Part II - Experimental Performance and Analytical Study of a Retrofitted Structural Model," by J.M. Bracci, A.M. Reinhorn and J.B. Mander, 12/8/92, (PB93-198315, A09, MF-A03).
- NCEER-92-0032 "Experimental and Analytical Investigation of Seismic Response of Structures with Supplemental Fluid Viscous Dampers," by M.C. Constantinou and M.D. Symans, 12/21/92, (PB93-191435).
- NCEER-92-0033 "Reconnaissance Report on the Cairo, Egypt Earthquake of October 12, 1992," by M. Khater, 12/23/92, (PB93-188621).
- NCEER-92-0034 "Low-Level Dynamic Characteristics of Four Tall Flat-Plate Buildings in New York City," by H. Gavin, S. Yuan, J. Grossman, E. Pekelis and K. Jacob, 12/28/92, (PB93-188217).
- NCEER-93-0001 "An Experimental Study on the Seismic Performance of Brick-Infilled Steel Frames With and Without Retrofit," by J.B. Mander, B. Nair, K. Wojtkowski and J. Ma, 1/29/93, (PB93-227510, A07, MF-A02).
- NCEER-93-0002 "Social Accounting for Disaster Preparedness and Recovery Planning," by S. Cole, E. Pantoja and V. Razak, 2/22/93, (PB94-142114, A12, MF-A03).
- NCEER-93-0003 "Assessment of 1991 NEHRP Provisions for Nonstructural Components and Recommended Revisions," by T.T. Soong, G. Chen, Z. Wu, R-H. Zhang and M. Grigoriu, 3/1/93, (PB93-188639).
- NCEER-93-0004 "Evaluation of Static and Response Spectrum Analysis Procedures of SEAOC/UBC for Seismic Isolated Structures," by C.W. Winters and M.C. Constantinou, 3/23/93, (PB93-198299).
- NCEER-93-0005 "Earthquakes in the Northeast - Are We Ignoring the Hazard? A Workshop on Earthquake Science and Safety for Educators," edited by K.E.K. Ross, 4/2/93, (PB94-103066, A09, MF-A02).
- NCEER-93-0006 "Inelastic Response of Reinforced Concrete Structures with Viscoelastic Braces," by R.F. Lobo, J.M. Bracci, K.L. Shen, A.M. Reinhorn and T.T. Soong, 4/5/93, (PB93-227486, A05, MF-A02).
- NCEER-93-0007 "Seismic Testing of Installation Methods for Computers and Data Processing Equipment," by K. Kosar, T.T. Soong, K.L. Shen, J.A. HoLung and Y.K. Lin, 4/12/93, (PB93-198299).
- NCEER-93-0008 "Retrofit of Reinforced Concrete Frames Using Added Dampers," by A. Reinhorn, M. Constantinou and C. Li, to be published.
- NCEER-93-0009 "Seismic Behavior and Design Guidelines for Steel Frame Structures with Added Viscoelastic Dampers," by K.C. Chang, M.L. Lai, T.T. Soong, D.S. Hao and Y.C. Yeh, 5/1/93, (PB94-141959, A07, MF-A02).
- NCEER-93-0010 "Seismic Performance of Shear-Critical Reinforced Concrete Bridge Piers," by J.B. Mander, S.M. Waheed, M.T.A. Chaudhary and S.S. Chen, 5/12/93, (PB93-227494, A08, MF-A02).

- NCEER-93-0011 "3D-BASIS-TABS: Computer Program for Nonlinear Dynamic Analysis of Three Dimensional Base Isolated Structures," by S. Nagarajaiah, C. Li, A.M. Reinhorn and M.C. Constantinou, 8/2/93, (PB94-141819, A09, MF-A02).
- NCEER-93-0012 "Effects of Hydrocarbon Spills from an Oil Pipeline Break on Ground Water," by O.J. Helweg and H.H.M. Hwang, 8/3/93, (PB94-141942, A06, MF-A02).
- NCEER-93-0013 "Simplified Procedures for Seismic Design of Nonstructural Components and Assessment of Current Code Provisions," by M.P. Singh, L.E. Suarez, E.E. Matheu and G.O. Maldonado, 8/4/93, (PB94-141827, A09, MF-A02).
- NCEER-93-0014 "An Energy Approach to Seismic Analysis and Design of Secondary Systems," by G. Chen and T.T. Soong, 8/6/93, (PB94-142767, A11, MF-A03).
- NCEER-93-0015 "Proceedings from School Sites: Becoming Prepared for Earthquakes - Commemorating the Third Anniversary of the Loma Prieta Earthquake," Edited by F.E. Winslow and K.E.K. Ross, 8/16/93.
- NCEER-93-0016 "Reconnaissance Report of Damage to Historic Monuments in Cairo, Egypt Following the October 12, 1992 Dahshur Earthquake," by D. Sykora, D. Look, G. Croci, E. Karaesmen and E. Karaesmen, 8/19/93, (PB94-142221, A08, MF-A02).
- NCEER-93-0017 "The Island of Guam Earthquake of August 8, 1993," by S.W. Swan and S.K. Harris, 9/30/93, (PB94-141843, A04, MF-A01).
- NCEER-93-0018 "Engineering Aspects of the October 12, 1992 Egyptian Earthquake," by A.W. Elgamal, M. Amer, K. Adalier and A. Abul-Fadl, 10/7/93, (PB94-141983, A05, MF-A01).
- NCEER-93-0019 "Development of an Earthquake Motion Simulator and its Application in Dynamic Centrifuge Testing," by I. Krstelj, Supervised by J.H. Prevost, 10/23/93, (PB94-181773, A-10, MF-A03).
- NCEER-93-0020 "NCEER-Taisei Corporation Research Program on Sliding Seismic Isolation Systems for Bridges: Experimental and Analytical Study of a Friction Pendulum System (FPS)," by M.C. Constantinou, P. Tsopelas, Y-S. Kim and S. Okamoto, 11/1/93, (PB94-142775, A08, MF-A02).
- NCEER-93-0021 "Finite Element Modeling of Elastomeric Seismic Isolation Bearings," by L.J. Billings, Supervised by R. Shepherd, 11/8/93, to be published.
- NCEER-93-0022 "Seismic Vulnerability of Equipment in Critical Facilities: Life-Safety and Operational Consequences," by K. Porter, G.S. Johnson, M.M. Zadeh, C. Scawthorn and S. Eder, 11/24/93, (PB94-181765, A16, MF-A03).
- NCEER-93-0023 "Hokkaido Nansei-oki, Japan Earthquake of July 12, 1993, by P.I. Yanev and C.R. Scawthorn, 12/23/93, (PB94-181500, A07, MF-A01).
- NCEER-94-0001 "An Evaluation of Seismic Serviceability of Water Supply Networks with Application to the San Francisco Auxiliary Water Supply System," by I. Markov, Supervised by M. Grigoriu and T. O'Rourke, 1/21/94.
- NCEER-94-0002 "NCEER-Taisei Corporation Research Program on Sliding Seismic Isolation Systems for Bridges: Experimental and Analytical Study of Systems Consisting of Sliding Bearings, Rubber Restoring Force Devices and Fluid Dampers," Volumes I and II, by P. Tsopelas, S. Okamoto, M.C. Constantinou, D. Ozaki and S. Fujii, 2/4/94, (PB94-181740, A09, MF-A02 and PB94-181757, A12, MF-A03).
- NCEER-94-0003 "A Markov Model for Local and Global Damage Indices in Seismic Analysis," by S. Rahman and M. Grigoriu, 2/18/94.

- NCEER-94-0004 "Proceedings from the NCEER Workshop on Seismic Response of Masonry Infills," edited by D.P. Abrams, 3/1/94, (PB94-180783, A07, MF-A02).
- NCEER-94-0005 "The Northridge, California Earthquake of January 17, 1994: General Reconnaissance Report," edited by J.D. Goltz, 3/11/94, (PB193943, A10, MF-A03).
- NCEER-94-0006 "Seismic Energy Based Fatigue Damage Analysis of Bridge Columns: Part I - Evaluation of Seismic Capacity," by G.A. Chang and J.B. Mander, 3/14/94, (PB94-219185, A11, MF-A03).
- NCEER-94-0007 "Seismic Isolation of Multi-Story Frame Structures Using Spherical Sliding Isolation Systems," by T.M. Al-Hussaini, V.A. Zayas and M.C. Constantinou, 3/17/94, (PB193745, A09, MF-A02).
- NCEER-94-0008 "The Northridge, California Earthquake of January 17, 1994: Performance of Highway Bridges," edited by I.G. Buckle, 3/24/94, (PB94-193851, A06, MF-A02).
- NCEER-94-0009 "Proceedings of the Third U.S.-Japan Workshop on Earthquake Protective Systems for Bridges," edited by I.G. Buckle and I. Friedland, 3/31/94, (PB94-195815, A99, MF-MF).
- NCEER-94-0010 "3D-BASIS-ME: Computer Program for Nonlinear Dynamic Analysis of Seismically Isolated Single and Multiple Structures and Liquid Storage Tanks," by P.C. Tsopelas, M.C. Constantinou and A.M. Reinhorn, 4/12/94.
- NCEER-94-0011 "The Northridge, California Earthquake of January 17, 1994: Performance of Gas Transmission Pipelines," by T.D. O'Rourke and M.C. Palmer, 5/16/94.
- NCEER-94-0012 "Feasibility Study of Replacement Procedures and Earthquake Performance Related to Gas Transmission Pipelines," by T.D. O'Rourke and M.C. Palmer, 5/25/94, (PB94-206638, A09, MF-A02).
- NCEER-94-0013 "Seismic Energy Based Fatigue Damage Analysis of Bridge Columns: Part II - Evaluation of Seismic Demand," by G.A. Chang and J.B. Mander, 6/1/94, (PB95-18106, A08, MF-A02).
- NCEER-94-0014 "NCEER-Taisei Corporation Research Program on Sliding Seismic Isolation Systems for Bridges: Experimental and Analytical Study of a System Consisting of Sliding Bearings and Fluid Restoring Force/Damping Devices," by P. Tsopelas and M.C. Constantinou, 6/13/94, (PB94-219144, A10, MF-A03).
- NCEER-94-0015 "Generation of Hazard-Consistent Fragility Curves for Seismic Loss Estimation Studies," by H. Hwang and J-R. Huo, 6/14/94, (PB95-181996, A09, MF-A02).
- NCEER-94-0016 "Seismic Study of Building Frames with Added Energy-Absorbing Devices," by W.S. Pong, C.S. Tsai and G.C. Lee, 6/20/94, (PB94-219136, A10, A03).
- NCEER-94-0017 "Sliding Mode Control for Seismic-Excited Linear and Nonlinear Civil Engineering Structures," by J. Yang, J. Wu, A. Agrawal and Z. Li, 6/21/94, (PB95-138483, A06, MF-A02).
- NCEER-94-0018 "3D-BASIS-TABS Version 2.0: Computer Program for Nonlinear Dynamic Analysis of Three Dimensional Base Isolated Structures," by A.M. Reinhorn, S. Nagarajaiah, M.C. Constantinou, P. Tsopelas and R. Li, 6/22/94, (PB95-182176, A08, MF-A02).
- NCEER-94-0019 "Proceedings of the International Workshop on Civil Infrastructure Systems: Application of Intelligent Systems and Advanced Materials on Bridge Systems," Edited by G.C. Lee and K.C. Chang, 7/18/94.
- NCEER-94-0020 "Study of Seismic Isolation Systems for Computer Floors," by V. Lambrou and M.C. Constantinou, 7/19/94, (PB95-138533, A10, MF-A03).

- NCEER-94-0021 "Proceedings of the U.S.-Italian Workshop on Guidelines for Seismic Evaluation and Rehabilitation of Unreinforced Masonry Buildings," Edited by D.P. Abrams and G.M. Calvi, 7/20/94, (PB95-138749, A13, MF-A03).
- NCEER-94-0022 "NCEER-Taisei Corporation Research Program on Sliding Seismic Isolation Systems for Bridges: Experimental and Analytical Study of a System Consisting of Lubricated PTFE Sliding Bearings and Mild Steel Dampers," by P. Tsopelas and M.C. Constantinou, 7/22/94, (PB95-182184, A08, MF-A02).
- NCEER-94-0023 "Development of Reliability-Based Design Criteria for Buildings Under Seismic Load," by Y.K. Wen, H. Hwang and M. Shinozuka, 8/1/94, (PB95-211934, A08, MF-A02).
- NCEER-94-0024 "Experimental Verification of Acceleration Feedback Control Strategies for an Active Tendon System," by S.J. Dyke, B.F. Spencer, Jr., P. Quast, M.K. Sain, D.C. Kaspari, Jr. and T.T. Soong, 8/29/94, (PB95-212320, A05, MF-A01).
- NCEER-94-0025 "Seismic Retrofitting Manual for Highway Bridges," Edited by I.G. Buckle and I.F. Friedland, to be published.
- NCEER-94-0026 "Proceedings from the Fifth U.S.-Japan Workshop on Earthquake Resistant Design of Lifeline Facilities and Countermeasures Against Soil Liquefaction," Edited by T.D. O'Rourke and M. Hamada, 11/7/94.
- NCEER-95-0001 "Experimental and Analytical Investigation of Seismic Retrofit of Structures with Supplemental Damping: Part 1 - Fluid Viscous Damping Devices," by A.M. Reinhorn, C. Li and M.C. Constantinou, 1/3/95.
- NCEER-95-0002 "Experimental and Analytical Study of Low-Cycle Fatigue Behavior of Semi-Rigid Top-And-Seat Angle Connections," by G. Pekcan, J.B. Mander and S.S. Chen, 1/5/95.
- NCEER-95-0003 "NCEER-ATC Joint Study on Fragility of Buildings," by T. Anagnos, C. Rojahn and A.S. Kiremidjian, 1/20/95.
- NCEER-95-0004 "Nonlinear Control Algorithms for Peak Response Reduction," by Z. Wu, T.T. Soong, V. Gattulli and R.C. Lin, 2/16/95.
- NCEER-95-0005 "Pipeline Replacement Feasibility Study: A Methodology for Minimizing Seismic and Corrosion Risks to Underground Natural Gas Pipelines," by R.T. Eguchi, H.A. Seligson and D.G. Honegger, 3/2/95.
- NCEER-95-0006 "Evaluation of Seismic Performance of an 11-Story Frame Building During the 1994 Northridge Earthquake," by F. Naeim, R. DiSulio, K. Benuska, A. Reinhorn and C. Li, to be published.
- NCEER-95-0007 "Prioritization of Bridges for Seismic Retrofitting," by N. Basöz and A.S. Kiremidjian, 4/24/95.
- NCEER-95-0008 "Method for Developing Motion Damage Relationships for Reinforced Concrete Frames," by A. Singhal and A.S. Kiremidjian, 5/11/95.

